Astronomy & Astrophysics manuscript no. output
August 5, 2022

The Gaia-ESO Public Spectroscopic Survey: Motivation, implementation, GIRAFFE data processing, analysis, and final data products⋆

G. Gilmore[1], S. Randich[2], C. C. Worley[1], A. Hourihane[1], A. Gonneau[1], G. G. Sacco[2], J. R. Lewis†[1], L. Magrini[2], P. François[3], R. D. Jeffries[4], S. E. Koposov[5,1], A. Bragaglia[6], E. J. Alfaro[7], C. Allende Prieto[8,9], R. Blomme[10], A. J. Korn[11], A. C. Lanzafame[12], E. Pancino[2,13], A. Recio-Blanco[14], R. Smiljanic[15], S. Van Eck[16], T. Zwitter[17], T. Bensby[18], E. Flaccomio[19], M. J. Irwin[1], E. Franciosini[2], L. Morbidelli[2], F. Damiani[19], R. Bonito[19], E. D. Friel[20], J. S. Vink[21], L. Prisinzano[19], U. Abbas[22], D. Hatzidimitriou[23,24], E. V. Held[25], C. Jordi[26], E. Paunzen[27], A. Spagna[22], R. J. Jackson[4], J. Maíz Apellániz[28], M. Asplund[29], P. Bonifacio[30], S. Feltzing[18], J. Binney[31], J. Drew[32], A. M. N. Ferguson[33], G. Micela[19], I. Negueruela[34], T. Prusti[35], H.-W. Rix[36], A. Vallenari[25], M. Bergemann[36,37], A. R. Casey[38], P. de Laverny[14], A. Frasca[39], V. Hill[14], K. Lind[40], L. Sbordone[41], S. G. Sousa[42], V. Adibekyan[42], E. Caffau[30], S. Daflon[43], D. K. Feuillet[18,36], M. Gebran[44], J. I. González Hernández[8], G. Guiglion[45], A. Herrero[8,9], A. Lobel[10], T. Merle[16], Š. Mikolaitis[46], D. Montes[47], T. Morel[48], G. Ruchti†[18], C. Soubiran[49], H. M. Tabernero[50], G. Tautvaišienė[46], G. Traven[17], M. Valentini[45], M. Van der Swaelmen[2], S. Villanova[51], C. Viscasillas Vázquez[46], A. Bayo[52,53], K. Biazzo[54], G. Carraro[55], B. Edvardsson[56], U. Heiter[11], P. Jofré[57], G. Marconi[41], C. Martayan[41], T. Masseron[8,9], L. Monaco[58], N. A. Walton[1], S. Zaggia[25], V. Aguirre Børsen-Koch[59], J. Alves[60], L. Balaguer-Núnez[26], P. S. Barklem[56], D. Barrado[61], M. Bellazzini[6], S. R. Berlanas[34], A. S. Binks[62,4], A. Bressan[63], R. Capuzzo–Dolcetta[64], L. Casagrande[65], L. Casamiquela[49], R. S. Collins[5], V. D'Orazi[25], M. L. L. Dantas[15], V. P. Debattista[66], E. Delgado-Mena[42], P. Di Marcantonio[67], A. Drazdauskas[46], N. W. Evans[1], B. Famaey[68], M. Franchini[67], Y. Frémat[10], X. Fu[69], D. Geisler[51,70,71], O. Gerhard[72], E. A. González Solares[1], E. K. Grebel[73], M. L. Gutiérrez Albarrán[47], F. Jiménez-Esteban[28], H. Jönsson[74], T. Khachaturyants[66], G. Kordopatis[14], J. Kos[17], N. Lagarde[49,75], H.-G. Ludwig[76], L. Mahy[10], M. Mapelli[25], E. Marfil[28], S. L. Martell[77], S. Messina[39], A. Miglio[78,6], I. Minchev[45], A. Moitinho[79], J. Montalban[78], M. J. P. F. G. Monteiro[42,80], C. Morossi[67], N. Mowlavi[81], A. Mucciarelli[78,6], D. N. A. Murphy[1], N. Nardetto[14], S. Ortolani[55], F. Paletou[82], J. Palouš[83], J. C. Pickering[84], A. Quirrenbach[76], P. Re Fiorentin[22], J. I. Read[85], D. Romano[6], N. Ryde[18], N. Sanna[2], W. Santos[43], G. M. Seabroke[86], L. Spina[87], M. Steinmetz[45], E. Stonkuté[88], E. Sutorius[5], F. Thévenin[14], M. Tosi[6], M. Tsantaki[2], N. Wright[4], R. F. G. Wyse[89], M. Zoccali[90], J. Zorec[91], and D. B. Zucker[92]

(Affiliations can be found after the references)

Received 01/2022; Accepted

ABSTRACT

Context. The Gaia-ESO Public Spectroscopic Survey is an ambitious project designed to obtain astrophysical parameters and elemental abundances for 100,000 stars, including large representative samples of the stellar populations in the Galaxy, and a well-defined sample of 60 (plus 20 archive) open clusters. We provide internally consistent results calibrated on benchmark stars and star clusters, extending across a very wide range of abundances and ages. This provides a legacy data set of intrinsic value, and equally a large wide-ranging dataset that is of value for homogenisation of other and future stellar surveys and Gaia's astrophysical parameters.
Aims. This article provides an overview of the survey methodology, the scientific aims, and the implementation, including a description of the data processing for the GIRAFFE spectra. A companion paper introduces the survey results.
Methods. Gaia-ESO aspires to quantify both random and systematic contributions to measurement uncertainties. Thus all available spectroscopic analysis techniques are utilised, each spectrum being analysed by up to several different analysis pipelines, with considerable effort being made to homogenise and calibrate the resulting parameters. We describe here the sequence of activities up to delivery of processed data products to the ESO Science Archive Facility for open use.
Results. The Gaia-ESO Survey obtained 202,000 spectra of 115,000 stars using 340 allocated VLT nights between December 2011 and January 2018 from GIRAFFE and UVES.
Conclusions. The full consistently reduced final data set of spectra was released through the ESO Science Archive Facility in late 2020, with the full astrophysical parameters sets following in 2022. A companion article reviews the survey implementation, scientific highlights, the open cluster survey, and data products.

Key words. Methods: observational - Galaxy: kinematics and dynamics - Galaxy: stellar content - Stars: abundances - Techniques: spectroscopy - Astronomical databases: surveys

Article published by EDP Sciences, to be cited as https://doi.org/10.1051/0004-6361/202243134

1. Introduction

This is one of two papers providing the overview of the Gaia-ESO Public Spectroscopic Survey of stellar populations. This survey has utilised the ESO VLT and multi-object FLAMES facility, and both GIRAFFE and UVES spectrographs, to derive astrophysical parameters and elemental abundances for some 100,000 stars. The companion survey overview paper, Randich et al. (2022), describes the primary scientific results, illustrating the outcomes of the many activities described in this paper. That paper also provides additional summary information on the open cluster aspects of Gaia-ESO. It is our intent in these two papers to document the origins, motivation, original case, structure as implemented, operation, and a summary of the outputs from the Survey. We also take care to identify those key individuals who led the work packages during the survey operation. In any large consortium it is a challenge to acknowledge due credit. In Gaia-ESO we have attempted to do this by identifying these individuals in this paper, and importantly by authorship policy - each key work package is described in its own paper, with lead authors the key individuals, as listed in this section below.

This paper is organised as follows. Following this introduction (Section 1), which includes the list of reference articles describing the Gaia-ESO Survey, in Section 2 we provide a summary overview of the science case for the survey, and introduce the envisioned legacy.

Section 3 introduces our ambition to define both measurement precision and accuracy, which explains our motivation for involving the many different spectroscopic analysis methodologies available in the community, with significant effort in subsequent homogenisation to provide a single recommended parameter set per star. In Section 4 we describe the survey working group (WG) structure and organisation. The match of scientific ambition to practical target selection for each aspect of the survey is described in Section 5. Section 6 provides the top-level overview of the target selection and sky coverage. It then describes the practical implementation effort, provided by WGs 0-6. As part of that effort we introduce our approach to maximise the Survey legacy, which leads to substantial calibration effort. Sub-section 6.5 describes the efforts to calibrate the survey, ensuring consistency which makes the survey results valuable for Gaia and allows cross-calibration with other present and future ground-based large spectroscopic surveys and the asteroseismology space missions. Section 7 describes the GIRAFFE data reduction pipeline developed and enhanced as part of the Gaia-ESO Survey, which generated the reduced spectra which are publicly released as a survey product. Within this, subsection 7.10 provides a more detailed discussion of sky subtraction, considering the various GIRAFFE settings we used and relevant astrophysical background sources. Section 8 describes the calculation of radial velocities, and their accuracies. This process also determines first-pass astrophysical parameters for each spectrum, useful as a starting point in later more detailed analysis. Section 9 provides an overview of the several approaches to spectrum analyses, and determination of the published recommended parameters. More detailed articles describing each method are referenced as appropriate. The astrophysical parameters and elemental abundances output from the various pipelines, nodes, and Working Groups must be calibrated onto a single internally consistent system, which is consistent with the calibration effort. This very challenging task is described in Section 10. Overview of the Survey, and the structure and operation of the data flows through the working and then survey databases is described in Section 11. The data released to the public through ESO Science Archive Facility (ESO SAF) data releases are explained in Section 12. Section 13 summarises the scientific and operational status of the Gaia-ESO Survey.

The Gaia-ESO Survey is an ESO public spectroscopic survey, targeting 10^5 stars, systematically covering all the major components of the Milky Way, from halo to star forming regions, providing an homogeneous overview of the distributions of kinematics and elemental abundances. The Survey utilises both medium ($R \simeq 20,000$) and high ($R \simeq 50,000$) resolution spectroscopy, and reaches faint enough to explore a significant range of Galacto-centric distances. This alone will contribute to our knowledge of Galactic and stellar evolution: when combined with Gaia astrometry, the Survey helps quantify the formation history and evolution of young, mature and ancient Galactic populations. With well-defined samples, based primarily on ESO-VISTA photometry for the field stars, and from a variety of photometric surveys of open clusters, the Survey quantifies the kinematic-multi-element abundance distribution functions of the bulge, the thick and the thin discs and the halo stellar components, as well as a significant sample of ~ 60 open star clusters, covering all accessible cluster ages and stellar masses. A brief overview is available at Gilmore et al. (2012), with an early progress report at Randich et al. (2013). These outline the prehistory of the project, and the partnership between ESO and the Gaia-ESO Survey team in developing and implementing this ambitious Public Spectroscopic Survey.

The Survey has obtained VLT/FLAMES spectra to quantify individual elemental abundances; yield precise radial velocities for a 4-D kinematic phase-space; map kinematic gradients and abundance - phase-space structure throughout the Galaxy; and follow the formation, evolution and dissolution of open clusters as they populate the disc. Several GIRAFFE settings, optimised for the astrophysical parameters of each target group, and parallel UVES spectra have been obtained for each surveyed open cluster. GIRAFFE spectra, with two settings, have been obtained for statistically significant samples of stars in all major stellar populations. These are supplemented by UVES spectra of an unbiased sample of G-stars within $\geq$ 1kpc of the Sun, providing the abundance distribution function for the local thin disc, thick disc and halo. The open cluster survey is described in a companion article (Randich et al. 2022). The Survey is designed to provide a legacy dataset that adds enormous value to the Gaia mission and ongoing ESO imaging surveys.

The Gaia-ESO Survey delivers the data to support a wide variety of studies of stellar populations, the evolution of dynamical systems, and stellar evolution. Gaia-ESO complements Gaia by using high-resolution spectra from UVES to measure the metallicity and detailed abundances for several chemical elements in ~ 5000 field stars with $V \leq 15$ and in ~ 2000 open cluster members down to $V \sim 16.5$. Depending on target signal-to-noise ratio (SNR), and astrophysical parameters, the Survey typically probes the two fundamental nucleosynthetic channels, nuclear statistical equilibrium (V, Cr, Mn, Fe, Co), and α-chain (Si, Ca, Ti). [Fe/H], [α/Fe], and some other element abundance ratios have been obtained from the lower resolution GIRAFFE spectra. The radial velocity (RV) precision for this sample is $\simeq 0.1\,\mathrm{km\,s^{-1}}$ to $\leq 5\,\mathrm{km\,s^{-1}}$, depending on target, with in each case the mea-

⋆ Based on observations collected at the ESO telescopes under programme 188.B3002, 193.B-0936, and 197.B-1074, the Gaia-ESO Public Spectroscopic Survey.

surement precision being that appropriate for a range of relevant astrophysical analyses.

The Gaia-ESO dataset supports analyses which aim to identify, on both chemical and kinematic grounds, phase-space substructures that bear witness to specific merger or starburst events. The dataset also allows mapping the dissolution of clusters, and the Galactic migration of field stars. The Survey not only supplies homogeneously determined element abundances, but also complementary astrophysical information for large samples of members of clusters with precise distances from Gaia. This information can be used to challenge models of stellar structure and evolution, as well as to test models of mass accretion from circumstellar discs into the star (Randich et al. 2018).

A substantial observational effort has been devoted to abundance calibration, establishing targets in common with other spectroscopic surveys, including observations of CoRoT and Kepler stars, and expanding the grid of "benchmark stars" which act as primary spectroscopic standards, to ensure maximal legacy value. The Gaia-ESO Survey additionally invested considerable effort in re-analyses of spectra already available in the ESO SAF, where scientifically complementary to the primary Survey.

The Survey consortium and operations was structured into a set of working groups, with the whole overseen by a Steering Committee. As a partial motivation for the Gaia-ESO Survey was to build an ESO-wide community ready to reap the vast scientific potential of Gaia, we explicitly included all groups in the ESO community active, at the time the Survey was designed, in precision stellar spectroscopy, with their ranges of expertise and methods. This provided the opportunity to cross-calibrate the various available methods, and identify possible systematic differences, particularly based on analyses of the well-quantified benchmark calibrator stars. The outcomes of all these methods were then homogenised into the recommended astrophysical parameters for each star which became available publicly through the ESO SAF (Sect 12), and also through the Gaia-ESO Survey archive hosted at the Wide Field Astronomy Unit, Edinburgh (WFAU) (Sect 11).

The big themes in astronomy require complementary space and ground based observations. To maximise the scientific output it is necessary to coordinate the European efforts. ESO and ESA have recognised this coordination necessity in various topics which can and must be addressed both from the ground and in space. Joint working groups have been nominated for selected topics and the fourth such group was central to this project. This ESA-ESO working group (chaired by Catherine Turon) addressed the topic of "Galactic Populations, Chemistry and Dynamics". The report of the working group was published in 2008 and remains up to date today (Turon et al. 2008). Many recommendations from that study are of relevance to this project, but the key ones can be summarised in two words covering both space and ground: Gaia and spectroscopy. Gaia began its science operations in July 2014. The Gaia-ESO public survey aimed to support the European stellar spectroscopy community to deliver full value from the Gaia potential for our Milky Way. The Gaia-ESO Survey had very ambitious goals. It included spectral types from O to M, all stellar populations, field and clusters, open and globular, all stellar ages. This ambition made it a particularly challenging endeavour. The spectroscopic data products are made available to the community in the same time frame as the intermediate Gaia catalogues. This allows the European and global - all survey products, like those of Gaia, are fully open-access - scientific community to address a multitude of galactic astronomy topics with the combined spectroscopic and Gaia data sets.

While this Survey was a substantial effort in its own right, and was the first dedicated stellar spectroscopic survey using 8-m class telescopes, it has been clear since early planning for Gaia that dedicated highly-multiplexed wide field spectroscopic facilities were needed for effective Gaia science exploitation. These are arriving, with many major surveys, with a range of spectral resolutions. These include (alphabetically) APOGEE (Ahn et al. 2014), Gaia-RVS (Gaia Collaboration et al. 2016), GALAH (De Silva et al. 2015), LAMOST (Cui et al. 2012), and RAVE (Steinmetz et al. 2006), among many others. MOONS (Cirasuolo et al. 2020), WEAVE (Dalton 2016) and 4MOST (de Jong et al. 2019) are among those in construction with major European involvement.

As a consortium-building exercise in preparation for these major long-term projects, a secondary ambition for the Gaia-ESO Public Spectroscopic Survey was to bring together the many high-quality stellar spectroscopy groups across Europe. Having all these groups applying their specific expertise, and learning to communicate and compare data and analyses, helped to build the successful consortia now carrying the subject forward.

Additionally, the project aspired to help identify and reduce the impact of the factors which lead to systematic scale differences between survey pipeline outputs. For this, a very major effort was committed to developing a homogeneous atomic and molecular line list relevant to abundance analyses of FGK-type stars in the relevant Gaia-ESO passbands 480-680 nm and 850-900 nm (Heiter et al. 2021). To ensure the highest homogeneity possible in the quantities derived, all the different Gaia-ESO spectrum analysis methods adopted the same atomic and molecular data, as well as the same set of model atmospheres to the extent possible - see sect 9.

In order to widen consistent cross-calibration possibilities between ground-based spectroscopic, asteroseismic and Gaia analyses, considerable overlaps of targets with CoRoT and Kepler stars were ensured, while significant samples of stars close to the equator (SDSS Stripe 82) were included. Substantial efforts were also invested in developing the Gaia Benchmarks calibrator stars, and ensuring consistency between that calibrator set and the overall Gaia-ESO elemental abundance and astrophysical parameter scales. Of course, the fundamental design of Gaia-ESO, with a substantial sample of open clusters of all available ages and abundances, extending to field stars with a wide range of ages and abundances, ensures the Gaia-ESO calibration is fundamentally tied to observationally-tested isochrones on stars with Gaia and spectroscopic data to ensure reliable cluster membership.

Publication of the full Survey overview in a single data release paper makes it difficult to ensure full credit is given to the leaders and members of the work packages who have invested considerable efforts to deliver this survey. Hence we decided not to follow the model of a single survey description paper at each of the data releases, but rather to describe the technical work in a series of specific articles. At the time of writing there are over 100 Gaia-ESO Survey articles already published by the consortium. We list here (Table 1) those which are reference and methods articles of direct relevance to understanding the final data products. The Gaia Benchmark Stars is a joint project to provide high-precision calibrator stars. Those references are also included in the Table.

Table 1: Gaia-ESO Survey Methods description papers

Article title	published reference
The Gaia-ESO Public Spectroscopic Survey	Gilmore et al. (2012)
The Gaia-ESO Large Public Spectroscopic Survey.	Randich et al. (2013)
The Gaia-ESO Survey: processing FLAMES-UVES spectra.	Sacco et al. (2014)
Fe I oscillator strengths for the Gaia-ESO survey.	Ruffoni et al. (2014)
The Gaia-ESO Survey: The analysis of high-resolution UVES spectra of FGK-type stars.	Smiljanic et al. (2014)
The Gaia-ESO Survey: Extracting diffuse interstellar bands from cool star spectra.	Puspitarini et al. (2015)
Gaia-ESO Survey: Analysis of pre-main sequence stellar spectra.	Lanzafame et al. (2015)
The Gaia-ESO Survey: Empirical determination of the precision of stellar radial velocities and projected rotation velocities.	Jackson et al. (2015)
The Gaia-ESO Survey Astrophysical Calibration.	Pancino et al. (2017a)
The Gaia-ESO Survey: the selection function of the Milky Way field stars.	Stonkutė et al. (2016)
A Grid of NLTE Corrections for Sulphur Lines in Atmospheres of Cool Stars for the Gaia-ESO Survey.	Korotin et al. (2017)
The Gaia-ESO Survey: double-, triple-, and quadruple-line spectroscopic binary candidates.	Merle et al. (2017)
Gaia-ESO Survey: INTRIGOSS—A New Library of High-resolution Synthetic Spectra.	Franchini et al. (2018)
Atomic data for the Gaia-ESO Survey. A line list for analysis of UVES and GIRAFFE observations of cool stars.	Heiter et al. (2021)
The Gaia-ESO Survey: detection and characterization of single-line spectroscopic binaries.	Merle et al. (2020)
The Gaia-ESO Survey: Spectroscopic-Asteroseismic analysis of the K2@Gaia-ESO stars.	Worley et al. (2020)
The Gaia-ESO Survey: Target Selection of Open Cluster Stars.	Bragaglia et al. (2022)
The Gaia-ESO Survey: The analysis of hot-star spectra.	Blomme et al. (2022)
The Gaia-ESO Survey: The analysis of the medium-resolution GIRAFFE spectra of FGK stars.	Worley & et al. (2022)
The Gaia-ESO Survey: Homogenisation of the multi-node astrophysical parameters sets.	Hourihane & et al, (2022)
The Gaia-ESO Survey: Spectroscopic-Asteroseismic analysis of the CoRoT@Gaia-ESO Stars.	Masseron & et al. (2022)
The Gaia-ESO Survey: Survey implementation, data products, open cluster survey, and legacy.	Randich et al. (2022)
The Gaia-ESO Public Spectroscopic Survey: motivation, implementation, GIRAFFE data processing, analysis, and final data products.	this paper
Gaia FGK benchmark stars: Metallicity.	Jofré et al. (2014)
The Gaia FGK benchmark stars. High resolution spectral library.	Blanco-Cuaresma et al. (2014)
Gaia FGK benchmark stars: Effective temperatures and surface gravities.	Heiter et al. (2015)
Gaia FGK benchmark stars: abundances of α and iron-peak elements.	Jofré et al. (2015)
Gaia FGK benchmark stars: new candidates at low metallicities.	Hawkins et al. (2016a)
Gaia FGK benchmark stars: a bridge between spectroscopic surveys.	Jofré et al. (2017a)
Gaia FGK benchmark stars: opening the black box of stellar element abundance determination.	Jofré et al. (2017b)
The Gaia FGK Benchmark Stars Version 2.1.	Jofré et al. (2018)
Benchmark ages for the Gaia benchmark stars.	Sahlholdt et al. (2019)

All Gaia-ESO Survey processed, calibrated and reduced data are available for unrestricted public access through the ESO Science SAF Facility web interface (Table 2).

Each data release has extensive documentation[1]. In addition to a summary of the release content - that for DR4 is below - the release documentation provides a summary overview of the

[1] available for example, DR4, at https://www.eso.org/rm/api/v1/public/releaseDescriptions/152

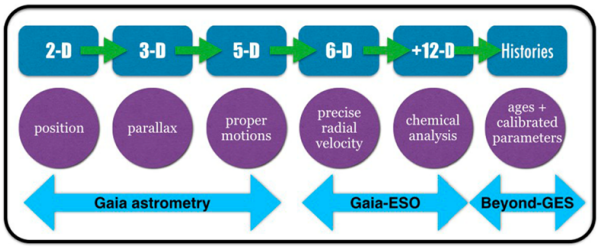

Fig. 1: The complementary contributions of astrometry, spectroscopy, field star and cluster isochrone and other age calibrations, and asteroseismology, to populating a high-dimensional description of Galactic stars.

observing and reduction operations, the types of targets, and explanation of the (many) keywords.

DR4.0, Dec 2020, delivers about 190,000 stacked, quality-controlled, 1-d spectra (R between 18000 and 54000) of 114,500 unique stellar targets. These stars were observed with GIRAFFE and UVES from 31.12.2011 to 26.01.2018, during the entire time execution of the survey. These targets were selected from all the major structural components of the Milky Way: bulge, thick and thin discs, halo, including open star clusters of all ages and masses. The 1-D spectra from Gaia-ESO DR4 augment or update the spectra published in the previous data releases.

The DR5 release of the final derived abundances and astrophysical parameters associated with the spectra published in DR4 was published on May 16 2022. The Advanced Products are described further below, and in the companion paper Randich et al. (2022).

2. Gaia-ESO Survey - proposal top-level science case

This section of this article essentially reproduces the key section of the original Gaia-ESO Survey proposal to ESO. We do this to bring into the public record the early context and history which led to the survey. We also in this way present the survey's original goals, to allow comparison of ambition and outcome. We avoid post-hoc justifications. This context also established the survey optimisation. As the choice of instrumentation was fixed, the variables available for optimisation are the wavelength settings, the signal-noise per pixel per object, and most significantly the number of targets required to meet the basic science goals. The text also puts in context the status of stellar spectroscopic surveys at the time, which was very much less rich than the situation now.

How disc galaxies form and evolve, and how their component stars and stellar populations form and evolve, are among the most fundamental questions in contemporary astrophysics. The Gaia-ESO survey has been formulated to contribute to those key questions, by enhancing our knowledge of the formation and evolution of the Galaxy and the stars that populate it. Gaia-ESO is a high statistical weight ($\simeq 10^5$ stars) spectroscopic survey which utilises the opportunity of a large telescope in the Southern Hemisphere to sample all the main components of the Galaxy, from star-forming regions to ancient halo stars. This survey has enormous value in its own right. However, its products are even further enhanced by Gaia astrometry and Gaia spectrophotometry and improved stellar parameters.

Understanding how galaxies actually form and evolve within our ΛCDM universe continues to be an enormous challenge (Peebles et al. 2011; Kormendy et al. 2010). Simulations of the aggregation of cold dark matter, complemented by direct studies of galaxies at high redshifts, suggest that galaxies grow through a sequence of merger/accretion events. However, theoretical models of galaxy formation, which necessarily involve modelling star formation and stellar evolution, rely more heavily on phenomenological models than on physical theory. Thus, these models require calibration with well-studied (nearby) test cases.

For example, star formation involves turbulence, magnetic reconnection, collisionless shocks, and radiative transfer through a turbulent medium. Similarly, the treatment of convection, mixing, equations of state at high density, opacities, rotation and magnetic fields can all significantly affect stellar luminosities, radii, and lifetimes at different evolutionary phases. We are also far from being able to simulate the coupled evolution of CDM and baryons from ab-initio physics. Observations are crucial to learning how galaxies and stars were formed and evolved, and what their structure now is (Bland-Hawthorn et al. 2010). Observations of objects at high redshifts and long look-back times are important for this endeavour, as is detailed examination of our Galaxy, because such "near-field cosmology" gives insights into key processes that cannot be obtained by studying faint, poorly resolved objects with uncertain futures.

Just as the history of life was deduced by examining rocks, we expect to deduce the history of our Galaxy by examining stars. Stars record the past in their ages, compositions, and in their kinematics. For example, individual accretion and cluster dissolution events can be inferred by detecting stellar streams from accurate phase-space positions. Correlations between the chemical compositions and kinematics of field stars enable us to deduce the history of star formation and even the past dynamics of the disc. The kinematic structure of the bulge reveals the relative importance in its formation of disc instability and an early major merger.

The study of open clusters is crucial to understanding fundamental issues in stellar evolution, the star formation process, and the assembly and evolution of the Milky Way thin disc. Theories of cluster formation range from the highly dynamic through to quasi-equilibrium and slow contraction scenarios. These different routes lead to different initial cluster structures and kinematics. Subsequent evolution depends on many factors, including the initial conditions, star formation efficiency and tidal interactions. Whilst hydrodynamic and N-body simulations are developing, a fundamental requirement is an extensive body of detailed observations. A complete comparison requires precise position and velocity phase-space information resolving the internal cluster kinematics, $\leq$ 0.5km/s. Even more sophisticated studies follow combination with Gaia astrometry. The velocity fields within the youngest clusters reveal their formation history, whilst the kinematics of the older clusters and the age dependence of their mass functions test theories of cluster destruction. Each star cluster provides a (near-)coeval snapshot of the stellar mass function. This survey contributes to testing stellar evolution models from pre-main sequence phases right through to advanced evolutionary stages. Much of the input physics in stellar models can be tested by its effects on stellar luminosities, radii and the lifetimes of different evolutionary phases. Homogeneous spectroscopy will provide estimates of stellar parameters and reddening for large samples of stars over a wide range of

Table 2: Gaia-ESO Survey ESO Science Archive Facility Data Releases

Name	Date	Unique targets	Spectra	Advanced Products
DR1	10-2013	3834	5654	no
DR2	02-2015	15093	27359	yes
DR3	08-2016	25534	44214	yes
DR4	12-2020	114500	190200	yes
DR5	05-2022	114324	202233	all products
DR5.1	late 2022	500	500	remaining stars

masses, in clusters with a wide range of ages and mean chemical compositions. Such data are essential in testing, calibrating, and refining both evolutionary tracks and stellar parameters derived from spectra.

When combined with Gaia astrometry, and supplemented by asteroseismology, these data isolate and probe all the theoretical uncertainties, whilst simultaneously identifying and quantifying important perturbing factors such as binarity, rotation, accretion and magnetic activity. The interplay of these difficult-to-model physical phenomena can only be dissected by studying a wide range of clusters the properties of which make one or the other effect dominate.

An important focus of the Gaia-ESO Survey is to ensure consistently derived (to the extent possible) and consistently calibrated astrophysical parameters on the widest possible range of stellar populations. These range from young open star clusters, through clusters with a range of ages and metallicities, to field stars young and old, metal-rich to metal-poor. By ensuring consistency across this wide range, the age-calibrations and element abundance ratios can be made consistent, quantifying evolution. The goal is to be able to combine Gaia-ESO age calibration using open cluster isochrones, asteroseismology calibrations, spectroscopic age indicators such as the [C/N] ratio in Red Giants, and Gaia data.

Of course, many ground-based surveys address these same general goals, while the *par excellence* step forward is the ESA Gaia mission, currently in its extended-mission phase.

A convenient way of picturing the Gaia – ground complementarity is looking at the dimensionality of data which can be obtained on an astrophysical object. Larger amounts of information of higher quality are the goal, to allow increasing understanding. Fig 1 (adapted from (Gilmore et al. 2012)) gives a cartoon view of this information set. There are four basic thresholds which we must pass. The first is to know a source exists, its position, and basic photometric data. Photometric surveys, such as those undertaken at VISTA and VST, which are source photometry for this survey, deliver this information. The second is to add the time domain – motions, including parallax, providing distances and speeds. Here Gaia is revolutionary. The third threshold is radial velocity, turning motions into orbits. While Gaia will provide radial velocities, the magnitude limit is several magnitudes brighter than that of the astrometry and the precision at fainter magnitudes is much below that of Gaia's proper motions. Gaia-ESO, together with other major spectroscopic surveys, is crucial to supplement Gaia spectroscopy. The fourth threshold is chemistry, and astrophysical parameters. These latter two both require spectroscopy, which is the key information from Gaia-ESO.

We must quantify the scale of the challenge for a stellar spectroscopic survey. The key to decoding the history of galaxy evolution involves chemical element mapping, which quantifies timescales, mixing and accretion length scales, and star formation histories; spatial distributions, which relate to structures and gradients; and kinematics, which relates to both the felt but unseen dark matter, and dynamical histories of clusters and merger events (Freeman & Bland-Hawthorn 2002). With Gaia, and calibrated stellar models, one can also add ages.

Manifestly, very large samples are required to define all these distribution functions and their spatial and temporal gradients. Orbit space is (only) three-dimensional because generic orbits in typical galaxy potentials admit three isolating integrals. The number of objects required to determine the underlying probability density of objects grows rapidly with the dimensionality of the space. So in the present case, if we have ten bins along each axis in integral space, corresponding to a resolution in velocity as coarse as ~ 6 km/s, we have 1000 bins in integral space. Then we wish to distinguish at a minimum between young stars, stars of intermediate age and old stars, and similarly, between stars with solar abundances, stars with abundances similar to those of disc clusters and of halo clusters. Thus each of the age, [Fe/H], and [α/H] axes must be divided into at least three bins, giving us 27 000 bins in the minimal six-dimensional space. Even with perfectly adapted bin sizes, an estimate of the density of stars in this space will have Poisson noise of order unity unless we have in excess of 10^5 stars. Similarly, defining the information content in the open cluster system requires adequate sampling of the four dimensional (age, metallicity, position in the Galaxy, mass/density) parameter space. Even considering the inhomogeneous (mostly abundance) measurements available in the literature, only a homogeneous survey of $\simeq 70$ clusters, containing $\simeq 5 \times 10^4$ stars, will have sufficient statistical power.

An illustration of the information content in abundance-kinematic surveys already available prior to the Gaia-ESO Survey is provided by the extensive review by Nissen (2013). Fig 16 of that review is shown as the top panel of Fig 2 here.

As a direct example of the evolution of the progress in observational constraints on Galactic evolution from stellar spectroscopic surveys between 2011, when the proposal for the Gaia-ESO Survey was submitted, and 2022, when the survey final data release was made public, we contrast the 2011-vintage upper panel Fig 2 with the lower panel Fig, topical results from a recent Gaia-ESO Survey analysis paper (Casali et al. 2019).

This figure illustrates the ability of chemical abundances and kinematic population assignments to sample the clear thin-thick disc distinction, the complexity of the halo populations, the considerable difference between Galactic halo satellites and Galactic halo field stars, and the very metal-rich inner-Galaxy stars. Ad-

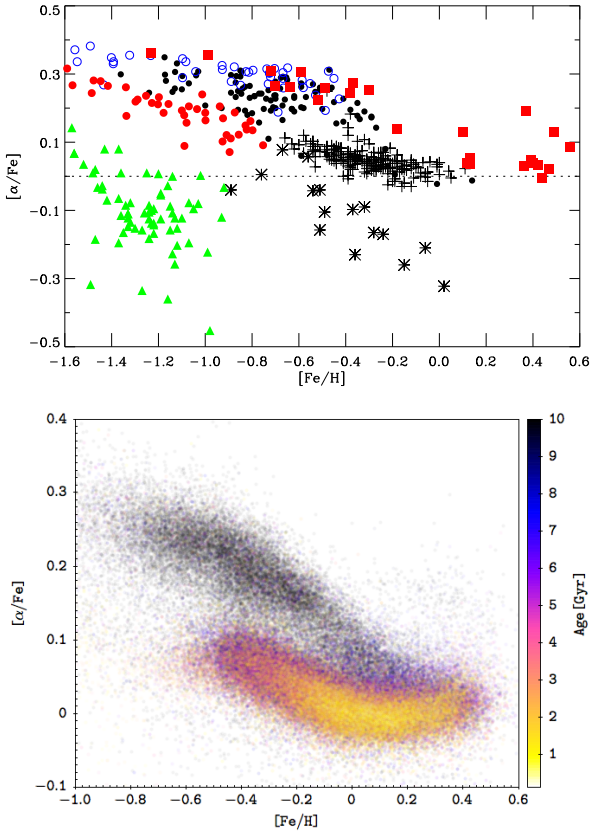

Fig. 2: [α/Fe] vs. [Fe/H] for various stellar populations. Upper: thin-disc stars from Reddy et al. (2003) are shown with plus symbols. Filled circles refer to thick-disc stars from Reddy et al. (2006) and Nissen & Schuster (2010). Filled (red) squares are microlensed bulge stars from Bensby et al. (2011). Open (blue) circles are high-α and filled (red) circles low-α halo stars from Nissen & Schuster (2010). Asterisks refer to stars in the Sagittarius dSph galaxy (Sbordone et al. 2007), and filled (green) triangles show data for stars in the Sculptor dSph galaxy from Kirby et al. (2009), for which the precision of [α/Fe] is better than 0.15 dex. This figure is taken from (Nissen 2013). Lower: [α/Fe] vs. [Fe/H] for various stellar populations, colour coded by age derived from the [C/N] chronometer calibrated from Gaia-ESO observed open clusters. The distinction between the high-alpha thick disc and the low-alpha thin disc is manifest. Also apparent is the age gradient down the thick disc sequence, continued in age after a discontinuous jump in [Fe/H] to [Fe/H]=-0.6 This identifies the last major merger in the Milky Way. This figure is taken from Casali et al. (2019).

ditionally, with newly developed age calibrations, the temporal evolution of the Milky Way begins to become quantified.

3. Survey strategy: defining both precision and accuracy for stellar abundances

Gaia-ESO includes stars with almost the full observationally available range of astrophysical parameters, hot to cool, young to old, metal-rich to metal-poor, pre-main sequence to evolved giants. Since a primary goal is to derive high-quality astrophysical parameters and elemental abundances across this wide range, it is clear that a range of different analysis pipelines is required. This immediately raises the challenge of homogenising and calibrating the outputs on to a consistent (set of) scales.

The challenges of stellar spectroscopy in the limiting regimes has been well summarised in two relevant recent review articles: "High-precision stellar abundances" (Nissen & Gustafsson 2018) and "Accuracy and precision of industrial stellar abundances" (Jofré et al. 2019). We retain the full titles of these articles since they very clearly define the complementarity they both provide.

The need for multiple approaches to maximise reliability is not a new concept. We note as one example the Segue Stellar Parameter Pipeline I - which involves 11 methods for $T_{\rm eff}$, 10 for $\log g$, 12 for Fe/H, though with considerable overlap among them. [Lee et al. (2008a), Lee et al. (2008b), Allende Prieto et al. (2008)].

Our need to cater for a very wide range in stellar astrophysical parameters is illustrated in Fig 3. This presents spectra for a set of about 100 stars in a young open cluster. The spectra are sorted by temperature (hottest at the top) with naturally the coolest stars also illustrating lower signal-noise data. The changing emission (Hα and Lithium in the lower panel) and absorption lines, and the range of astrophysical parameters which must be handled is apparent. The top panel is Giraffe HR9B, the lower HR15N (see Table 7).

Calibration of spectroscopic analyses between authors and across methods has been a requirement ever since the subject began. Typically in very large surveys iterative increases in accuracy and precision are achieved with experience, and by detailed studies of individual data sets. For example, Hawkins et al. (2016b) reanalyse the APOGEE DR12 APOKASC subsample, to show the importance of linelist selection and the treatment of microturbulence to ensure robust metallicity scales and elemental abundance ratios. The lesson learned is that careful treatment of the important astrophysical parameters involved in abundance determinations, augmented by analysis of a set of "benchmark" stars, provides abundance results which do not need later empirical scaling to match independent literature studies. Another example of systematics which require careful treatment is given by Venn et al. (2012), their Fig 5, showing the large and wavelength-dependant continuum scattering corrections required.

In spite of best efforts, some analysis limitations are discovered only at science verification analysis level. For example, Piatti (2019) notes the apparent but entirely spurious dispersion in a study of NGC188, indicating an apparent dispersion of 0.16dex in [Na/Fe]. He concludes "Therefore I warn users of large spectroscopic surveys to be extra careful when finding peculiar abundance results". This caveat emptor applies fully to Gaia-ESO Survey results.

Robust astrophysical analyses require that parameters derived from several different pipelines are as much as is feasible on a single consistent scale. This is a fundamental requirement which does not require new justification. It is not always completely easy to do. We illustrate this by considering the successive (re-)analyses of the star Boo-1137, a metal-poor red giant member of the Bootes-I ultra-faint dwarf galaxy, based on a single VLT spectrum with the same settings and typical quality as those relevant to the Gaia-ESO Survey. This star was discovered by Norris et al. (2010a), and subsequently studied by Norris et al. (2010b), and by Gilmore et al. (2013). The analysis of Gilmore et al. (2013) was a full double-blind study, compara-

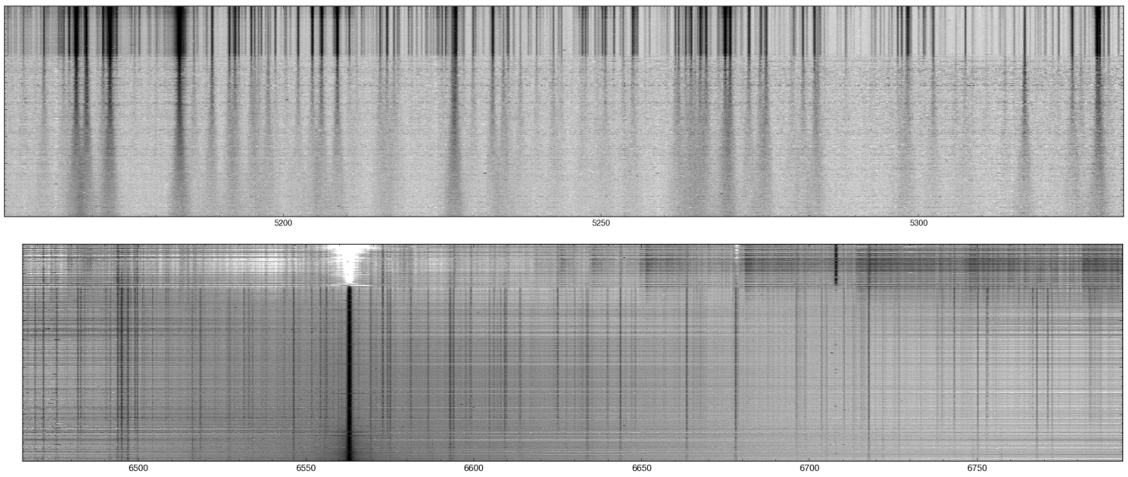

Fig. 3: Gaia-ESO Survey stars in a typical young open cluster. This presents a single Giraffe setup of about 100 stars with spectra scaled to illustrate the dynamic range, and sorted in temperature (hottest at the top). The top panel is Giraffe HR9B, 514-535nm, the lower HR15N, 644-682nm. This illustrates the wide range of astrophysical parameters, and hence appearances of the spectrum, which must be managed in a wide-ranging stellar survey.

ble in methodology and methods with the analyses of Gaia-ESO stellar spectra by several nodes acting independently.

The starting point of this example is that Norris et al. (2010b) derived an abundance ratio [Mg/Fe] = +0.47, while Gilmore et al. (2013) derived [Mg/Fe] = +0.26 from the same spectrum. Clearly the difference between the derived values is entirely a consequence of different analyses. How do such differences arise, and what lessons should be learned for multi-node survey calibration and homogenisation?

The first point to note is the importance of data selection. The double-blind analysis of Gilmore et al. (2013) showed the desirability to restrict the wavelength range under consideration. This generated changes in both Mg and Fe abundances, with opposite sign. There is a further change of note: the adopted Solar abundances. The 2010 study adopted the Solar abundance from Asplund et al. (2006), while the 2013 study adopted those of Asplund et al. (2009). These individually small changes all affect the derived elemental abundance ratio cumulatively.

This simple example illustrates the desirability of independent double-blind analyses to identify the parameter ranges in which specific analysis systems are optimised. It also illustrates the need to isolate and fix parameters which can be controlled, such as line lists, model atmospheres and adopted scale or benchmark references, that being the Sun in this case.

It also of course highlights the need to bring all the node results together into a consistent homogenised whole. For Gaia-ESO Working Group 15 carried out this last critical task. In the rest of this paper we describe the many steps and very substantial investment of effort which was required to implement the multi-analysis approach introduced above.

Homogenisation of analyses from several independent studies of the same spectra improves more than (just) reliability of the derived parameters. An additional advantage, and indeed a robust sanity check on the whole process, is its effect on the homogenised H-R diagram. This is described more in section 10, but is illustrated here by an example in Fig 4. Reductions of method-specific systematics, essentially calibrating away limits on the relevant parameter range in which a method is robust, are

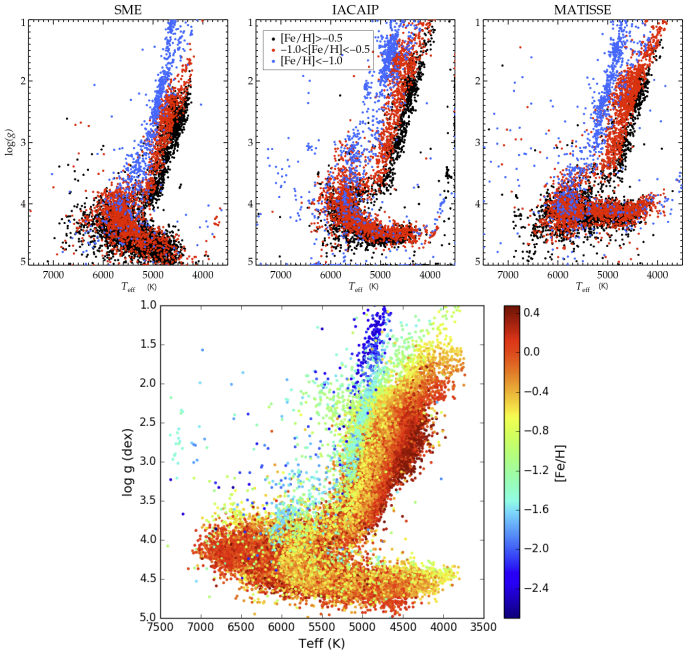

Fig. 4: Before homogenisation and after - initial method-specific systematic differences can be homogenised away if one has many methods available in a single study. The three top panels present results from specific nodes (see Sect 9 for detail), while the lower panel shows the outcome of homogenisation, further colour-coded by [Fe/H] to make clear the dispersion is now real astrophysical dispersion. The systematic effects apparent in the top three panels have been substantially reduced.

apparent. A full description of how the Gaia-ESO approach was implemented, showing node-level and homogenised HRDs, is available in Randich et al. (2022), especially figures 10 and 11 of that paper.

4. Structure of the Gaia-ESO Survey project team

As with all ESO public surveys, the Gaia-ESO Spectroscopic Survey Consortium role and responsibilities are defined through a Survey Management Plan, which is a Memorandum of Understanding between ESO and the Co-PIs, Gilmore and Randich. This defines what is essentially described in this paper, the structure and responsibilities of the survey team, and the deliverable data products for release through the ESO SAF.

In order to implement those formal requirements, in a consortium with originally some 400 Co-Investigators from some 100 Institutes, with a commitment to 300 VLT nights of data, a formal structured set of internal Working Groups with clearly defined responsibilities was established. An overview Steering Group supervised survey management, while annual reports to and bi-annual reviews by ESO panels monitored technical and scientific progress. Internal communications relied heavily on a dedicated wiki system, newsletters, and annual whole-Consortium meetings (pre-Covid).

Among the minor but significant challenges in bringing together such a large number of established spectroscopic analysis groups was efficient data exchange. Indeed it is a valuable legacy product of the survey that the community has learned to adopt a standard data format for both results and data - FITS - and has become familiar with handling very large and complex data files.

4.1. How it came together

Development of the large and ambitious Gaia-ESO Survey project involved many people and much time and effort. The range of expertise required to be able to select and observe suitable targets, reduce the data, analyse the spectra and deliver science verification for the ambitious very wide range of astrophysical targets was assembled and organised. The two branches of community interest were brought together, with one group with more expertise focussed on young stars and star clusters, the other on field stars. This ensured a single ambition, to build internal survey-wide consistency, with analyses anchored from clusters and their isochrones, then extending to the widest accessible range of ages and abundances.

All interested European spectroscopic analysis groups were invited to join, ensuring that essentially all widely-used analysis packages were involved, and the requisite range of expertise and effort was available. Although the observational approach for the open clusters was already optimised, from community experience with FLAMES, for the field stars many simulations were implemented, to optimise the selection of available observing setups, and targeted signal-noise ratios. The considerable effort to develop the data reduction pipelines and data management system was identified. All this took place prior to and shortly after submission of the survey proposal to ESO in March 2011.

Following acceptance of the survey by ESO, the detailed implementation plans, from target selection, through observing, data reduction, data analysis and science verification, to the expected survey products leading to a substantial public archive, were specified in a Survey Management Plan between ESO and the Co-Principal Investigators.

In the early stages of planning to ensure maximal value from the range of approaches involved, it was clear that a small number of critical issues needed to be addressed. This included from the astrophysical view adoption of an optimal single astrophysical line-list (Heiter et al. 2021), use of the (developing) Gaia Benchmark Stars as prime calibrators, dedicated data processing pipelines (UVES at Arcetri, GIRAFFE at Cambridge) and data archives, and efficient and effective ways to move spectra and derived parameters to and from the analysis teams and homogenisation Working Groups. For this last activity adopting a FITS structure for all files proved very beneficial. Regular specialist and team-wide meetings facilitated the smooth operation of this whole process. The rest of this section describes the implemented structure in more detail.

4.2. Project organisation

An overview of the Gaia-ESO Survey data flow process is presented in Fig 5. The tasks are distributed among 19 Working Groups (WGs), WG0 to WG18, each of which has a coordinator - see Table 3, and an active membership.

The tasks of the Working Groups are to implement the data flow, from target selection and characterisation, through preparation of the ESO OB observing files, observing, pipeline data processing, detailed spectrum analyses, astrophysical parameter quality/sanity checking and homogenisation, to science quality control, through to preparation, documentation and delivery of external data products to both ESO and a dedicated public archive.

In addition to the Working Group leads, a significant number of individuals have provided exceptional efforts to deliver the Gaia-ESO Survey, they are listed in Table 4. These have been credited by identification as "Builders", a recognition which provides co-authorship rights on survey papers. Among their duties has been to provide internal refereeing of survey papers prior to their journal submission.

The two Co-PIs, Gerry Gilmore & Sofia Randich, led the survey jointly, with Gilmore being specifically responsible for the field star and calibration efforts, and Randich for the open cluster work. Both were assisted and supported by a dedicated Project Office team listed in Table 5, whose work was critical to successful delivery of the final survey products. In addition, survey-wide and management issues were supported by and overseen by a Steering Group (Table 6) of senior scientists representing the broad range of Institutes and subjects involved in the survey.

5. Gaia-ESO Survey observational strategy

The Gaia-ESO Survey observing strategy has been designed to deliver the top-level survey goals. The observations include Milky Way (MW) field observations, Open Cluster observations, and calibration observations of different targets, such as radial velocity standard stars, benchmark stars, globular clusters, CoRoT red giants and Kepler K2 red giants.

The Gaia-ESO Survey observations were performed with the multi-object optical spectrograph FLAMES mounted on UT2 at the VLT (Pasquini et al. 2002). FLAMES is a multi-object system, feeding an intermediate (GIRAFFE) and a high resolution (UVES) spectrograph with a field of view 25 arcmin in diameter.

The choice of setups and integration times were optimised through extensive simulations and tradeoffs for the field stars, while previous observational experience dictated the open cluster settings and requirements. The field star simulations were led by Vanessa Hill, and proved to be reliable and accurate by the survey observational results. The essential decision was that, given that the amount of observing time per star was fixed by the

Fig. 5: A science data processing perspective of the Gaia-ESO Survey structure. The small purple ovals identify the 26 processing and analysis nodes which are described in later sections of this paper.

Table 3: Gaia-ESO Survey Working Group organisational structure

Working Group	Task	Coordinator(s)	Reference article
WG 0	Paranal Observing Team	Thomas Bensby	this paper
WG 1	Cluster Membership Analysis	Emilio Alfaro	Bragaglia et al. (2022)
WG 2	Auxiliary Data for Cluster Target Selection	merged with WGs 1 & 4	
WG 3	Galactic Field and Plane Target Selection	Carine Babusiaux, Sergey Koposov	this paper
WG 4	Cluster Stars Target Selection	Angela Bragaglia	Bragaglia et al. (2022)
WG 5	Calibrators & Standards	Elena Pancino	Pancino et al. (2017a)
WG 6a	OB/fposs generation [Field]	Thomas Bensby	this paper
WG 6b	OB/fposs generation [clusters]	Ettore Flaccomio	Bragaglia et al. (2022)
WG 7a	Raw Data Pipelines: GIRAFFE	Jim Lewis, Mike Irwin	this paper
WG 7b	Raw Data Pipelines: UVES	Germano Sacco	Sacco et al. (2014)
WG 8a	Radial Velocities: GIRAFFE	Sergey Koposov, Rob Jeffries	this paper; Jackson et al. (2015)
WG 8b	Radial Velocities: UVES	Germano Sacco	Sacco et al. (2014)
WG 9	Discrete Classification	Sergey Koposov	this paper
WG 10	GIRAFFE FGK-star Analyses	Clare Worley; Carlos Allende-Prieto	Worley & et al. (2022)
WG10	WG 10 - initial team	Alejandra Recio-Blanco	Recio-Blanco et al. (2014)
WG 11	UVES FGK-star Analyses	Rodolfo Smiljanic; Andreas Korn	Smiljanic et al. (2014)
WG 12	PMS-Star Spectrum Analyses	Alessandro Lanzafame	Lanzafame et al. (2015)
WG 13	OBA-Star Spectrum Analyses	Ronny Blomme	Blomme et al. (2022)
WG 14	Non-standard Objects, Dictionary	Sophie Van Eck, Tomaz Zwitter	Van Eck & et al. (2022)
WG 15	Survey Parameter Homogenisation	Patrick Francois	Hourihane & et al, (2022)
WG 16	Survey Progress Monitoring	Gerry Gilmore & Sofia Randich	this paper & Randich et al. (2022)
WG 17	CASU Operational Datacentre	CASU/Mike Irwin	this paper
WG 18	Survey Internal Archive	WFAU/Nigel Hambly	this paper

requirement to observe 10^5 stars, and the amount of survey observing time ESO was making available, field star observations were optimised by two equal-length observations, one HR10, one HR21. This maximised the number of stars for which element abundance ratio data could be derived. This observing approach was planned to deliver median signal-to-noise ratio per

Table 4: Gaia-ESO Survey Builders

Name	Name	Name	Name
	G Gilmore	S Randich	
M Asplund	J Binney	P Bonifacio	J Drew
S Feltzing	A Ferguson	R Jeffries	G Micela
I Negueruela	T Prusti	H-W Rix	A Vallenari
E Alfaro	C Allende Prieto	C Babusiaux	T Bensby
R Blomme	A Bragaglia	E Flaccomio	P Francois
N Hambly	M Irwin	S Koposov	A Korn
A Lanzafame	E Pancino	A Recio-Blanco	R Smiljanic
S Van Eck	N Walton	A Bayo	M Bergemann
K Biazzo	G Carraro	A Casey	M Costado
F Damiani	B Edvardsson	E Franciosini	A Frasca
A Gonneau	U Heiter	V Hill	A Hourihane
R Jackson	P Jofré	C Lardo	P de Laverny
J Lewis	K Lind	L Magrini	G Marconi
C Martayan	T Masseron	L Monaco	L Morbidelli
L Prisinzano	G Sacco	L Sbordone	S Sousa
C Worley	S Zaggia	T Zwitter	

Table 5: Gaia-ESO Survey Project Office Team

	Institute
Anais Gonneau	Cambridge
Anna Hourihane	Cambridge
Germano Sacco	Arcetri
Clare Worley	Cambridge

Table 6: Gaia-ESO Survey steering group

Name	Function	Affiliation	Country
Gerry Gilmore	Co-PI	Institute of Astronomy	UK
Sofia Randich	Co-PI	INAF Obs Arcetri	I
Martin Asplund	Steering Group	ANU/MPA	Aus/D
James Binney	Steering Group	Oxford	UK
Piercarlo Bonifacio	Steering Group	Paris	Fr
Janet Drew	Steering Group	Hertfordshire/UCL	UK
Sofia Feltzing	Steering Group	Lund	Se
Annette Ferguson	Steering Group	Edinburgh	UK
Rob Jeffries	Steering Group	Keele	UK
Giusi Micela	Steering Group	Palermo	I
Ignacio Negueruela	Steering Group	Alicante	Sp
Timo Prusti	Steering Group	ESA	ESA
Hans-Walter Rix	Steering Group	MPIA	D
Antonella Vallenari	Steering Group	Padova	I

pixel (SNR) spectra of 25 in HR21 and 10 in HR10, given system performance and the apparent brightness distribution of the targets. For the field-star UVES parallel sample the comparable SNR target was 40. In the event these requirements were delivered. Table 1 and section 2 in Randich et al. (2022) provide a detailed discussion of delivered system performance, which closely matched expectation. The field star observational approach was therefore not changed during the survey.

Considerable experience with the VLT system was available for the open cluster aspects of the survey. There median SNR targets ranging from 30 to 75 were planned for the various GIRAFFE settings, and 75 to 150 for UVES. Corresponding exposure times were of course target specific, depending on age, distance and extinction. In some cases for open cluster targets more pointings were required to cover the whole cluster area and complete membership candidates, slightly reducing the initially planned number of cluster targets with the reward of higher quality results. A full discussion of the overall survey delivered performance, with additional focus on the open cluster science is available in Randich et al. (2022) Observations were restricted

Table 7: Properties of the GIRAFFE setup modes that are used in the Gaia-ESO Survey. Resolution improved in February 2015 following refocus efforts.

Setup	central wavelength (nm)	wavelength range (nm)	resolution < 02-2015	resolution >02-2015
HR3	412.4	403-420	24800	31400
HR4	429.7	419-439	20350	24000
HR5A	447.1	434-458	18470	20250
HR5B	446.4	437-455	26000	archive
HR6	465.6	453-475	20350	24300
HR9B	525.8	514-535	25900	31750
HR10	548.8	533-561	19800	21500
HR14A	651.5	630-669	17740	18000
HR14B	650.5	638-663	28800	archive
HR15N	665.0	644-682	17000	19200
HR21	875.7	848-898	16200	18000

Table 8: Properties of the UVES setup modes that are used in the Gaia-ESO Survey

Setup	central wavelength (nm)	wavelength range (nm)	resolution
U520	519	414-621	47000
U580	580	476-684	47000

to $+10^\circ \geq$ DEC $\geq -60^\circ$ whenever possible to minimise airmass effects.

The observing strategy for the Gaia-ESO Survey was tailored to match the requirements of the individual populations being observed. Table 7 shows the GIRAFFE setups employed in Gaia-ESO Survey observations, their wavelength coverage and their resolutions. Table 8 presents comparable data for UVES. Table 9 describes the stellar populations observed and enumerates the GIRAFFE setups employed. Calibration and standard stars were observed in all the setups listed in the two tables.

Observation blocks were implemented in a manner which splits a single observation into two equal length exposures. This aids in the detection of transient features such as cosmic rays. For most observing modes a much shorter exposure is inserted with the simultaneous calibration ("simcal") arc lamp switched on. This allows for the wavelength zeropoint drift to be monitored over the course of the night. One observing mode (HR21) does not use simcal observations as there are a number of very bright arc lines in that wavelength region which saturate even in short exposures. For this one mode wavelength drift can be monitored using the night sky lines.

6. Target selection and observations [WG0-WG6]

The survey includes the Galactic inner and outer bulge, inner and outer thick and thin discs, the halo and known halo streams. There is special focus on open clusters at all ages, and on solar neighbourhood field stars, as these trace both stellar and Galactic evolution, complement Gaia astrometry, and will benefit most from the most precise Gaia data. The sky coverage achieved is shown in Fig 6.

Table 9: GIRAFFE modes used for each project within the Gaia-ESO Survey

Survey Area	Typical magnitudes	GIRAFFE setups used
Bulge	$I = 15$	HR10,21
Halo/Thick Disc	$15 \leq r \leq 18$	HR10,21
Outer thick disc	$r \leq 18$	HR10,21
Open clusters (early type)	$I \leq 19$	HR3,4,5A,6,14A
Open clusters (late type)	$I \leq 19$	HR15N
Calibrator clusters	various	all modes
Benchmark Stars	$I \leq 15$	all modes
Radial Velocity standards	various	all modes

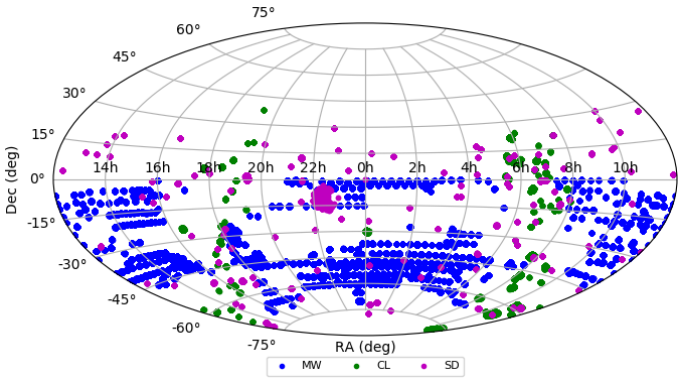

Fig. 6: The sky distribution of Gaia-ESO Survey observed fields for all observations broken down by field-type: Milky Way fields (MW), clusters (CL), standards and calibration fields (SD). The clump of SD fields around 22h, -10 deg includes the Kepler K2 red giants introduced as standards in July 2016.

Open clusters. Cluster selection is optimised to fine-sample the age-[Fe/H]-radial distance-mass parameter space. Open clusters in all phases of evolution (except embedded), from $\sim 10^6$ Myr up to $\sim$ 8 Gyr are included, sampling different environments and star formation conditions. For all clusters we use GIRAFFE to target faint cluster members (down to V= 19), while UVES fibers are fed with brighter or key objects (down to V= 16.5), to be used for accurate abundance determination or for which better precision in RV is required. The several GIRAFFE set-ups employed are listed in Table 9. Setups HR03/04/05A/06/14A contain a large number of spectral features used to derive RVs and astrophysical characteristics (e.g., temperature, gravity, wind) of early-type stars; HR15N is instead the most commonly used grating for late-type stars; this accesses a large enough number of lines to derive RVs, as well as to retrieve key information on the star characteristics (e.g., temperature, Li, accretion rates, chromospheric activity, rotation). For UVES, CD3 is most suitable both for early-type (520 nm setting) stars and late-type members (580 nm setting). Cluster FPOSS configurations are typically observed at least twice to identify binaries.

Bulge survey. Here the prime targets are K giants, including the red clump (I = 15 typically). These dominate the relevant CMD selection. Two GIRAFFE settings are needed (HR21, HR10), implying up to 4H/fibre setup, depending on the field and the extinction. This measures Mg, Ca, Ti for most stars, and Si, Cr, Mn, and Ni for many stars. The bulge RGB is clearly visible in CMDs at $b \leq 45°$, so this survey extends that far. In low extinction regions, brighter gK stars can be observed with UVES 580-nm parallels to sample both bulge and inner Galaxy populations. In the event scheduling limitations (the focus on the VLTI SgrA* science, and overrides to implement spectroscopy of micro-lensed bulge dwarfs) reduced the available effort on the inner Galaxy and Bulge.

Halo/thick disc survey. Primary targets are r=17-18 F+G stars, with the bluer, fainter F stars probing the halo, brighter, redder F/G stars probing the thick disc. SDSS analyses show a clear thick disc/halo transition in the range $17 \leq r \leq 18$. The spectra allow measurement of both iron-peak elements and alpha elements, for stars down to [M/H]≤ -1.0. In fields crossing known halo streams (eg Sgr), stream K giant candidates are also observed. A subset of fibres was allocated to specially selected candidate members of rare but astrophysically important stellar populations, such as extremely metal poor stars. The fields are distributed in the whole sky, but predominately in the Galactic cap (SGC, NGC) and bulge regions. This minimises scheduling clashes with the cluster targets, and ensures southern and northern fields for scheduling, and photometric overlap with SDSS, PS1, and ESO/VST.

Outer thick/thin disc, 2-4 kpc from the Sun. These fields have distant F/G stars as prime targets, and 2 settings, as for the halo in both requirements and measurables. This well-defined low latitude sample probes 2-4 kpc, more than a radial scale length. In addition, 25% of the fibres are allocated to candidate K giants (r$\leq$ 18), which probe the far outer disc, warp, flare and Monoceros stream.

Solar Neighbourhood. UVES parallels for the field surveys are dedicated to an unbiased sample of order 5000 G-stars extending $\geq$ 1 kpc from the Sun, to quantify the local detailed elemental abundance distribution functions. The sample is photometrically-selected to ensure all possible ages and metallicities for unevolved stars and subgiants are sampled. UVES 580-nm setting is adopted. These are parallel observations, requiring no dedicated time.

6.1. Observational Working Group activities: WG0 to WG6

In these sections we provide a brief summary of the efforts required to obtain observations at the VLT. These efforts include target identification and selection, creation of the ESO Observing system OB and FPOSS files, which control the observations and the fibre allocations respectively, and operation of the VLT and data quality real-time checking during observations. These processes were required for the three main target classes: field stars, cluster stars, and calibrator and standard stars.

6.2. WG0 - Paranal observing team

The Working Group 0 Coordinator was Thomas Bensby. In addition to coordinating the observing team, and carrying out many runs, he checked all necessary observing files prior to each run, and ensured suitable records were available to optimise completion of sets of observations.

Observations for the Gaia-ESO Survey took place during 59 scheduled observing runs in the period 31.12.2011-26.01.2018. The observers were drawn (largely) from a small experienced team, Table 10, including ESO Support astronomers when they were available. This minimised needless travel and ensured fully experienced and efficient observers were available.

Table 10: The core Paranal Observing Team.

Observer	Institute
T. Bensby	Lund Observatory
A. Bayo	Universidad de Valparaiso
G. Carraro	Universita' di Padova
G. Marconi	ESO
C. Martayan	ESO
L. Monaco	Universidad Andres Bello
L. Sbordone	ESO
S. Zaggia	Osservatorio Astronomico di Padova

A report on the observing outcomes, including sky conditions, is included in Randich et al. (2022).

6.3. WG3, WG6a - Field star target selection and observation preparation

Field star target selection was initially defined by Carine Babusiaux and Gerry Gilmore, with the regular target files creation being done by Sergey Koposov. The selection function for the Gaia-ESO Survey field star observations is described in additional detail in Stonkutė et al. (2016). We provide an overview here.

Field stars were primarily selected for observation with GIRAFFE from (J, H, K_s) VISTA imaging, using the photometry derived by the Vista Hemisphere Survey (VHS; (McMahon et al. 2013)), ensuring excellent recent astrometry, and thus further increasing the value of the ESO VISTA surveys. For the brighter UVES parallel sample, 2MASS (Skrutskie et al. 2006) was used. The VHS near-IR photometry was chosen because there was, at the time, no publically available recent optical photometry covering a sufficiently wide sky area to ensure targets could be prepared with reliable astrometry and photometry. Reliable close-epoch astrometry was a critical requirement given that the observations were through relatively small fibres, so that the brighter acquisition and guide stars must be on the same astrometric system as the fainter target stars, with proper motions either known, or irrelevant through epoch matching. To ensure that the JHK selection matched the halo-thick disc division apparent from SDSS optical photometry, fields with both SDSS and VHS photometry were used to define the actual selection, as illustrated in Fig 7.

The primary GIRAFFE targets are r=17-18 F+G stars, with the bluer, fainter F stars probing the halo, brighter, redder F/G stars probing the thick disc. SDSS analyses show a clear thick disc/halo transition in the range $17 \leq r \leq 18$ – Gaia-ESO uses the equivalent selection from VISTA JHK photometry, as illustrated in Fig 7 and Fig 8.

The main GIRAFFE target selection selecting these is made from stars with

$$0.00 \leq (J - K_s) \leq 0.45; 14.0 \leq J \leq 17.5.$$

This selection is complemented with candidate red-clump giants from the same population, which are selected in

$$0.40 \leq (J - K_s) \leq 0.70; 12.5 \leq J \leq 15.0.$$

Stars are selected with an equal number per magnitude and per 0.1mag colour bin in these ranges, as illustrated in Fig 8. Additional targets are selected in same CMD-selection to allow for fibre-positioner limits on target acquisition.

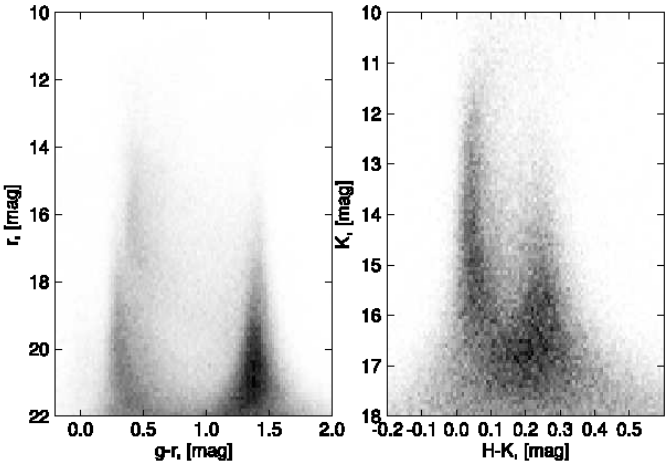

Fig. 7: LHS: SDSS high-latitude photometry illustrating the two blue-star populations, $0.3 \leq (g - r) \leq 0.6$. The bluer, becoming dominant at fainter magnitudes, is the halo. The less blue, becoming less dominant at $r \sim 17$, is the thick disc. RHS: the same stars observed in VHS [K_s, H-K_s] photometry, which is the source of photometry applied by Gaia-ESO.

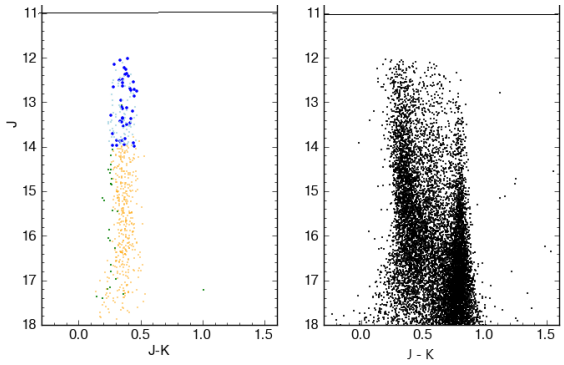

Fig. 8: Target selection for the field-star survey. The left colour-magnitude diagram shows the selected stars for both GIRAFFE and UVES, the right CMD shows the parent sample in that field from which the targets are selected. The larger blue points brighter than J=14 are the primary UVES target. Fainter yellow points are the primary GIRAFFE targets

.

In parallel UVES fibres are dedicated to a special selection. These field-star UVES parallel targets are chosen according to their near-infrared colors to be FG-dwarfs/turn-off stars with magnitudes down to J = 14 mag. The goal was to observe a sample of approximately 5000 FG-type stars within 2 kpc of the Sun to derive the detailed kinematic-multi-element distribution function of the solar neighborhood. This sample includes mainly thin and thick disc stars, with a sufficiently broad colour selection to include stars of all ages and metallicities, including also a small fraction of local halo stars. For these targets the VHS photometry is saturated, so 2MASS is used. The target selection is based on 2MASS photometry (point sources with quality flags "AAA"). The CMD box is defined by $12 \leq J \leq 14$ and $0.23 \leq (J - K) \leq (0.45 + 0.5 \times E(B - V))$, the Schlegel et al.

(1998) map being used to determine the extinction E(B-V). The targets selected before April 2012 had a brightest cut on J of 11 instead of 12 . When there were not enough targets the red edge was extended. When there were too many potential targets an algorithm selected roughly an equal number of stars per magnitude bin with the rest being marked as lower priority. Further illustration of the field star target selection, including more discussion of higher density and higher extinction fields is available in Stonkutė et al. (2016).

6.4. WG1, WG4, WG6b - open cluster star target selection and observation preparation

The considerable work on open cluster star selection was coordinated by Angela Bragaglia, and described in Bragaglia et al., in prep.

The open cluster survey has the very ambitious aim to cover the age-metallicity-distance-mass parameter space which is realistically available observationally. Depending on the stellar spectral type, open cluster stars are observed with different GIRAFFE setups and two UVES settings. For the hot/massive stars, the GIRAFFE setups HR3, HR4 (introduced only in 2016), HR5A, HR6, HR9B, and HR14N are employed, while HR15N is used for cool stars on the main sequence, pre-main sequence, and giant candidates. The corresponding choices for UVES are the U520 and U580 setups. The final data release includes spectra, radial velocities, rotational velocities, stellar parameters, metallicity, and detailed abundances for 62[2] open clusters observed by Gaia-ESO (plus approximately 20 clusters reanalysed from the ESO SAF).

The open clusters show a large variety of cluster ages, evolutionary phases, spectral types and luminosities, and the choice of instrument/setup needs to take this into account. For cool stars, normally the fainter cluster members ([pre-]main sequence or turn-off stars) are observed using GIRAFFE HR15N (sometimes HR09B for turn-off stars), while for the brighter stars (typically evolved giants or bright [pre-]main sequence cluster candidates) UVES parallels are employed (with the U580 setup). Limiting magnitudes for cool stars (later than A-type) are V=16.5 and V=19 mag for UVES and GIRAFFE respectively. Different magnitude ranges are covered in clusters where hot stars are observed with the blue gratings. An overlap in magnitude between the GIRAFFE and UVES samples is present normally and a number of stars are observed with both instruments for inter-calibration purposes. For more details, see Bragaglia et al. (2022).

Within each cluster, the target selection procedure was implemented differently between GIRAFFE and UVES, but uniformly across clusters. Namely, for GIRAFFE, with which we aim to observe unbiased and inclusive samples, cluster candidates are essentially selected on the basis of photometry. We used proper motions and radial velocities and other membership indicators (like e.g., X-ray emission) only to define the photometric sequences and the spatial extent of the clusters. In other words, we employed existing information on membership only to discard secure non-members, lying far from the cluster sequences. For UVES, with which we aim to target more secure cluster members, we instead employed membership information from the literature (e.g. v_{rad}, Li abundance, Hα), whenever available. More details on the target selection within clusters and preparation of the OBs can be found in Bragaglia et al. (2022).

[2] One cluster is actually double, NGC 2451A and NGC 2451B; one candidate, Loden 165, turned out not to be a cluster after all.

6.5. WG5 - Calibration and standard star target selection and observation preparation

The Gaia-ESO Survey primary calibration strategy, based on targeted observations of globular clusters, open clusters, and field stars, was coordinated by Elena Pancino, and is described more fully in Pancino et al. (2017a).

Gaia-ESO dedicated considerable effort to define calibration stars - clusters, special fields, CoRoT and Kepler-K2 fields, stars which are Gaia calibrators, etc, to ensure Gaia-ESO is optimally calibrated, and that other major surveys can be calibrated onto compatible parameter scales. We recall that a primary goal of Gaia-ESO is to ensure all stellar populations, from young to old, hot to cool, metal-rich to metal-poor, are on as consistent a calibrated scale as is feasible. This of course imposes severe challenges on the calibration strategy. In addition, especially for field stars where only a single star could be observed by the full fibre system, there is obvious pressure to identify bright targets, so that twilight observations could be used as much as possible.

The survey team also analysed the ESO SAF for abundance calibrations, and complementary data. The large-scale (AMBRE-Worley et al. (2016a)) re-reduction of the ESO SAF is being done consistently with the Gaia-ESO Survey, to ensure maximum value. Relevant archive data, specifically high signal-noise ratio observations with the Gaia-ESO setups of targets consistent with the Gaia-ESO selection, were re-analysed as part of this survey, to ensure maximum consistency across all datasets. Open cluster selection is based on a critical analysis of available data in the archive, in order not to re-observe cluster members for which spectra with the required set-up and signal-noise ratio are already available. Calibration targets were deliberately selected to optimise the archive value, by allowing available spectra to be re-calibrated onto our abundance system.

The Standard cluster fields included in the survey, with spectra released as part of the public data release, are: calibration observations of stars in the globular clusters M12, M15, M2, NGC104, NGC1261, NGC1851, NGC1904, NGC2808, NGC362, NGC4372, NGC4590, NGC4833, NGC5927 and NGC6752 which meet our data quality selection threshold for inclusion; and calibrating open clusters observed in a range of setups to aid in inter-setup calibration (Berkeley 32, M67, Melotte 71, NGC2243, NGC2420, NGC2477, NGC3532, NGC6253, NGC6553).

In addition, much work was devoted to observing and improving the parameters of the Gaia Benchmark stars. The Gaia Benchmarks are a much broader project to support Gaia, but which also provides a set of primary calibrators adopted and extended by Gaia-ESO. The project is intended to provide a global set of well-understood standards of value to all spectroscopic surveys (Jofré et al. 2017a).

To add further calibration weight, with specific ambition to ensure the asteroseismic and spectroscopic $\log g$ scales are consistent, and also to include age calibration, special efforts in the calibration programme were focussed on stars observed by CoRoT ((Masseron & et al. 2022) and as part of the Kepler K2 mission (Worley et al. 2020).

7. GIRAFFE data reduction pipeline [WG7]

Gaia-ESO uses two spectrographs, both fed by the FLAMES fibre system. The higher resolution UVES data (table 8) are processed at Arcetri observatory by a team lead by Germano Sacco (WG7b). Their processing pipeline is based on the pipeline provided by ESO, and improved for this survey. This work is described in full in Sacco et al. (2014).

The remainder of this section describes the GIRAFFE processing pipeline. This was developed by the late Jim Lewis of the Cambridge Astronomical Survey Unit (CASU). This processing system is the basis for that to be implemented for the future WEAVE and 4MOST survey facilities. This text description is lightly edited from Jim's final description of this one of his many and much valued contributions to astronomy surveys. It provides an experienced perspective and a valuable introduction to the challenges in pipeline processing surveys with a very wide range of stellar astrophysical parameters. The logical flow is summarised in Fig 9.

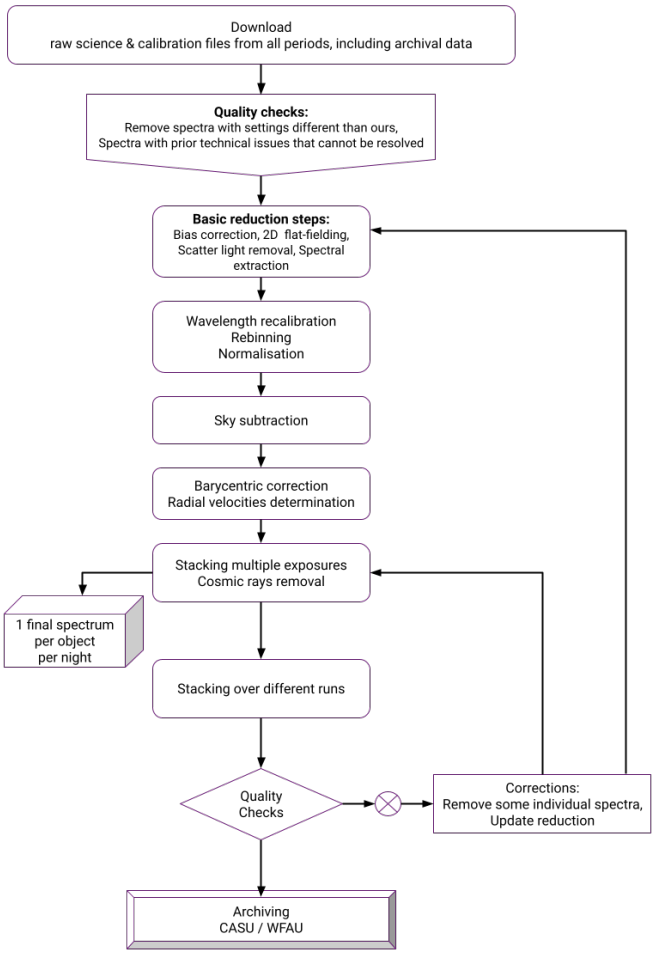

Fig. 9: Flowchart of the reduction processes for the GIRAFFE spectra.

Fig 10 shows some example spectra from several of the GIRAFFE setups.

Reduction of GIRAFFE spectra involves the following steps:

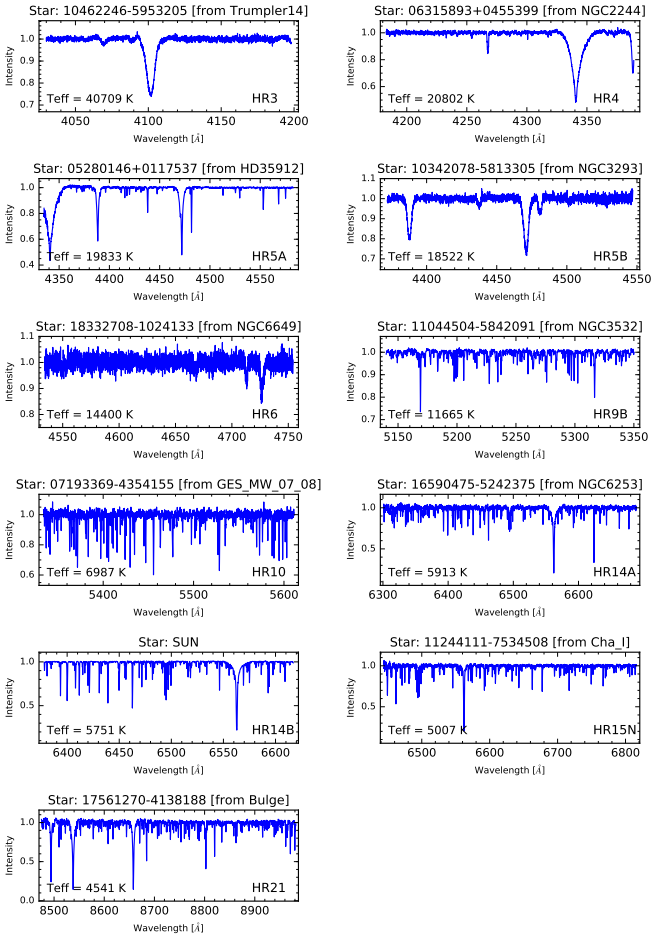

Fig. 10: Example spectra from several GIRAFFE setups.

- Default basic processing, including bias subtraction; cross-talk and scattered light removal; bad pixel masking; flat-fielding; wavelength calibration; extraction.
- Wavelength recalibration of each extracted spectrum using sky emission lines, for red wavelength settings, or almost-simultaneous short simcal observations for the bluer settings.
- Combining sky fibres for the determination of the master sky spectrum for each integration and subtracting (master or local, as scientifically appropriate) from individual extracted objects.
- Combining the individual integrations into co-added spectra, after measuring the RV, checking for binarity, and velocity shifting to the heliocentric frame. Co-added spectra are used then to reject cosmic rays from individual spectra.

7.1. Bias correction

The bias for a given row in the detector is determined from the mean of the same row in the detector underscan region. At this point the input data are integers and hence a clipped mean is used rather than the median in order to avoid quantisation of the bias estimate at the 1 ADU level.

7.2. 2-D flat field

Flat field correction is done for a number of reasons. First of all it removes the inter-pixel quantum efficiency variations in the detector. It is also useful for taking out the large scale background variations that arise due to the camera optics. For the latter it is common to do dome flat observations with the same grating, filter and fibre module as the science exposure. The flat field spectra can be extracted in the same way as the science spectra and then divided into the science spectra. This should result in an object spectrum with a background shape that is much closer to the true continuum of the object. However as 1d spectra are the result of a summation across the point-spread function of the fibre, any information on the quantum efficiency variation of the individual pixels is lost. What is needed are dome flat exposures that are taken with the grating and filter set as for the science observations but without the fibre module. This would help ensure uniform illumination of the entire detector, including the inter-fibre regions where the scattered light contribution is estimated. This is common practice with longslit spectroscopic observations.

Unfortunately this sort of longslit flat field is not something that is done with GIRAFFE and it appears not to be possible. There is a maintenance slit in GIRAFFE that is used to do instrumental health-check exposures and dome flat sequences are often done as part of a rolling program of maintenance observations. These, however are not dispersed, nor are they filtered and, as flat fields are wavelength dependent, will not be a very accurate model of the inter-pixel sensitivity variation in a science observation for a given wavelength setup. Nevertheless, applying these flats to the science data delivers a very evident reduction in noise. Tests have also shown that these dome flats are quite stable over the course of several months. With that in mind it was decided to apply these flats to the science and calibration observations before extraction.

7.3. Spectral extraction and 1-D flat field

The spectra are extracted using the optimal extraction method outlined in Marsh (1989) which is designed to work on 2d spectral profiles that are highly curved. The extraction profiles are fitted to dome flat exposures that are done during the daytime using the same grating angle and filter setup as the science exposures done the previous night. During the fitting procedure the contribution of scattered light is estimated from the inter-fibre regions and subtracted off at each point in the raw fibre data.

The dome-flat spectra are extracted using the fitted extraction profiles. The average flux in all of the extracted dome flat spectra in a given exposure is calculated and then each of the flat spectra is divided by this average. This ensures that the differences in fibre throughput are corrected.

Science spectra are extracted using profiles that are appropriate for the GIRAFFE setup used in the observations. The 1d flat field is then used to do the large scale continuum and fibre throughput correction mentioned above.

7.4. Wavelength solution and corrections

The wavelength solution for a given grating/filter setup is tied to Thorium-Argon exposures done during the day. The solution for each spectrum is determined independently through identification of arc lines and doing a standard polynomial fit to the pixel positions and wavelengths.

The wavelength solutions are quite stable, but some drift in the zero point does exist. To measure this we use the aforementioned simcal observations for most of the setups employed. Simcal observations consist of five fibres which are illuminated by the arc lamp and located roughly uniformly across the detector. The arc lines are identified exactly the same way as for the arc exposures and a mean shift is calculated from the change in pixel positions of the arc lines between the two exposures for those fibres. The correction for a spectrum is done as an interpolation of the simcal shifts for the nearest two simcal fibres.

For the HR21 setup where we do not use the simcal arcs, it is possible to monitor the wavelength drift by using the night sky lines that exist in the individual science spectra. These can be identified in the extracted spectra and the inferred wavelength from the standard solution can be compared with a set of known sky line wavelengths to measure the drift.

7.5. Rebinning

All spectra for a given setup are rebinned using a linear interpolation onto a common wavelength scale with common endpoints. In doing the rebinning we take into account the wavelength solution found from the arc exposures, the wavelength solution corrections found from either simcal or skyline offset measurements and the heliocentric correction for each object. This results in spectra on a uniform linear wavelength grid with 0.05Å pixels, centred on the heliocentric system. Thus the spectra have only been interpolated once, which minimises the correlation between adjacent pixels.

7.6. Normalisation

Within the analysis groups of the Gaia-ESO Survey there was a desire to have spectra normalised such that the continuum shape was completely removed. This is not something that can be done in a general way with the Gaia-ESO Survey as there is such a large variety of stellar types in the samples. The pipeline produces a normalised spectrum using a sliding window filter to model out the continuum. The results are reasonably good and are certainly sufficient for the purpose of measuring cross correlated velocities. However serious analysis that requires a normalised spectrum should include a normalisation procedure that is optimised for the type of star being investigated. Results from the specialised working group analyses produce results very different from the pipeline outcomes for stars with non-typical properties. These include common types, OBA stars and young pre-main sequence stars, where considerable specialist processing is critical for reliable analyses.

7.7. Sky subtraction

All spectra need to have a background (sky) correction applied. What can be difficult is determining exactly how much to subtract off. The OBs for the Gaia-ESO Survey are designed so that there are between 10-20 sky fibres per field and of course these are observed simultaneously with the science objects. What one gets in each fibre can depend on spatial variations in the night sky as well as the presence of real astronomical background (e.g. emission nebulosity). The Gaia-ESO Survey spectra are taken in

a variety of astronomical environments and hence working out a general solution to the background subtraction is not a straightforward problem. In practise we combine all the sky fibres in a given exposure into a single high signal master sky spectrum. If the observation is done in a wavelength region where there are many sky lines, then for each science spectrum a scale factor is calculated, which is applied to the master sky before it is subtracted from the science spectrum. This scaling only applies to the HR21 setup. In setups with wavelength regions without sky emission lines, this scale factor is assumed to be one.

There is a need to provide for cases where there is a strong variation in the astronomical environment of the stars being observed. This is often the case when observing in active star forming regions. To this end more complex sky subtraction algorithms are required.

7.8. Sky background estimation

It is not obvious that there is a single "best" way to correct Gaia-ESO Survey spectra for background emission. The idea in a nutshell is to form an estimate of the background emission from both astronomical and atmospheric sources that is affecting the spectrum of a science object. This estimated background spectrum can then be subtracted on a pixel by pixel basis from the input science spectrum to give an output spectrum that consists of emission from the object alone. Unfortunately getting enough information to form that estimated background spectrum can in some cases be extremely difficult and it might well be that obtaining a result in which one can have full confidence is impossible.

When assessing the best way to remove background emission from Gaia-ESO Survey spectra, it is important to understand the nature and origin of the features in any background spectrum. If we look at a Gaia-ESO Survey spectrum that has not yet been background corrected, but which is on a linear wavelength scale and not corrected to heliocentric, that spectrum will consist of contributions from the following sources:

- The object spectrum – all features and continuum are shifted by the star's line-of-sight velocity combined with its heliocentric correction.
- Unresolved stellar light – this is generally quite small (unless we are observing in high density regions such as the galactic centre) and will mainly consist of continuum emission. Any such light will be redshifted to a variety of velocities, and this may result in very broad features.
- Emission lines from a surrounding nebular component – these features originate in HII regions and the like. They will be shifted by the recessional velocity of the emitting gas and the heliocentric motion. Furthermore these features may be broadened and skewed by local internal kinematics.
- Emission lines, absorption (telluric) lines and continuum originating in the earth's atmosphere – these features are in the earth's rest frame.
- Solar light – residual solar light comes from moon light and the zodiacal light and broadly speaking will be in the solar system rest frame.

The method used to sample the background emission is to assign a number of fibres to (what appear to be) background positions. These are spread around the field in order to give as broad a sample as possible of the background conditions in the area. Correcting the background can be done in several ways. Some possibilities are:

- 1) Create an average background spectrum from all of the background spectra in a given observation. Subtract this from each object. This is a 'vanilla' correction. This is what must be done in the absence of any sort of prominent atmospheric emission features in the wavelength region. Without such features it is impossible to to say with any certainty whether the amount of continuum emission being subtracted is correct.
- 2) Create an average background spectrum from all of the background spectra in a given observation. Use prominent emission features to work out a scaling factor between this mean spectrum and the object spectrum you wish to correct. Then scale the mean background spectrum and subtract it from the object spectrum. Note that this scale factor is not an attempt to correct for fibre throughput – that has been done at the flat-fielding stage. It is rather an attempt to model out the differences in the background emission across the field. The scaling is done so as to minimise the emission lines in the stellar spectrum.
- 3) Take one or more background spectra that lay in spatial proximity to an object and average these. If there are emission features, then scale the mean spectrum before subtracting. This is the method used if the background emission is varying rapidly in the spatial sense. In extreme cases one can allocate a dedicated background fibre for each object, but this has not been done for the Gaia-ESO Survey.
- 4) If emission lines exists and they are all atmospheric, then simply remove them by interpolating between two pixels on either side of each of the lines. Then remove a scaled amount of the continuum. Such regions are then flagged with a zero weight to help those fitting the spectra later on. If the emission is nebular, then this is probably not a good thing to do. Both the stars and the background may have the same emission lines and it's important to try and subtract out the correct amount of each. Also, the continuum emission and the nebular emission arise from completely different physical properties and to base the continuum estimation on the flux of the nebular lines risks getting the continuum subtraction badly wrong.

The problem becomes more interesting when the object spectrum that we want to recover has emission and absorption features of its own in common with the background (for example, Hα). That is now not a case of scaling the background spectrum so that we have no more emission features in the corrected spectrum (as with method number 2 above). We want to subtract just enough to remove the background contribution, but no more. If the background emission source is uniform and at exactly the same recessional velocity as the object, this can be achieved by averaging all the sky fibres. But this just simply does not happen in real star-forming systems. By and large there will be gradients in the velocity and in the flux of emission lines across the field. When this happens then averaging all the background fibres together to form a mean sky is clearly incorrect. This situation requires special consideration by users. An example applied to Gaia-ESO spectra of the young cluster γ Vel is given in Damiani et al. (2014a). Bonito et al. (2020) explore the issue of sky subtraction where nebular emission contributes to emission lines of interest for star forming regions, for NGC 2264 (Hα, and forbidden emission lines including [SII], [NII]).

A more complex but real-world scenario is where there are background spectra emission lines from both gas in the vicinity of the object and from the earth's atmosphere. The atmospheric lines in the background spectra will match in wavelength to those in the object spectra. But in general there will be a wavelength offset between the gas emission lines for a background spectrum and those in an uncorrected object spectrum as the fibres used for these spectra will sample the emitting gas in two separate places where the local kinematics may well differ.

7.9. Sky subtraction approach adopted for each GIRAFFE setup

7.9.1. HR5A, HR6 and HR9B

Background spectra for HR5A, HR6, and HR9B do not show any emission lines and they all show some of the characteristic absorption features of the solar spectrum. For GIRAFFE setups such as these with no emission lines, we have to employ option 1 outlined in the previous section. In general the continuum emission in the background spectra is small and a 10-20% error in the background correction does not make a great deal of difference in the final object spectrum (unless, of course, that object is very faint).

7.9.2. HR3 and HR4

Background spectra for HR3 and HR4 do have some background nebulosity and hence there is a small emission line at λ4101 which is Hδ. As this is a nebular line it would be wrong to scale the mean background to try and remove it. In the absence of this line a vanilla subtraction is all that can be done. Where the line exists then one can shift the mean sky spectrum so that the Hδ lines coincide and then do a vanilla subtraction.

7.9.3. HR10

In the HR10 (H548.8) setup there is a very strong emission in the form of the [OI] λ5577 atmospheric line, and also three weaker atmospheric OH lines. Although the intensity of 5577 in general varies across the field of view, the shape of the line and its central wavelength is reasonably stable (notwithstanding any changes in the line-spread function across the detector due to the camera optics). For that reason it is possible to use the intensity of this line to work out an individual scaling factor that can be applied to a mean background spectrum before subtracting it from each object spectrum. Because of the stability of this line's position and shape it corrects out reasonably well. Because the other lines are so weak by comparison, we do not include them in the scaling calculation.

Tests show that correction using the 'vanilla' method described above clearly overcorrects the sky subtraction. Correction by scaling to the line provides much better correction. The HR10 setup with good signal-noise allows application of method 4, which is simply to work out a scale factor which we use to correct the continuum and then just cut out the line residual. This provides a small cosmetic improvement over intensity-scaling.

7.9.4. HR21

In the HR21 (H875.7) setup there is a large number of atmospheric emission lines. These not only vary in intensity across the field, the intensity of the lines vary with respect to each other. The lines at λ8493 and λ8505 show definite changes in their flux ratios between the concurrently-observed spectra. This is a sky background spatial variation. This effect means that it might not always be possible to define a single scaling factor which will remove all of the lines equally well. Also as many of these lines are blends the intensity variation will alter their blended shapes across the field. This means that even if a scale factor that is consistent with all the line intensities can be defined, there may still be significant residual emission after background correction. Where appropriate residual line artefacts can be clipped from the spectra - the key result is that the weight map contains the relevant astrophysical information for later analysis.

7.9.5. HR14 & HR15N

The HR14 and HR15N setups have both a large number of atmospheric lines and (when observing young clusters) nebular lines. As mentioned before, this has the potential of causing a lot of trouble because the sets of lines are in two different velocity frames of reference. Any attempt to shift the mean background spectrum so that the positions of the nebular lines match will mean shifting the atmospheric lines out of coincidence.

Another problem with nebular lines in the background spectrum is that they will be affected by the internal kinematics of the emitting gas and this will vary across the field. As such if we seek to use a master sky which is a mean of all the sky spectra in an exposure, we will have mean line profiles that look nothing like the lines we want to correct.

There is a further issue here on the question of whether we should be scaling nebular lines to a mean background spectrum at all. The objects themselves may well have one or more of these lines and scaling a mean background so that nebular lines are removed is in essence forcing an astrophysical scenario where the objects cannot have emission lines. This is further complicated by the velocity offsets that may occur between the background and the object, for example a star with an expanding circumstellar shell. An example analysis of Gaia-ESO HR15N spectra for the young cluster γ Vel is given in Damiani et al. (2014a).

7.10. Outcome methods adopted

In what follows we summarise how the background subtraction algorithms were optimised for the final data releases.

- HR5A, HR6 and HR9B – We use the vanilla algorithm.
- HR3 – The Hδ line that sometimes appears is nebular in origin. If it does appear then the mean background spectrum can be shifted so that the lines coincide. Then a vanilla correction can be done. The continuum in most cases is mainly solar in origin and this has nothing to do with the physical process that gives rise to a nebular line. Scaling the spectrum to remove the line would probably cause an error in the amount of continuum to be removed. In the absence of the emission line, just subtract a mean background spectrum.
- HR10 – The λ5577 line is atmospheric in origin and hence it is safe to use it to work out a scale factor. The residual line itself is removed using the clipping method. The pixels where the line is removed are given a zero weight. The scale factor calculated from the line ratio can then be used to subtract out the correct amount of continuum.

– HR21 – All of the lines are atmospheric in origin, hence we treat this in the same manner as for HR10.

– HR14 and HR15 – These can have both atmospheric and nebular emission. In the case where no nebular emission is present, then we treat the spectra in the manner outlined for HR10. In the presence of emission lines we adopt a two-pass procedure. The first is to create a mean background spectrum with nebular lines that are clipped out. This is scaled by the atmospheric line ratios, which will correct the continuum. The atmospheric lines are then clipped out. Then a second background spectrum with no atmospheric lines and with a mean continuum of zero is shifted in wavelength space so that the nebular lines coincide. These are subtracted using a scale factor of 1. This method sometimes leaves ugly remnants in the spectra, because the line profile shapes are different. But this is a scientifically more valid way of dealing with the problem.

– If a science analysis is interested in the emission features of stars in the Gaia-ESO Survey it will be necessary to go back to the spectra that are not background corrected. Using multi-component fits and velocity information it may be possible to recover the true emission line that belongs to the stellar object. This however is not something that can be done in bulk in a data reduction pipeline.

7.11. Stack multiple exposures

The observations are generally broken up into at least two exposures. The rebinned and sky corrected spectra are coadded using the information in the variance spectra to form a final spectrum for each object for a given night. It is at this point that any artefacts such as cosmic rays are removed.

7.12. Cross-correlation velocities

The pipeline also does a simple cross correlation of each spectrum relative to a selection of model atmospheres. This gives a first pass estimate of the radial velocity, surface gravity, metallicity and effective surface temperature of each star. A much better estimate of these parameters is generated initially in the Radial Velocities WG (WG8 & WG9) and finally through the full spectroscopic analyses in the specific Working Groups. This sanity checks for variable radial velocity before co-adding.

7.13. Stacking over different runs

In order to achieve the desired signal to noise many stars are being observed over the course of several runs. The final spectra that are released to the analysis groups are those that have been coadded over all the observing runs that have been done, with in all cases check for radial velocity variability before addition. These final stacks are also cross-correlated as specified in section 7.12 to give initial estimates of velocity, surface gravity, effective temperature and metallicity.

8. Radial velocities [WG8] and first-pass classification [WG9]

8.1. GIRAFFE spectra

The work of WG8 and WG9 has been led, and largely implemented, by Sergey Koposov. The two WGs were in effect merged in to a single set of operations, as described below.

Koposov et al. (2015) introduces the Radial Velocity methodology, building on the earlier development of precise radial velocities from GIRAFFE spectra by Koposov et al. (2011) in studies of the internal kinematics of dSph galaxies. Jackson et al. (2015) investigates the delivered velocity precision as a function of stellar type, signal to noise ratio and observing setup. The maximum achieved precision is of the order of 0.25 km/s, matching the initial goal.

After pipeline processing to remove instrumental signatures, extracted individual GIRAFFE spectra with their variance spectra and quality control flags are available. Telluric lines, cosmic rays in cases of single exposures and known defects are masked. Astrophysical emission lines are detected and fitted, but not considered during the radial velocity processing. The method utilises the direct pixel-fitting process described by Koposov et al. (2011). This is not a cross-correlation method, which is known to be non-optimal, but proceeds by fitting observed data by model spectra derived from a spectral library. The essence is to ensure one is working with a minimally rebinned spectrum with reliable variance associated with each pixel. As described in Koposov et al. (2015), which this description follows, the Gaia-ESO spectra are rebinned by the pipeline, which generates correlated noise in the spectra. It is necessary to utilise appropriately the full covariance spectrum calculated during reduction, or an appropriate validated scaling of the errors. Each spectrum is then fitted by a suitable subset of a large spectral library. This provides a first-pass estimate of both the stellar parameters (T_{eff}, log g, [Fe/H], [α/H]) and the radial velocity.

For performance reasons, two iterations are repeated. First, to optimise the radial velocity, keeping the stellar astrophysical parameters fixed, followed by an iteration to optimise the stellar parameters while keeping the radial velocity fixed. We also iterate starting from random stellar parameters to reduce the likelihood of being trapped in a local minimum in the fitting surface. Where the signal-noise ratio is sufficiently high, the stellar Vsin$i$ is also fitted.

Given these initial estimates, the next step is to adopt a Gaia-ESO optimised grid of model spectra. The Gaia-ESO model grid was calculated for the survey using the same methodology as that for the AMBRE project, which is described by de Laverny et al. (2012). This is a high-resolution ($\mathcal{R} \geq 300,000$) grid using Turbospectrum (Alvarez & Plez 1998), MARCS model atmospheres (Gustafsson et al. 2008) , and the dedicated Gaia-ESO line list (Heiter et al. 2021). The grid covers $3000K \leq T_{eff} \leq 8000K$, $0 \leq \log g \leq 5$, $-5 \leq$ [Fe/H] $\leq +0.5$, and $0.0 \leq [\alpha/Fe] \leq 0.8$.

Given the first-pass parameter estimates, for a given set of stellar parameters $\omega = \{T_{\rm eff}, \log g, [{\rm Fe/H}], [\alpha/{\rm Fe}]\}$ we first produce a flux-normalised synthetic spectrum $S(\lambda, \omega)$ at wavelengths λ by interpolating spectra from a surrounding grid. We redshift our interpolated spectrum by velocity V such that the normalised synthetic flux at an observed point λ is given by $S\left(\lambda\left[1+\frac{V}{c}\right], \omega\right)$, where c is the speed of light. The observed continuum is modelled as a low-order polynomial, with order set to a higher value for spectra with signal-noise $\geq$ 20, with

coefficients b_j which enter multiplicatively:

$$M(\lambda, \omega, v, \{b\}) = \sum_{j=0}^{N-1} b_{channel,j} \lambda^j \times S\left(\lambda\left[1 + \frac{V}{c}\right], \omega\right) \quad (1)$$

The continuum in each observed channel is modelled separately. We convolve the model spectrum with a Gaussian line spread function (LSF) (with free parameter $\mathcal{R}$) to match the resolving power in each channel, and resample the model spectrum to the observed pixels $\{\lambda\}$. Although the spectral resolution $\mathcal{R}$ in each channel is reasonably well-known, refocusing of the GIRAFFE spectrograph during the survey improved the quoted spectral resolution. For this reason we chose to include the spectral resolution $\mathcal{R}$ as a nuisance parameter with reasonable priors and marginalise them away. After convolution with the LSF, binning to the observed pixels $\{\lambda\}$ and assuming Gaussian error σ_i, the probability distribution $p\,(F_i|\lambda_i, \sigma_i, \omega, V, \{b\}, \{\mathcal{R}\})$ for the observed spectral flux F_i is:

$$p\,(F_i|\lambda_i, \sigma_i, \omega, V, \{b\}, \{\mathcal{R}\}) = \frac{1}{\sqrt{2\pi\sigma_i^2}} \exp\left(-\frac{[F_i - M_i]^2}{2\sigma_i^2}\right). \quad (2)$$

Under the implied assumption that the data are independently drawn, the likelihood of observing the data D, given our model, is found by the product of individual probabilities:

$$\mathcal{L} = \prod_{i=1}^{N} p\,(F_i|\lambda_i, \sigma_i, \omega, V, \{b\}, \{\mathcal{R}\}) \quad (3)$$

and the probability $\mathcal{P}$ of observing the data is proportional up to a constant such that:

$$\begin{aligned} \mathcal{P} &\propto \mathcal{L}\,(D|\theta) \times \mathcal{P}r\,(\theta) \\ \ln \mathcal{P} &= \ln \mathcal{L}\,(D|\theta) + \ln \mathcal{P}r\,(\theta) \end{aligned} \quad (4)$$

where $\mathcal{P}r(\theta)$ is the prior probability on the model parameters θ.

This analysis describes the joint probability distribution of an identified template and an associated target star radial velocity. In practice we evaluate the probability for a grid of radial velocities - essentially a uniform prior on radial velocity - and for our grid of templates, again assuming a uniform prior. The resulting 2-D probability distribution can be marginalised over appropriate parameters to determine the maximum likelihood a posteriori estimate of the velocity and the velocity error, and similarly to determine the parameters of the best-fitting template.

8.2. GIRAFFE radial velocity accuracy

It is well-known that although the formal radial velocity precision derived from cross-correlation or pixel-fitting methods can be almost arbitrarily small for sufficiently high S/N spectra, the actual precision achievable with most spectrographs is generally limited by systematic effects. This includes instrument flexure, uncertainties in the wavelength calibrations, Line Spread Function (LSF) variation/asymmetry and template mismatches. This systematic component has to be included in the total error budget. We have found this systematic error between the HR21 and HR10 setups to be around 300 m s^{-1} from large numbers of Gaia-ESO Milky Way spectra. It is important to note that this systematic component is not expected to be present when comparing

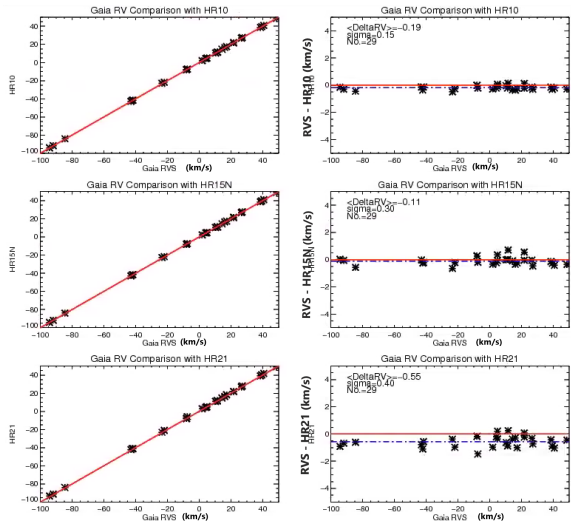

Fig. 11: Comparison of radial velocities determined for the Gaia Radial Velocity Standards by the Gaia ESO Survey pipeline for various GIRAFFE instrumental setups with the reference values for the same stars from Soubiran et al. (2018). The red lines are the one-one relation, blue lines fitted offsets.

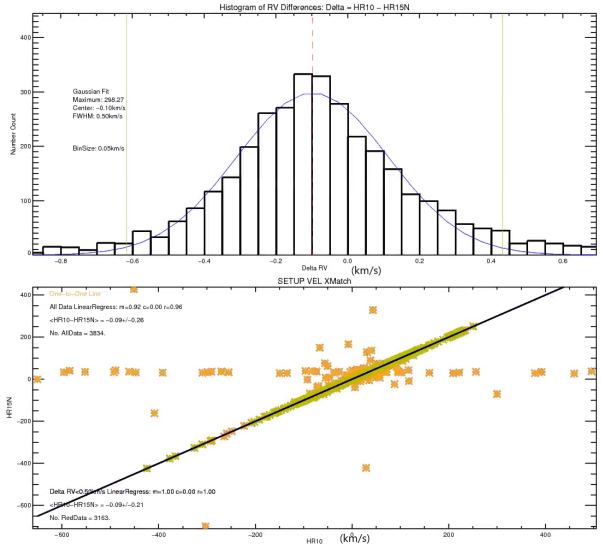

Fig. 12: A comparison of the Gaia ESO Survey radial velocity pipeline results for the stars in common between the GIRAFFE HR15N and HR10 instrumental setups. The agreement is very good, with the offset between the two scales determined to be -0.09±0.26 km/s.

RVs obtained from spectra using the same setup in sequential exposures, but it becomes important when comparing RVs from different nights, or between setups. We include this systematic error floor in suitable comparisons hereafter.

The range of instrumental setups in which a star is observed, and hence the number of available spectra with associated radial velocities, varies per star. Calibrators, for example, have typically been observed with a broader range of instrumental configurations and will thus have a relatively greater number of

radial velocity determinations than a typical field star. Additionally, particular analysis nodes and Working Groups deliver revised estimates of the radial velocities for their targets of interest that they determine during their specialised analysis for the parametrisation of these spectra. Thus, as with most of the quantities derived from the spectral analysis, multiple radial velocity results are available per star, and these need to be homogenised to produce a single recommended radial velocity per star.

As part of the homogenisation by WG15 of the available radial velocities for each star, different instrumental setups were compared, and offsets were applied to bring the radial velocities on to the same scale. The radial velocities from the HR10 setup were used to establish the zeropoint of the radial velocity scale due to their good agreement with the literature values of the Gaia Radial Velocity Standards (Soubiran et al. (2018); see Fig 11). Fig 12 shows an example of the cross-match between different instrumental setups and the offset found and applied during homogenisation. A more complete description of the radial velocity accuracy and zeropoint as a function of stellar and observational parameters is presented in Jackson et al. (2015), while an updated version is presented in the accompanying paper (Randich et al. 2022).

8.3. UVES radial velocities

Determination of radial velocities from the high-resolution UVES spectra is described fully in the UVES processing description paper (Sacco et al. 2014), and updated in the companion article (Randich et al. 2022).

We provide a brief summary from that paper here for convenience.

Radial velocities are derived by cross-correlating each spectrum with a grid of synthetic template spectra. The grid is composed of 36 spectra convolved at the FLAMES-UVES spectral resolution. It covers seven effective temperatures (T_{eff} = 3100, 4000, 5000, 6000, 7000, 8000 K), three surface gravities (log g = 2.5, 4.0, 5.0), and two values of metallicity ([Fe/H] = 0.0, −1.0).

Each spectrum is cross-correlated with all the spectra of the grid, using the IRAF task FXCOR masking the Balmer lines (Hα and Hβ) and regions of the spectra with strong telluric lines. To derive the radial velocity, the cross-correlation function (CCF) with the highest peak is selected and the peak is fitted with a Gaussian function to derive its centroid. This procedure fails for very early-type stars with an effective temperature above the highest temperature of our grid, which are characterised by the presence of no, or very few, absorption lines other than the Balmer lines. Radial velocities for these stars are treated separately by the dedicated Working Group WG13.

To estimate the precision of the velocities, we used the differences between velocities measured from the lower (RVL) and upper (RVU) spectra, which are measured independently by the pipeline. Assuming identical uncertainties on the velocities from the two wavelength ranges, and since there is no systematic offset between lower and upper spectra (median(RVU - RVL) = 0.007 km/s), the empirical error on the velocities derived by our pipeline is defined to be $\sigma_{\rm UL} = ({\rm RV_U} - {\rm RV_L})/\sqrt{2}$. The statistical error on a radial velocity is equal to the 68th percentile rank of the distribution of these empirical errors, after outliers have been removed, and corresponds to σ = 0.18 km/s.

Since the upper and the lower spectrum are calibrated using the same arc lamp, our approach for the error estimate does not take into account the error due to the variations of the zero point of the wavelength calibration. In order to estimate this source of uncertainty, we used spectra of targets observed multiple times in different epochs. Similarly to the above case, the empirical error is estimated as $\sigma = |\Delta RV|/\sqrt{2}$ where $|\Delta RV|$ is the difference between two observations of the same target performed on different nights. The distribution of this empirical error is much wider than the distribution of the errors $\sigma_{\rm UL}$; the 68th percentiles are σ_U = 0.38 km/s and σ_L = 0.40 km/s for the lower and upper ranges, respectively. This proves that the variations of the zero point of the wavelength calibration are the main source of uncertainty. Therefore, we adopt $\sigma \sim 0.4$ km/s as the typical error for the radial velocities derived from the FLAMES-UVES spectra of the Gaia-ESO Survey.

9. Spectrum analyses (WG10,WG11,WG12,WG13,WG14)

The spectrum analyses have been performed in five Working Groups; Working Group 10 analysed GIRAFFE spectra of normal FGK stars; Working Group 11 analysed UVES spectra of normal FGK stars; Working Group 12 analysed cool pre-main sequence stars; Working Group 13 analysed hot OBA stars; Working Group 14 has two roles, one to process unusual and complex objects, such as white dwarfs and spectroscopic binaries, and also to develop project wide data quality flags.

The goal of the working groups was to process extracted spectra to refine astrophysical parameters, to deliver elemental abundances to a level appropriate for the relevant stellar type and available signal-noise ratio, to derive stellar properties (e.g. activity, accretion, rotation whenever relevant) and to provide detailed analysis-level quality-control. Each Working Group had a similar structure, involving a set of "nodes", each of which processed (a subset of) the spectra using its preferred analysis methods and software.

The structure of the Working Groups for spectrum analysis provided close coordination between the teams, ensuring the optimum range of analyses would be applied to the various stellar and data types as appropriate. The methodologies are all established, all publicly well-documented, forming the basis of most modern spectrum analyses in the literature. Below we provide a general description of the input data, as well as of the strategy and methods followed.

Input The main input to the spectrum analyses consists of reduced spectra. These have been put on a wavelength scale, have been velocity shifted to a barycentric reference frame, and have been pipeline normalised. Quality information is also provided, including variance spectra, Signal-Noise ratio, non-usable pixels, and any other relevant output from the spectrum processing. Additional inputs are the radial and rotational velocities derived by Working Group 8, photometric data, and first guess atmospheric parameters derived by Working Group 9. For cluster stars, cluster distances and reddening values are also available as input to the spectrum analysis.

Line lists, atomic and molecular data ($gf-$values, broadening constants, etc.) appropriate for the different categories of targets and spectral intervals are compiled by dedicated efforts and made available survey-wide to the analysis nodes. These actions are taken to ensure homogeneity in the derived quantities. Similarly, all the nodes participating in the analyses have adopted a fixed set of model atmospheres, which is sufficiently broad to be optimised for each class of survey astrophysical targets.

Analysis: strategy and methods The five Working Groups delivering the spectrum analysis all follow a similar approach, summarised in the following.

- The data analysis was both distributed and duplicated among the nodes contributing to each working group. Specifically, more than one group analyses and produces results for (nearly) all relevant survey targets. This duplication of different methods allows, given performance comparison of the results, production of a set of recommended parameters. It also, through rigorous quality control, provided a quantitative estimate of both random and method-dependent uncertainties. In the event of discordant results for a specific star, individual checks could be conducted. Quality monitoring and outlier detection were performed throughout the survey. Monitoring of homogeneity was conducted by the analysis teams, in coordination with Working Group 15 (see below). The decision on the final recommended values was the responsibility of Working Group 15.
- A first pass analysis was performed, followed by a more refined analysis. The first pass analysis quality checked the preliminary classification parameters and provided astrophysical parameters, which, together with the information on photometry from the target selection procedure, were input to subsequent analyses.
- Depending on the star's spectral-type and characteristics, appropriate optimal tools, software, and model atmospheres were used; however, some methodologies in common to all Working Groups could be identified.
  The methods to derive astrophysical parameters and abundances could be roughly divided in two broad categories. The first one includes the main types of parameterisation methodology, such as exhaustive search algorithms, global optimisation methods, projection algorithms, pattern-recognition methods, and Bayesian parameterisation approaches. The second one consists of more classical approaches, based on measurements of equivalent widths of absorption lines and inversion codes (spectral synthesis), or use of curves of growth for particular lines/elements (e.g., Li). Equivalent widths were measured with (semi-)automatic codes by fitting Gaussian profiles to the lines. The available codes included DAOSPEC, ARES, and SPECTRE.
  Specific methods were used in special subsets of the sample (e.g., Hα wings, line-depth-ratios). In most cases the codes were automatic, and proven to be able to handle large scale data volumes.

More specific details on the analysis of the different types of stars/spectra are given in the following sections. The WG10 homogenisation was carried out with reference to the results of the WG11 homogenisation, since many stars were in common, thus WG11 is described first.

9.1. Working Group 11: UVES spectra of "normal" FGK stars

The operation of Working Group 11 (WG11) is described more fully in the article "The Gaia-ESO Survey: The analysis of high-resolution UVES spectra of FGK-type stars", Smiljanic et al. (2014). Further details on updates implemented for the final Gaia-ESO data release are given in Worley & et al. (2022). A total of 13 different nodes participated in the analysis described in Smiljanic et al. (2014).

The methodologies are described in the Appendix A of Smiljanic et al. (2014) and summarised in Table 11. An exception is the Arcetri node which did not participate in earlier WG11 analysis cycles and is described in Lanzafame et al. (2015). Here, we give just a brief summary of the codes used by each node for completeness:

Arcetri: Equivalent widths of the Li and the nearby Fe line were measured with Gaussian fitting. Abundances were determined with a set of curves of growth (Franciosini et al. 2022) determined from a grid of synthetic spectra computed with the methods and tools described in de Laverny et al. (2012) and in de Laverny et al. (2013) and adopting the AMBRE linelist of Guiglion et al. (2016).

CAUP: Equivalent widths were measured with the Automatic Routine for line Equivalent widths in stellar Spectra code (ARES, Sousa et al. 2007, 2015). Atmospheric parameters and chemical abundances were determined with MOOG (Sneden et al. 2012).

EPINARBO The EPINARBO node was composed of subnodes located at several institutes that contributed during the different phases of the project, including: Laura Magrini (INAF-Arcetri); Angela Bragaglia and Paolo Donati (INAF-Bolgna); Antonella Vallenari, Tristan Cantat-Gaudin and Rosanna Sordo (INAF-Padova); and University of Indiana (Eileen Friel and Heather Jacobson). Equivalent widths were measured with DOOp (Cantat-Gaudin et al. 2014), a wrapper that allows improved and automated use of DAOSPEC (Stetson & Pancino 2008). Atmospheric parameters and abundances were determined with the Fast Automatic MOOG Analysis code (FAMA, Magrini et al. 2013) which automates the use of MOOG (Sneden et al. 2012).

IAC-AIP: The code FERRE (see Allende Prieto et al. 2014, and references therein) was used. The strategy was to find, for each observed spectrum, the atmospheric parameters of the best fitting model among a grid of pre-computed synthetic spectra.

LUMBA: The LUMBA UVES analysis pipeline is fully described in Gavel et al. (2019). The pipeline made use of the Spectroscopy Made Easy code (SME, Valenti & Piskunov 1996; Piskunov & Valenti 2017) for computing on-the-fly synthetic spectra that were used to determine atmospheric parameters and chemical abundances. Departures from Boltzmann and Saha statistics were considered for iron lines which are prominently used in the derivation of stellar parameters.

Nice: The MATrix Inversion for Spectral SynthEsis (MATISSE, Recio-Blanco et al. 2006) algorithm was used. The code used a method that projects the observed spectrum onto functions determined from the linear combination of a pre-computed grid of synthetic spectra. The UVES analysis of the Gaia-ESO setups proceeded as described in Worley et al. (2016b).

OACT: The OACT node used the code ROTFIT (Frasca et al. 2003, 2006). The method consisted in a χ^2 minimisation of the

residuals between the observed spectrum and a set of reference spectra. In this case, a library of observed spectra, from the ELODIE archive (Prugniel & Soubiran 2001), was used as reference.

UCM: The code STEPAR (Tabernero et al. 2019) was used to determine atmospheric parameters based on equivalent widths automating the use of MOOG (Sneden et al. 2012). Equivalent widths were measured with the Tool for Automatic Measurement of Equivalent width (TAME, Kang & Lee 2012).

Vilnius: Equivalent widths were measured with DAOSPEC (Stetson & Pancino 2008). The node developed its own wrapper to automate the use of the MOOG code (Sneden et al. 2012) for the determination of atmospheric parameters and chemical abundances. Although most abundances were computed from the equivalent widths, a few selected species were analyzed with spectrum synthesis. The Vilnius node was the only provider of carbon and nitrogen abundances from the synthesis of C_2 and CN molecular features, and oxygen abundances from the synthesis of the forbidden oxygen line at 6300 Å.

In total, WG11 analyzed 8175 sets of UVES spectra from 6987 individual stars. This number includes all the UVES spectra also analyzed by WG12 (pre-main sequence stars). A fraction of the stars observed in young open clusters as candidate pre-main sequence stars are indeed normal FGK-type stars, which are better suited for analysis by the WG11 methodologies. Their inclusion among the WG11 sample ensures they receive similar treatment as the remaining sample. The decision about which final result to adopt (from WG11 or WG12) is a later step performed by WG15.

The final data products resulting from this analysis, with a breakdown by contributing node, include: lithium abundances (from the Arcetri node only); chromospheric activity indicators (from the OACT node only); abundances of carbon, nitrogen, and oxygen (from the Vilnius node only); atmospheric parameters (from the nodes CAUP, EPINARBO, IAC-AIP, LUMBA, Nice, OACT, and UCM); and other chemical abundances (from the nodes CAUP, EPINARBO, LUMBA, and Vilnius).

With respect to the description presented in Smiljanic et al. (2014), the most important change in WG11 procedures concerns the homogenisation process, i.e., the process of combining the multiple measurements of a certain quantity into a final recommended value, with well characterised uncertainties. For this final release, we made use of a hierarchical Bayesian inference method. Details will be given in Worley & et al. (2022), here we only summarise its most important aspects.

The concept and first implementation of the Bayesian approach to combine the multiple measurements was developed internally to Gaia-ESO by Andrew Casey (2014-2017, private communication). His implementation was used for producing the WG11 results available in the Gaia-ESO internal data release 5[3]. For the final analysis (which corresponds to the Gaia-ESO internal data release 6), we built upon his ideas and initial work to develop a slightly different implementation of the Bayesian approach.

The concept is the following. Let us assume that a certain star "n" is characterised by a parameter with value $\mathbf{true.param}_n$. What a node "i" returns after the analysis is a noisy measurement of that parameter, $\mathbf{param}_{i,n}$. We assume that the effects of the node measuring that parameter can be separated into two components: a stochastic error of Gaussian nature ($\mathbf{random.err}_i$, which is a property of the node) and a systematic offset ($\mathbf{bias}_{i,n}$, which is given by a function that is a property of the node and whose value was computed for that star). In that case, we can write something like:

$$\mathrm{param}_{i,n} \sim dnorm(\mathrm{true.param}_n, \mathrm{random.err_i}) + \mathrm{bias}_{i,n} \quad (5)$$

where dnorm(μ,σ) stands for the normal distribution of mean = μ and standard deviation = σ. The symbol "$\sim$" indicates that the left part of the equation ($\mathbf{param}_{i,n}$) is a result of a random draw from the right part of the equation. Numerically, we actually add the bias term to $\mathbf{true.param}_n$ inside the Normal distribution. If a node is affected by a certain bias, it is not really measuring from a distribution centred around the true value, but from a distribution centered around the biased value. We further assume that we can parametrise the bias as a quadratic function of the measured parameter, to capture its variation across the parameter space.

Using a multi-dimensional Normal distribution, we generalise this idea for the case where several nodes are providing measurements of the same quantity. Instead of a standard deviation, the multi-dimensional Normal is characterised by a covariance matrix with terms that take into account the stochastic error of each node and also the correlations among the nodes.

This is all written as a Bayesian hierarchical model where the parameters are inferred using MCMC simulations. The first step is to estimate the terms of the covariance matrix and the coefficients of the quadratic bias function of each node. That is done using a set of calibrators for which reference values, and associated uncertainties, of the parameter in question are known. In practice, we write the reference value, and its uncertainty, as a Gaussian prior to the true value of the parameter. The second step consists in applying the biases and the covariance matrix to the remaining sample to invert, from the measurements, the most likely true value of the parameter (and its uncertainty).

For obtaining values of $T_{\rm eff}$, we used as reference calibrators the *Gaia* benchmark stars (Heiter et al. 2015; Jofré et al. 2018). For the case of log g, in addition to the *Gaia* benchmark stars, we also included the sample of giants with asteroseismic gravities obtained from K2 (Worley et al. 2020) and CoRoT data (Masseron et al., in preparation). For the metallicities, stars from the sample of open and globular clusters listed in Tables 7 and 8 of Pancino et al. (2017a) were used in addition to the *Gaia* benchmark stars. Cluster members were either adopted from Pancino et al. (2017b) or defined using radial velocities.

By applying the same biases and the covariance matrix to the calibrators, we estimated our capacity of recovering the reference values. The comparison shows our estimate of the systematic errors in $T_{\rm eff}$, log g, and [Fe/H] to be of the order of 85 K, 0.14 dex, and 0.09 dex, respectively. However, we remark that this budget necessarily includes the errors in the reference scales themselves. Comparisons between the $T_{\rm eff}$ and log g values obtained from the Bayesian analysis for cluster members against theoretical isochrones demonstrate that robust parameter values were obtained. We defer a more detailed description of these (and other) tests to Worley & et al. (2022).

For the chemical abundances, the first step for determining biases and the covariance matrix is not possible, because of the

[3] https://github.com/andycasey/ges-idr5

Table 11: Overview of the WG11 Nodes that participated in the analysis of the last Gaia-ESO data release.

Node	Method	Analysis lead	Data products
Arcetri	Equivalent widths	Elena Franciosini	Lithium abundances
CAUP	Equivalent widths	Vardan Adibekyan,	
Elisa Delgado-Mena, Sergio Sousa	Stellar parameters, abundances		
EPINARBO	Equivalent widths	Laura Magrini	Stellar parameters and ab
IAC-AIP	Library of synthetic spectra	Michael Weber	Stellar parameters
LUMBA	On-the-fly spectrum synthesis	Alvin Gavel	Stellar parameters and ab
Nice	Library of synthetic spectra	Clare Worley	Stellar parameters
OACT	Library of observed spectra	Antonio Frasca and Katia Biazzo	Stellar parameters and ac
UCM	Equivalent widths	Hugo Tabernero	Stellar parameters
Vilnius	Equivalent widths, spectrum synthesis	Arnas Drazdauskas, Gražina Tautvaišienė	Stellar parameters and ab

lack of a reference sample. In this case, we implemented a simplified inference model that estimates at the same time the best abundance and the covariance matrix. In this sense, the method essentially returns a weighted mean, but where the weights (and possible correlations) are estimated simultaneously through the node to node comparisons. For the abundances, we work on a line-by-line basis, i.e., taking into account separately each spectral line measured by each node. We adopt the solar abundances of Grevesse et al. (2007) as a strong solar prior (to be reproduced within $1\sigma = 0.01$ dex). When available, chemical abundances for the *Gaia* benchmark stars (Jofré et al. 2015) are used as weaker priors.

9.2. Working Group 10: GIRAFFE spectra of "Normal" FGK stars

The operation of Working Group 10 is described more fully in Worley & et al. (2022), Recio-Blanco et al. (2014) and Worley et al. (2020). The analysis teams (nodes) that participated in the final Gaia-ESO data release are summarised in Table 12.

There is a significant overlap between the WG10 and WG11 nodes hence the description of the methodologies of Arcetri, CAUP, EPINARBO, IAC (see IAC-AIP), Lumba, OACT and Vilnius can be found in the WG11 section above. The additional WG10 node is MaxPlanck:

MaxPlanck: This method determined stellar parameters and magnesium abundance through the use of neural networks described in Kovalev et al. (2019). A training set of synthetic spectra was generated using the MARCS stellar atmosphere models and the Gaia-ESO line list (Heiter et al. 2021).

In total, WG10 analyzed 158809 GIRAFFE spectra from 92348 individual stars. The summary of the number of spectra and number of stars per GIRAFFE setup is given in Table 13.

For the parameter analysis, the nodes were able to analyse each setup individually but also determine parameters by analysing the HR10 and HR21 spectra together. Thus the homogenisation was carried out as four setups: HR15N, HR9B, HR10|HR21, HR21-Bulge. For the HR10|HR21 setup all results from HR10+HR21 and HR10-only were combined. For HR21-Bulge only the results for the bulge fields and the calibration stars (FGK benchmarks, CoRoT, K2, Globular Clusters, Calibrating Open Clusters) were homogenised.

The homogenisation per setup was determined using the bayesian inference method developed for the WG11 analysis (as described above) and adapted for WG10. See Worley & et al. (2022) for a description of this method. The reference set in each case was based on the cross-match of each WG10 setup to the WG11 sample, the FGK Benchmarks, and the other WG10 setups, primarily HR15N, in a bootstrapping approach. Thus the WG10 setups were homogenised directly onto WG11 and to the other WG10 setups. This gave the per star homogenisation per setup.

Quality diagnostics showed that the agreement between the WG10 setups and WG11 was excellent and so no further calibrations were needed for the parameters. To generate the final per star dataset for WG10, when a star was present in multiple setups, a priority procedure was implemented to take the parameters from the most appropriate setup based on the observing programme and science goals. See Worley & et al. (2022) for the quality diagnostics and priority procedure. The final WG10 homogenisation of the node analyses resulted in 78005 stars with stellar parameters.

The chemical abundance homogenisation was carried out combining all node results for all setups for each element for each star. In this way the separate setups were treated together as a single non-continuous spectrum per star. The reference set was the cross-match to WG11 which as a sample included a range of standards and science targets. This meant the WG10 abundances were put directly onto the WG11 abundance scale.

9.3. Working Group 12: Cool pre-main sequence stars

Working Group 12 made use of specialised methods for analyzing spectra of young, low-mass stars, particularly not-embedded pre-main sequence stars. The analysis took chromospheric activity and possible mass accretion into account. Both UVES/U580 and GIRAFFE/HR15N spectra were analyzed.

Six nodes contributed to the analysis: INAF–Osservatorio Astrofisico di Arcetri, Centro de Astrofisica de Universidade do Porto (CAUP), Università di Catania and INAF–Osservatorio Astrofisico di Catania (OACT), INAF–Osservatorio Astronomico di Palermo (OAPA), Universidad Complutense de Madrid (UCM), and Eidgenössische Technische Hochschule Zürich (ETH).

The operation of Working Group 12 is described more fully in the article "Gaia-ESO Survey: Analysis of pre-main sequence stellar spectra" Lanzafame et al. (2015). Here, a brief summary and some updates are reported.

A summary of the parameters obtained by WG12 is reported in Table 14. A distinction is made amongst *raw*, *fundamental*, and *derived* parameters. The Hα emission equivalent width (W(Hα)), the Li absorption equivalent width (W(Li)), the Hα width at 10% of the line peak (Natta et al. 2004), and the Hα full width at zero intensity (FWZI) are considered *raw* parame-

Table 12: Overview of the WG10 Nodes that participated in the analysis of the final Gaia-ESO data release.

Node	Method	Analysis responsible	Data products	Setups Analysed
Arcetri	Equivalent widths	Elena Franciosini	Lithium abundances	HR15N
CAUP	Equivalent widths	Andressa Ferreira	Abundances	HR10, HR21, HR15N
EPINARBO	Equivalent widths	Laura Magrini	Stellar parameters and abundances	HR15N, HR9B
IAC	Library of synthetic spectra	Carlos Allende-Prieto	Stellar parameters	HR10, HR21
LUMBA	On-the-fly spectrum synthesis	Diane Feuillet and Karin Lind	Stellar parameters and abundances	HR10, HR21, HR15N
MaxPlanck	Neural networks	Maria Bergemann and Mikhail Kovalev	Stellar parameters and activity	HR10, HR21
OACT	Library of observed spectra	Antonio Frasca and Katia Biazzo	Stellar parameters and activity	HR15N, HR9B
Vilnius	Equivalent widths and spectrum synthesis	Šarūnas Mikolaitis	Stellar parameters and abundances	HR10, HR21

Table 13: Summary of the number of spectra and stars per GIRAFFE setup.

Setup	No. Stars	No. Spectra
HR15N	25785	26550
HR9B	3473	4161
HR10	59722	60579
HR21	66542	67519
Total	92348	158809

Table 14: Output parameters of the Gaia-ESO PMS analysis (WG12). The number of stars for which each parameter was derived is indicated for the GIRAFFE/HR15N and UVES/U580 setup separately. For the Li equivalent width, only the number of stars with $W(\mathrm{Li}) > 100$ Å, is reported. For the veiling, only stars for which $r > 0$ are counted. See text for a description of the symbols used.

Parameter	GIRAFFE/HR15N	UVES/U580
raw		
$W(\mathrm{H}\alpha)$	2826	476
$W(\mathrm{Li})$ (>100 Å)	3570	46
Hα 10%	2149	47
FWZI	4783	0
fundamental		
$T_{\rm eff}$	14211	merged with WG11
$\log g$	6499	merged with WG11
γ	14166	...
[Fe/H]	11018	merged with WG11
ξ	...	merged with WG11
$v \sin i$	12753	merged with WG11
$r > 0$	352	...
derived		
$\Delta W(\mathrm{H}\alpha)_{\rm chr}$	2826	476
$\Delta W(\mathrm{H}\beta)_{\rm chr}$	...	256
$F(\mathrm{H}\alpha)_{\rm chr}$	2726	436
$F(\mathrm{H}\beta)_{\rm chr}$	...	224

ters as these are directly measured on the input spectra and do not require any prior information. They are used to identify pre-main-sequence (PMS) stars and optimise the evaluation of the fundamental parameters in ROTFIT (Frasca et al. 2006), one of the two methods used. In addition to $T_{\rm eff}$, $\log g$, and [Fe/H], the fundamental parameters derived include also micro-turbulence velocity (ξ), projected rotational velocity ($v \sin i$), veiling (r, see, e.g., Hartigan et al. 1988), and a gravity-sensitive spectral index (γ, see Damiani et al. 2014b). Finally, the derived parameters are those whose derivation requires prior knowledge of the fundamental parameters: chromospheric activity indices ($\Delta W(\mathrm{H}\alpha)_{\rm chr}$ and $\Delta W(\mathrm{H}\beta)_{\rm chr}$) taken as equivalent width difference with respect to an inactive template with the same fundamental parameters, and chromospheric line fluxes ($F(\mathrm{H}\alpha)_{\rm chr}$ and $F(\mathrm{H}\beta)_{\rm chr}$) evaluated from the chromospheric activity index and the expected flux at the continuum.

Fundamental parameters were inferred by the OACT node using ROTFIT (Frasca et al. 2006) and by the OAPA node using a spectral indices method (Damiani et al. 2014b). The spectral indices results are considered valid below a given threshold of blending due to rotational broadening. In the case at hand, the limits are $v \sin i < 90$ km/s for $T_{\rm eff}$, $v \sin i < 30$ km/s for $\log g$, and $v \sin i < 70$ km/s for [Fe/H]. Comparison with benchmark stars have shown the ROTFIT application to HR15N spectra produces strong biases for $T_{\rm eff} > 6200$ K, and therefore all ROTFIT results are disregarded in this range. When both methods produce valid results, it was imposed that substantial agreement exists before averaging them. Comparison with benchmarks and results from photometry have led to the following homogenisation criteria:

- The spectral index method was taken as reference $T_{\rm eff}$. The two methods were averaged when $\Delta T_{\rm eff} < \pm 220$ K for $T_{\rm eff} < 4000$ K, $\Delta T_{\rm eff} < \pm 360$ K for $4000 < T_{\rm eff} < 5000$ K, and $\Delta T_{\rm eff} < \pm 300$ K for $T_{\rm eff} > 5000$ K. Otherwise only the spectral index value is recommended.
- $\log g$ are averaged only if the two results differ by < 0.3 dex. Otherwise, only the ROTFIT results is given if $\log g_{\rm OACT} > 4.2$ and $\log g_{\rm OAPA} > 5.0$. In all other cases, no $\log g$ is given.
- When both methods produce [Fe/H] the values are averaged.

Besides the ($T_{\rm eff}$, $\log g$, [Fe/H]) triad, WG12(OACT) also recalculated radial velocities for clusters badly affected by nebular lines (NGC2264, NGC6530, Trumpler14, NGC2451) after applying an alternative different sky background subtraction.

The projected rotational velocity $v \sin i$ from HR15N was also recalculated by OACT using a cross-correlation technique and masking emission features in young stars. Changes in the spectrograph resolution were also taken into account. Upper limits are given when the error is larger than the $v \sin i$ value itself or when $v \sin i \leqslant 7$ km s^{-1}, which is the limit imposed by the GIRAFFE resolution.

9.4. Working Group 13: OBA stars

The operation of Working Group 13 is described more fully in the article "The Gaia-ESO Survey: The analysis of hot-star spectra" Blomme et al. (2022).

In Working Group 13 (WG13), eight Nodes worked on the analysis of the O-, B- and A-type spectra. These were selected from observations made with the HR3/4/5A/6/14A GIRAFFE setups and their corresponding UVES data. Some archive data were also processed. The temperature range covered by WG13 is large, and most of the Nodes cannot fully cover that range. Two types of analysis were used by the Nodes. The first one was based on a carefully selected set of diagnostic photospheric spectral lines, and radiative transfer calculations were used to fit the profiles in detail. The second one used the full observed spectrum, comparing it to theoretically generated ones. In the comparison, weights can be used to stress the importance of certain spectral regions. After the Nodes have derived the stellar parameters, their results are homogenised and the abundances are determined. More details of the WG13 work are given in Blomme et al. (2022).

ROBGrid Node. The ROBGrid Node used theoretical spectra from the literature and compared them to the observations, to derive the stellar parameters ($T_{\rm eff}$, $\log g$, and metallicity – if not too different from solar metallicity). Each observed spectrum was compared to all theoretical spectra to find the best fit. For each comparison, the radial and projected rotational velocities are determined using a cross-correlation technique (David et al. 2014, their Eq. 7) with a rotationally broadened theoretical spectrum. To judge the goodness-of-fit the χ^2 for that comparison is calculated. The final stellar parameters (as well as the radial and projected rotational velocity) are determined by the theoretical spectrum having the minimum χ^2. In a larger loop around this fitting procedure, we also refined the normalisation of the observed spectrum. ROBGrid does not determine errors of the stellar parameters, but assigned errors that were derived in the homogenisation phase. The Node also does not provide abundances of individual elements, because the abundances that went into the literature models cannot be changed.

ROB Node. The ROB Node used a three-step approach to determine the stellar parameters and abundances. First the stellar parameters were estimated from a limited number of diagnostic H Balmer, Fe, and Mg absorption lines. Next, the detailed profiles of a more extensive set of diagnostic lines were fit by an iteration over $T_{\rm eff}$, surface gravity ($\log g$), line-of-sight microturbulence velocity (ξ), and metallicity ([M/H]). Finally, abundances were measured from selected sets of sufficiently (medium-strong to) strong lines. To explore the parameter space, we calculated a large homogeneous grid of synthetic spectra with the LTE radiative transfer code Scanspec[4] (Lobel 2011). The error bars range from $\sim$ ±150 K for $T_{\rm eff} < 8500$ K to $\sim$ ±250 K for $T_{\rm eff} > 11\,000$ K. The metallicities and element abundances have error bars ranging from ±0.05 dex to ±0.1 dex,

MGNDU Node. The MGNDU node analysed data from the UVES 520 setup. The spectra were renormalised as in Gebran et al. (2016), and the radial velocities redetermined because a high radial velocity accuracy is important for the MGNDU procedure (Paletou et al. 2015; Gebran et al. 2016). The procedure used is a combination of Principal Component Analysis (PCA) and a Sliced Inverse Regression (SIR). It starts by compiling a learning database using synthetic spectra. The model atmospheres for this database were calculated using the latest version of the ATLAS9 code (Kurucz 1992; Castelli & Kurucz 2003; Sbordone et al. 2004). Synthetic spectra were calculated from these models, using the SYNSPEC48 LTE code Hubeny & Lanz (1992) and the line list of Gebran et al. (2016). Once the learning database has been constructed, it can be applied to any observed spectrum to derive the stellar parameters (Kassounian et al. 2019). The average uncertainties for the inverted parameters are around 150 K for $T_{\rm eff}$, 0.35 for $\log g$, 0.15 for [M/H], and 2 km s^{-1} for $v \sin i$. No elemental abundances, other than Fe, are determined by MGNDU.

Liège Node The Liège Node covers the temperature range 10 000 to 32 000 K, corresponding to the range of B-type stars. A least-square minimisation was used to fit the observed normalised spectra with a grid of solar-metallicity, synthetic spectra computed with the SYNSPEC program on the basis of non-LTE TLUSTY (Lanz & Hubeny 2007) and LTE ATLAS (Kurucz 1993) model atmospheres. We first determined the radial velocity and projected rotational velocity (macroturbulence is not included). The full wavelength domain was used to determine the effective temperature and surface gravity. The typical 1-σ uncertainties are ~750 K for $T_{\rm eff}$, ~0.15 for $\log g$, ~15 km s^{-1} for $v \sin i$ and ~2 km s^{-1} for the radial velocity. For the abundance determination, we considered He, C, N, Ne, Mg, and Si. We found the best χ^2 fit of a grid of rotationally-broadened synthetic spectra to the observed line profiles of He I λ4471, C II λ4267, N II λ4630, Ne I λ6402, Mg II λ4481, Si II λ6371, and Si III λ4568-4575, from which we derived the abundances. The line profile calculations used the non-LTE code DETAIL/SURFACE originally developed by Butler (1984). More details about the version of the code currently used and the model atoms implemented are given in Morel et al. (2006) and Morel & Butler (2008).

ON Node The ON Node started by determining $v \sin i$ from the He I lines. Stellar parameters and abundances were then determined using theoretical spectra calculated with the fully non-LTE spectral synthesis code SYNSPEC and a new grid of line-blanketed non-LTE model atmospheres calculated with TLUSTY (Hubeny & Lanz 1995, 2017). The grid covers $T_{\rm eff}$ between 14 000 and 33 000 K, and surface gravity between 3.0 and 4.5. The Hydrogen lines of the GIRAFFE spectra are compared to these theoretical spectra to find the combinations of $T_{\rm eff}$ and $\log g$ that can reproduce the observed H profiles. The effective temperature was then determined from the ionization balance of Si II-Si III-Si IV. Next, a range of microturbulence velocity ξ is explored and the corresponding abundances of C, O, and Si are determined. By requiring the abundances to be independent of line strength, their final values are derived. The uncertainties on the individual parameters are 1000 K for $T_{\rm eff}$, 0.15 for $\log g$, 15 % for $v \sin i$, and 2 km s^{-1} for ξ.

IAC Node The IAC node analyses the O and early B-type stars using large grids of synthetic spectra computed with the non-LTE FASTWIND stellar atmosphere code (Santolaya-Rey

[4] http://alobel.freeshell.org/scan.html

Table 15: Overview of the WG13 Nodes. Listed are the effective temperature range covered by the Node, the spectral analysis technique used, the stellar parameters that are determined, the elements for which abundances are determined, and the number of spectra processed.

Node	$T_{\rm eff}$ range	Technique	Parameters determined	Abundances	# spectra
ROBGrid	3000 – 50 000 K	χ^2 minimisation with grid of theoretical spectra	$T_{\rm eff}$, $\log g$, [M/H], $v_{\rm rad}$, $v \sin i$[a]	–	8667
ROB	6000 – 12 000 K	Fe - Fe$^+$ ionisation balance of diagnostic photospheric lines	$T_{\rm eff}$, $\log g$, [Fe/H], ξ, $v \sin i$[a]	C, O, Mg, Al, Sc, Fe	517
MGNDU	5000 – 15 000 K	PCA and SIR	$T_{\rm eff}$, $\log g$, [M/H] , $v_{\rm rad}$, $v \sin i$	–	186
Liège	10 000 – 32 000 K	χ^2 minimisation with grid	$T_{\rm eff}$, $\log g$, $v_{\rm rad}$, $v \sin i$[a]	He, C, N, Ne, Mg, Si	696
ON	14 000 – 33 000 K	Non-LTE synthesis and Si ionisation balance	$T_{\rm eff}$, $\log g$, $v \sin i$[a]	C, O, Si	184
IAC	22 000 – 55 000 K	χ^2 minimisation with grid of FASTWIND models	$T_{\rm eff}$, $\log g$, $v \sin i$, $v_{\rm macro}$	He	268
Mntp	30 000 – 45 000 K	χ^2 minimisation with grid of CMFGEN models	$T_{\rm eff}$, $\log g$, $v \sin i$, $v_{\rm macro}$	–	55
LiègeO	20 000 – 45 000 K	CMFGEN	$T_{\rm eff}$, $\log g$, $v \sin i$, $v_{\rm macro}$	He, C, N	293

Notes. [(a)] What is listed here as $v \sin i$ is actually the total line-broadening parameter, which can include other effects, such as macroturbulence.

et al. 1997; Puls et al. 2005). First, a Fourier transform plus goodness-of-fit method determines the projected rotational velocity and the macroturbulent broadening. A χ^2 approach is then used to compare the observed diagnostic lines (Hα, Hγ, Hδ, He I λ4387, He I λ4471, He I λ4713, He I+II λ6678, He II λ4541 and He II λ4686) to the theoretical spectra. From this we determine effective temperature ($T_{\rm eff}$), surface gravity ($\log g$), Helium abundance ($N_{\rm He}/N_{\rm H}$), microturbulence (ξ), wind-strength parameter[5] (Q) and the exponent of the wind velocity-law[6] (β). Typical uncertainties are of the order of ±1000 K in $T_{\rm eff}$, ±0.10 in $\log g$, ±0.15 in $\log Q$ and ±0.03 dex in Helium abundance.

Mntp Node The Mntp node relied on a pre-computed grid of synthetic spectra, calculated with the non-LTE code CMFGEN (Hillier & Miller 1998). The projected rotational velocity of each star was derived from the Fourier transform of Si III λ4552 and/or He I λ4713. By convolving the theoretical spectra with the instrumental profile, the rotational profile and a radial-tangential macroturbulence profile, the value for the macroturbulence was determined. A χ^2 approach was used to find the best-fit spectrum, concentrating on those spectral lines that are sensitive to effective temperature and surface gravity. Typical uncertainties are 2500 K on $T_{\rm eff}$ and 0.15 on $\log g$.

LiègeO Node The LiègeO Node used the CMFGEN non-LTE atmosphere code (Hillier & Miller 1998) to analyze the O- and early B-type stars. A grid of CMFGEN models was constructed covering the range $T_{\rm eff}$ = 27,000 to 36,000 K, and surface gravity 3.0 to 4.3. These models include the effect of the stellar wind. The spectra are convolved with a rotation profile and a radial-tangential macroturbulence profile. For the O-type stars, the ionization balance between He I and He II is used to determine the effective temperature. For B-type stars, we used Si III and Si IV, with He I λ 4471 and Mg II λ 4481 as a secondary diagnostic. Carefully selected lines of Carbon and Nitrogen were used to determine the abundances.

Homogenisation Once the different nodes have delivered the stellar parameters, the results were homogenised. Node results for the benchmark stars are used to introduce corrections, but this could only be applied for the ROBGrid results as the other nodes did not analyse a sufficient number of benchmark stars. The recommended values for the stellar parameters are then determined as a weighted sum of the different node results (for details, see (Blomme et al. 2022)). Contrary to the practice in other Working Groups, these recommended stellar parameters values are not used in determining the abundances; instead the Node stellar parameters are used. Abundances are determined for only a small number of stars, with little overlap between the nodes. Where there was overlap, the recommended abundances are determined by a straight average of the node abundances.

9.5. Working Group 14: Non standard objects, quality flags

The aim of Working Group 14 (WG14) was to identify and characterise outlier objects. The majority of outlier objects were initially steps up the data processing and verification learning curve, and after improvement and iteration became obsolete. This was an invaluable contribution to survey quality control. For further information see Van Eck & et al. (2022). WG14 scanned all Gaia-ESO Survey spectra, using a mix of goodness-of-fit spectrum-matching outputs, and diagnostic analyses such as the shape of cross-correlation functions, looking for outlying data. the most significant are outlined below. In order to detect and characterise an anomaly most efficiently, a dedicated dictionary has been defined. This dictionary is briefly described in Sect. 9.5.1. WG14 could then systematically investigate specific types of outlying features potentially affecting all Gaia-ESO data (i.e. whatever the object spectral type is), namely emission line objects and binary/multiple objects, as described below (Sect. 9.5.2 and Sect. 9.5.3, respectively). Science verification illustrations of the value of the work of WG14 are available in: "The Gaia-ESO Survey: Catalogue of Hα emission stars" (Traven et al. 2015), "The Gaia-ESO Survey: double-, triple-, and

[5] Q is defined as $Q = \dot{M}/(v_\infty R)^{1.5}$ (Puls et al. 1996), where $\dot{M}$ is the mass-loss rate, v_∞ the terminal velocity of the wind, and R the stellar radius.

[6] The velocity in the stellar wind is given by $v(r) = v_\infty(1 - R_*/r)^\beta$, where R_* is the stellar radius of the star.

quadruple-line spectroscopic binary candidates" (Merle et al. 2017), and "The Gaia-ESO Survey: detection and characterisation of single-line spectroscopic binaries" (Merle et al. 2020).

9.5.1. Gaia-ESO Survey dictionary

The complete dictionary During analyses many nodes and Working Groups were flagging various types of outliers but with idiosyncratic naming conventions. It seemed desirable to use a common dictionary. This dictionary should convey information that is at the same time useful, exact and exhaustive for Gaia-ESO Survey-consortium data-processing users, but also for later use external to the survey consortium, without demanding too-much specialist project-specific knowledge. It was primarily the task of WG14 to flag outliers in such a way.

This dictionary has been defined with three main sections. First, a technical section (TECH) listing mainly data and data-product issues: data reduction, S/N, analysis issues and result quality issues, separately for parameter and abundance determination issues. These flags have been very useful to trace back data reduction problems or main analysis problems encountered by the nodes, and so in many cases the problematic flagged data has been able to be replaced by improved-quality data. Second, a peculiarity (PECULI) section, listing peculiarities possibly affecting the spectra, was introduced, listing for example binarity or emission line characterisation, as well as anomalous line and molecular absorption. Third, a comment (Remark) section was included, listing specific classes of stars, so that if any WG and nodes, in the course of their analysis, recognised a peculiar type of object, they could flag it as such. This section was however not used as much as the two other ones. A 3-level confidence flag (A,B,C), complementing each flag, has been introduced. For each data release, a first-pass analysis was performed beforehand, flagging most prominent issues, so that this information could be conveyed to the various nodes during their analysis phase.

The simplified dictionary In the final data release of recommended results, a significant number of flags are potentially available. A compromise is needed between providing too-much information to be helpful for an end-user, and failing to flag important information. In the event WG15 compromised with a simplified set of flags. These focus on the processing and quality-control issues noted above, and some astrophysically-interesting products, discussed below. The larger set of information is available in the full node-level information also made available.

9.5.2. Emission line detection and classification

Automated fits to the profile of detected emission lines are feasible. The most relevant for Gaia-ESO is Hα. The fitting used two independent Gaussian profiles and a third component accounting for nebular emission allowed distinction of several morphological types of Hα line profiles with the introduction of a simplified classification scheme. The spectra were sorted into eight distinct morphological categories: single component emission, emission blend, sharp emission peaks, double emission, P-Cygni, inverted P-Cygni, self-absorption, and emission in absorption. A quantitative discussion of the degree of variability of Hα emission profiles, which is expected for young, active objects, was also possible thanks to multiple observations. As proof of principle of the utlity of this approach, Traven et al. (2015) discussed the properties of Hα emission stars across the sample of 22035 spectra from a Gaia-ESO Survey internal data release after 22 months of observation. These are observed with the GIRAFFE instrument and largely to stars in young open clusters. A catalogue of stars with properties of their Hα emission line profiles, morphological classification, analysis of variability with time and the supplementary information from the SIMBAD, VizieR, and ADS databases was published. The relevant flags and parameters are published.

9.5.3. Binarity and radial-velocity variability detection

SB1 Although Gaia-ESO was not designed as a radial-velocity survey, most stars are observed more than once, with the subsequent radial velocity determinations being checked, and as appropriate flagged, for variability at the pipeline processing stage (Sect 8. In WG14 a more careful analysis was carried out. The aim, apart from intrinsic interest, is to identify multi-component spectra and to alert other WG/nodes analyses that atmospheric parameters should not be used for these system components; SB-specific pipelines should be used instead. This proceeded in two stages. The first involved analysis of the shape of the pipeline-generated cross-correlation functions (CCF). The CCF will be distorted from symmetry if stacking spectra uncorrected for unrecognised but true radial-velocity variations. This prompted an investigation of the individual spectra radial velocity determinations, looking for evidence for spectroscopic binaries with one visible component (SB1). The Gaia-ESO Survey internal data releases were investigated to identify and characterise SB1. A statistical χ^2-test was performed on the CCF's for stars characterised by at least two observations and a signal-to-noise ratio larger than three. The resulting sample of candidate RV variables was cleaned from contamination by pulsation/convection-induced variables using Gaia DR2 parallaxes and photometry. Monte-Carlo simulations using the NASA/HEASARC SB9 catalogue of spectroscopic orbits allowed estimation of the detection efficiency. Thus we could correct the SB1 rate to evaluate the Gaia-ESO SB1 binary fraction and its dependence on effective temperature and metallicity. This analysis remains to be completed for the full Gaia-ESO dataset, but for a proof of principle analysis using part of the data (Merle et al. 2020) found 641 (resp., 803) FGK SB1 candidates at the 5σ (resp., 3σ) level. The orbital-period distribution was estimated from the RV standard-deviation distribution. After correcting for the detection efficiency and selection biases, the SB1 frequency could be estimated, and its dependence on metallicity and spectral type could be constrained .

SB2 For double-lined and higher-multiplicity spectroscopic binaries one similarly can detect and flag binarity/multiplicity (SBX, X$\geq$ 2) for stars from the cross-correlation function (CCFs) of the Gaia-ESO spectra with spectral templates. Due to the large number of spectra, WG14 automated the task analysing the successive derivatives of the CCF. The use of successive derivatives allowed the de-blending of multicomponent CCFs. The code written to perform this task provides: i) the number of peaks detected in the CCF, ii) radial velocities corresponding to the peak maxima.

As a proof of principle this method was applied (Merle et al. 2017) on the fourth Gaia-ESO internal data release and allowed the detection of 354 SBn candidates (342 SB2, 11 SB3, and even one SB4), of which only nine candidates were known in the literature. This implies that about 98% of these SBn candidates are new, illustrating the known incompleteness of such studies at faint magnitudes. Among the SB2 candidates, detailed analysis (including follow-up observation on the SALT telescope) of the unique SB4 (four peaks in the CCF) reveals that CNAME 08414659-5303449 (HD 74438) in the open cluster IC 2391 is a physically bound stellar quadruple system. This very rare discovery indicates the success of teh approach.

Building on this success, Van der Swaelmen & et al. (2022) (see also Van der Swaelmen et al. 2018) improved the detection by designing specific cross-correlation masks (called NACRE masks) which produce more narrow CCFs, and therefore allow detection of SB2 with a smaller radial velocity difference. Our investigation showed that the HR21 wavelength range, around the near-infrared Ca II triplet, tends to host numerous strong and saturated lines (compared to the HR10 wavelength range) that broaden the CCFs. The new NACRE masks exclude these strong features to keep only weak, mildly-blended atomic lines and produce more narrow CCFs. We therefore re-computed the CCFs for the approximately 150000 individual HR10 and HR21 spectra and analysed them with DOE. The resulting flags are in the released dataset.

9.5.4. t-SNE flagging

The t-SNE node employed a semi-automatic approach to classification of spectra. This means that we manually assigned labels to groups of spectra that share a similar morphology, where the groups of spectra are revealed by the dimensionality reduction (clustering) technique t-SNE (for more details see Traven et al. 2017). Our intention was not to provide highly reliable classification labels for every spectrum, rather we identified most of the common outstanding peculiarities in the whole dataset, with spectra labelled up to the limits of our semi-automatic procedure. The benefit of this method is the ability to discover different kinds of unexpected peculiarities/features/issues as well as provide a clear overview of the structure of the whole spectral dataset (distinction between dwarfs/giants, hot/cool stars, etc.).

We produced classification results for the four Gaia-ESO setups (HR14A, HR15N, HR21, UVES-U580) that displayed at least a few well defined and interesting groups of spectra after analysis. We emphasise that this is not an exhaustive classification, since a person is needed to identify and name the different peculiar groups, however apart from that the t-SNE framework developed allows for a very efficient inspection and also updates to the classification as the dataset grows with time.

One of the strongest and most abundant features that we recognised in the t-SNE spectral classification are incorrectly subtracted nebular emission lines (HR14A, HR15N), along with other reduction issues. Some interesting objects with intrinsic emission in the Hα and CaII lines are likewise revealed by t-SNE. We also provided an interactive interface to the t-SNE maps dubbed the "GES Explorer", which is available internally to the Gaia-ESO collaboration, and can serve as a powerful exploratory tool for the Gaia-ESO dataset. In that way this t-SNE effort provides flags of value, particularly for analyses of young stars.

10. Survey parameter homogenisation WG15

Fuller information on the work of WG15 can be found in Hourihane & et al, (2022). The core team members were Patrick Francois, Anais Gonneau, Anna Hourihane, Laura Magrini and Clare Worley.

The aim of this WG was to ensure that the data products generated by the spectrum analyses are coherent, the resulting stellar atmospheric parameters and abundances homogenous, the parameters are calibrated onto an identified (set of) external calibrator objects, and the process is fully documented, supporting the data releases. This homogenisation process is a key aspect of analysis quality control, and proceeds through a double iteration. The first part of this homogenisation process is done inside each Working Group, where in particular the outputs of the different node-based analysis tools are compared and combined. Bringing together a final "best" parameter set requires, in addition to the internal analyses, careful analysis of calibration targets, and targets observed in more than one setting and instrument. In general systematic calibration scale and zero offsets between analysis groups, and between target classes and fundamental benchmark stars were found to be small by the end of the survey, for the final processing iteration. during the survey teams identified many causes of systematics and mitigated them. Some remain, as for example in radial velocity zero point offset between setups as discussed in Sect 8 and illustrated in Fig 11 and Fig 12. All systematic remaining offsets are corrected. The sanity check on the outcome of this on the HRD scatter pre- and post-processing is shown in Fig 4 above.

The homogenisation process is based on the homogenised results issued by the working groups WG10, WG11, WG12 and WG13 and the flags from WG14. During the first internal release, the results released by the WGs were obtained per spectrograph setup and not per individual object (cname). We verified that the benchmark star results (stellar parameters) coming from the different setups gave consistent results.

For later data releases the homogenisation process was performed in two steps. First we homogenised the stellar parameters, namely $T_{\rm eff}$, $\log g$, [Fe/H] and ξ, and delivered to the WGs a file containing all the targets with an homogenised set of stellar parameters. From that parameter set, updated abundances were computed by the nodes of the different WGs and the resulting abundances were set on the same scale by the WGs. The resulting updated abundance files then came back to WG15 to perform the element by element abundance homogenisation. Two more steps are needed to produce the final WG15 file, radial velocity homogenisation and the homogenisation of the flags.

10.1. Stellar parameter homogenisation

The aim of the homogenisation process is to put the astrophysical parameter results of the analyses of the different Working Groups WG10, WG11, WG12 and WG13 on a common scale. To allow a calibration of the work of the different WGs, Gaia-ESO has been designed to have several sets of stars in common amongst the analysis WGs. A set of FGK benchmark stars is analysed by all WGs except WG13 (hot stars) for which a special set of benchmark stars has been used. The benchmark stars have their atmosphere fundamental parameters determined by independent means. They are used as reference for the parameter scale. In addition to using the stars in common between WGs to perform the homogenisation process, we also used the objects

(open and globular clusters) that have been observed and processed by several WGs. In particular, a set of clusters referenced as calibration clusters has been observed in a range of instrumental setups to aid in inter-setup and inter-WG calibration. For example, the stars in NGC 6705 are observed in all setups, and are in common to all WGS, thus making this cluster a fundamental inter-calibrator for the whole survey.

10.1.1. Absolute parameter scale

The first step in the homogenisation process is to map the results of each WG on to the absolute external scale represented by the benchmark stars and to ensure internal consistency of the WG results with this scale. For the WG10 results, checks are performed to ensure that good agreement is found between the joint analysis of the HR10-HR21 setups and the literature results for the benchmark stars. Care has also been taken to verify that the other WG10 setups (HR21 alone, HR15N and HR09B) are mapped onto the HR10-HR21 scale. For WG11, we checked the agreement of the results for both setups U520 and U580. We also searched for potential corrections among the three setups U520 U580 and HR15N that have been used by WG12 for the analysis of the benchmark stars. Several warm benchmark stars added during the project have been used by WG13 to set their scale on the literature data. Stars in common amongst the WG13 setups were also considered to check the internal consistency of the WG13 results. A priority order has been recommended by WG13, based on their evaluation of the reliability of the outcomes, and adopted by WG15 for their results. The adopted sequence is" HR3|HR5A|HR6|HR9B|HR14", "HR5A|HR6|HR9B|HR14A","HR3|HR15A|HR6","HR14","HR9B" and "U520".

10.1.2. Relative parameter scale

Once the WGs results have been mapped onto the benchmark scale, the results of each WG for the whole sample of stars need be checked with respect to each other. As the full set of stars observed by Gaia-ESO covers a larger range of stellar parameters than the benchmark stars, it is mandatory to perform a series of checks. To evaluate any possible offsets between WGs we use the stars in common between different WGs that give us a direct estimate of any differences between WGs' results.

A second test is to plot the Hertzprung Russell diagram of Milky Way stars from the different WGs in the same metallicity range and compare these distribution with the theoretical : see Fig 4 above for an example.

A third test uses the member stars in open and globular clusters, which are both considered to be composed of chemically homogenous populations. Clusters are particularly important in the process of homogenisation as they allow us to put stars that are not common between WGs on a common scale as hot, massive cluster stars and pre-main sequence stars.

Globular clusters are important as they cover a wide range in metallicity for which both GIRAFFE and UVES observations were completed. They were investigated for $T_{\rm eff}$, $\log g$, [Fe/H] offsets between U580 and HR10+HR21 samples.

Open clusters analysed in Gaia-ESO can be divided into two categories, intermediate-age/old clusters (with ages $\leq$ 100 Myr up to several Gyr) and young clusters with younger ages that may have massive stars (mass $\leq$ 8 $M_{\odot}$). To allow a comparison of the results of the different WGs and a final homogenisation of the whole Gaia-ESO Survey results, several open clusters are observed in more than one setup and are analysed by several WGs. These so-called intercalibration clusters give a solid basis to perform the comparison of the results between different WGs and different setups. The best example is the open cluster NGC 6705 analysed by the four WGs as noted above. For both open and globular cluster, an important check is to estimate qualitatively the agreement with a theoretical isochrone (PARSEC).

The homogenisation and the offsets applied to the different WGs results follow a sequence described in detail in Hourihane & et al, (2022). If a star has results in more than one WG, then the selection of the recommended set of parameters is based on the setup used and/or the competence of each on the analyses on that type of star. An example is that the results for stars with $T_{eff} \geq 7000K$ all come from WG13. Another example is to give priority to the results coming from UVES over GIRAFFE spectra. For multiple exposures of the same benchmark stars, we have selected the one with the highest signal-to-noise ratio (S/N).

10.2. Abundance homogenisation

The task of the abundance homogenisation is based on the determination of the offsets in the abundances of the individual elements between the different WGs. Stars in common between WGs or cluster member stars observed by several WGs are used to evaluate these offsets.

The abundances were determined by the analysis nodes and WGs based on the recommended parameters that were the product of the WG15 homogenisation. As the large wavelength range and the high resolution of the UVES spectrograph permit a more precise determination of the stellar parameters and abundances than GIRAFFE spectra, the homogenisation process for the WG10 abundances uses the WG11 results as the baseline. WG13 results are treated separately as the hot stars are suspected to have abundance anomalies and do not follow the general trends found in FGK stars. The lithium abundance is also treated separately. For the other elements, the first step is to check the solar and the benchmark abundances and look for possible offsets with respect to the literature values. The abundances measured in the stars in common between WGs are then compared to check for possible offsets. The abundance ratios vs $[Fe/H]$ determined in the open clusters (both calibration and science open clusters) are then computed for the different WGs to check for anomalies. The same work is also performed on globular clusters. Median elemental differences between WG10 and WG11 are determined and used to find offsets and/or trends as a function of metallicity. The Milky Way stars abundances are also compared to literature data (Bensby et al. 2014; Battistini & Bensby 2015, 2016; Reddy et al. 2006; Pereira et al. 2017; Takeda et al. 2016) and checked for offsets and trends as a function of metallicity.

10.3. Radial velocity homogenisation

The Gaia Radial Velocity standard stars have been investigated as part of the homogenisation of the Gaia-ESO radial velocities and the Gaia-ESO HR10 RVs have been found to have zero offset from the reference values for these stars (Soubiran et al. 2018). Therefore, HR10 RVs were taken as the zero point for the Gaia-ESO RVs. The HR10 RVs come from the pipeline of Sect 8. Only RVs from the stacked, singlespec spectra from which the

stellar parameters and abundances were determined are considered here. For investigation of the RV variations between individual or nightly stacked spectra, see Jackson et al. (2015) and Sect 9.5.3.

Offsets were calculated between each of the setups and the zeropoint of the Gaia-ESO RV scale, HR10. The offsets were then applied to put the other setups onto the HR10 scale. For WG13, RVs have been based on a combination of WG13 setups.

Where the HR10 setup was not available, the radial velocity was sourced from the same setup as that from which the parameters were selected. Potential offsets were applied when the RVs were taken from a different setup to HR10. These offsets are calculated on the basis of stars in common between the setups. The order of priority in which RVs from the different setups were selected was: HR10, HR15N, U580, HR21, HR9B, HR3, HR5A, HR6, HR14A, HR14B, U520, HR4, HR5B.

10.4. Flag homogenisation

The homogenisation is based on the dictionary of flags produced by WG14. We compared the flags produced by the different WGs and searched for possible conflicts. In general, all the flags from the WG Recommended files are included with any duplicates removed. Details can be found in Hourihane & et al, (2022).

11. Survey progress monitoring and data publication (WG16, WG17, WG18)

Survey progress monitoring is a major task, sufficiently critical to efficient survey progress that the relevant WG (WG16) was led by the Co-PIs directly, ably supported by the dedicated Project Office team. Survey progress is a complex mix of management, communications, and book-keeping. Management involves monitoring the progress of all WGs involved in data preparation, processing, and analysis. The key aspect for this WG was the book-keeping. Reliable and quantitative information must track, for every target star, the number of observations attempted, achieved, and still awaited. The processing status of each observation must be tracked, and updated as each WG deposits data in the operational database. SNR data for each spectrum, SNR data for each object, including repeats and different settings, and necessary additional information prior to object readiness for science analysis, must all be maintained for all 10^5 targets. For the clusters the same information must be maintained both for the individual targets and for the clusters as a whole. In particular, the fractional completion of data taking and processing for each cluster must be tracked.

Internal data management of data products was designed around the ESO FITS raw data structure. The extracted, wavelength calibrated and sky subtracted spectra are in a 2d "image" with the corresponding fibre information in binary table extensions. Processing and quality control information is propagated through the FITS header. The outputs from all later stages of processing are incorporated in further binary table extensions. This model, where all relevant information about an observation is kept in the same container file, was developed by the Cambridge Astronomical Survey Unit (CASU) team for the VISTA pipelines, and cuts bookkeeping tasks down to a minimum.

11.1. Operational database (WG17)

The Gaia-ESO project utilised both an operational database, based in Cambridge at CASU, and a dedicated archive, based in Edinburgh, to hold all relevant information, to complement the primary public stable archive, which is that of ESO. This approach builds on the operational VISTA (and other projects) systems hosted at CASU, Cambridge, and at the Wide Field Astronomy Unit (WFAU), Edinburgh. It is a proven and successful model, and proved essential to support the survey data flow. In particular, this approach kept separate the day-to-day processing, the spectrum analyses, and all activities in which data are being determined or updated, from all those science activities which should be based on readily accessible static information.

The operational database held all data while it remained incomplete, or subject to change. All observation preparation WGs submitted all relevant data associated with target selection, up to and including OB preparation, to the operational database [WG1-WG6]. Raw data from ESO were added. Pipelines [WG7-WG9] operated on the raw data, generated pipeline reduced and extracted spectra, with associated variances, quality control (QC) info, RVs and classification outputs, and wrote these back to the operational database. An aspect of the QC is the quantitative SNR data, also supplied to ESO through the regular survey progress reports. Spectrum analysis groups [WG10-WG15] read, but do not modify, these spectra, carry out their analyses, and deliver back FITS-table results to the operational database. These tables are attached to each relevant spectrum, allowing the progress monitor to be updated.

Subsequent processing stages collated and incorporated available existing information such as photometric indices, proper motions, and also appended derived radial velocities and stellar atmosphere parameters in additional FITS table extensions. Further processing stages involving common tasks such as continuum estimation and normalisation to unity are readily incorporated by including extra FITS extensions. The philosophy is to keep the same file architecture throughout and minimise bookkeeping and versioning issues by always attaching information directly to the files. This also has the advantage of removing direct dependency on availability of access to external databases. To minimise resampling of spectra we also maintained extracted spectra in natural units (e.g. pixel-based fluxes) and use FITS table extensions and/or FITS header information to specify conversions to physical units, should this ever be appropriate and required, and/or to zero-velocity systems.

We use the Gaia DPAC model - all data are stored in the central repository, taken out for use/analysis, and have parameters returned. No process adjusts the spectra, except by resetting the master spectrum if needed when the whole process restarts from scratch. No data processing WG talks directly to the archive. When the spectrum teams agree their job is converged for some source, all relevant data become fixed.

At this stage all data are copied to the permanent Gaia-ESO archive, hosted at WFAU Edinburgh, and become available internally to the survey consortium to begin science quality control.

11.2. Internal survey archive (WG18)

After pipeline processing, including atmospheric parameter and abundance determination etc., the spectroscopic survey data were made available to the consortium for quality control, science verification and preliminary analysis via a bespoke archive

system. This system acts not only as the 'internal' archive system for the consortium, but also as a publicly accessible portal that provides enhanced database–driven products to facilitate world community exploitation of prepared static releases of survey data. Metadata associated with the products available in the archive complies with the corresponding VO Data Models, in particular with the VO Spectrum Data Model. This follows the tried–and–tested Vista Data Flow System (VDFS) model developed by Cambridge and Edinburgh, for UKIRT–WFCAM, VISTA-VIRCam and VST survey data, and supports both internal team science verification, and provides a global archive system complementary to that provided by ESO.

The Gaia-ESO Survey archive design follows proven models, and includes the following features:

- back–end relational database management system store
- a near–normalised relational design to track all data, metadata and provenance through the pipeline and subsequent analysis stages
- simple interface applications for the novice user
- tabular data (i.e. catalogues) available through ConeSearch protocols
- SQL interface and relational model exposed to users through interactive web forms for more complicated usage scenarios
- integration of multi–wavelength catalogue data and image thumbnails
- publication of spectroscopic data to the VO through the Simple Spectral Access Protocol
- publication of all tabular data (e.g. input catalogues, derived physical quantities for targets etc.) to the VO through the Table Access Protocol (thereby making them accessible to sophisticated client–side exploration and analysis utilities such as TOPCAT)
- finally, cross-linking to the Gaia EDR3 star identifications is provided in the ESO SAF, while updated cross-matching to the Gaia-ESO CNAME identifiers will be provided as a Gaia data product with future Gaia data releases.

The internal CASU Gaia-ESO archive is hosted at Cambridge/CASU. [7]

The public Gaia-ESO Survey archive is Edinburgh/WFAU. [8]

The primary public data archive is the ESO Science Archive Facility. [9]

12. Gaia-ESO Survey public data products

This section introduces the final data release content. A fuller description of this is provided in the companion paper (Randich et al. 2022), while the detailed final set of homogenisation processes is described in the WG15 paper Hourihane & et al, (2022).

All spectra and derived parameters and abundances are available through the ESO Science Archive Facility [10] and the dedicated WFAU portal. [11]

Preliminary data releases have been available through these archives during the survey. The set of reduced spectra, apart from data for 592 objects now also released, have been available through the ESO SAF since December 2020.

[7] http://casu.ast.cam.ac.uk/gaiaeso/
[8] http://ges.roe.ac.uk/
[9] http://archive.eso.org/cms.html
[10] http://archive.eso.org/cms/data-portal.html
[11] http://ges.roe.ac.uk/pubs.html

Summary survey statistics are provided here in Table 16 for the relative numbers of survey and archive spectra, Table 17 for the total number of spectra by spectrograph setup, and Table 18 for the cross-matches between setups.

The survey yielded 185795 GIRAFFE spectra for 108473 unique stars and 16438 UVES spectra for 7141 stars (see Table 16) , most of which were observed at two different epochs. The products delivered at the end of the survey include all the extracted spectra, with relevant ancillary information, and value added deliverables.

Each source has a unique CNAME identifier, in standard coordinate format, and is cross-matched to the Gaia EDR3 identifiers. The Gaia cross-match will be maintained as part of future Gaia data releases.

The final data release includes, for all targets with completed observations:

Advanced Data Products - reduced data These are the outputs of Working Groups 0-9.

- One-dimensional, wavelength calibrated, sky-subtracted, normalised, UVES and/or GIRAFFE spectra for each survey target. Where no RV variability is detected, co-added sum spectra are provided, in addition to single-epoch spectra. UVES spectra are provided as sets of single echelle orders and a merged spectrum
- The associated variance spectrum
- Associated quality control information
- Supplementary value-added data include:
- The photometry (and additional membership information for clusters) used to select the targets
- The class of target - cluster, standard, etc
- Selected matched multi-wavelength photometric data where available
- Object classification
- Radial velocity and its error distribution function
- Analysis for RV variability
- Projected rotational velocity and error estimate (where relevant)

Advanced Data Products - astrophysical parameters Advanced data products from expanded and refined spectral analysis, calibrated using the current Gaia-ESO calibrations. These are the outputs of iterative homogenisation and quality control involving Working Groups 10-15, and survey consortium science verification analysis.

- Whenever possible stellar astrophysical parameters: effective temperature, surface gravity
- Whenever possible stellar metallicity [Fe/H]
- Whenever possible [α/Fe] ratios
- Measurements of stellar activity or mass accretion/ejection rates, for cluster members (where relevant)
- Quantitative mass loss estimates, for early-type stars
- Elemental abundances, with the specific elements depending on target type.
- Quantitative uncertainties on the delivered quantities, derived from the multiple reduction systems implemented

The final data-release includes homogenised values for all deliverables listed above for all stars, calibrated onto the final Gaia-ESO calibration system. Halpha, tSNE and BIN flags are

Table 16: Gaia-ESO Survey Final Data Set: numbers of spectra

	Gaia-ESO	ESO Archive	Total Spectra
UVES	14484	1954	16438
GIRAFFE	178698	7097	185795
TOTAL	193182	9051	202233

Table 17: Gaia-ESO Survey Final Data Set: numbers of unique sources by setup

Total	U580	U520	HR10	HR21	HR15N	HR3	HR4	HR5A	HR5B	HR6	HR9B	HR14A	HR14B
115614	6641	500	59722	66542	40973	2228	1253	2072	107	2121	3873	2252	107

Table 18: Gaia-ESO Survey Final Data Set: number of cross-matches by setup

	U520	HR10	HR21	HR15N	HR3	HR4	HR5A	HR5B	HR6	HR9B	HR14A	HR14B
U580	110	171	249	869	31	9	26	1	26	162	70	1
U520	-	55	61	77	22	0	22	1	22	104	22	1
HR10	-	-	58354	3834	181	167	181	1	181	253	211	1
HR21	-	-	-	3805	181	167	181	1	181	253	211	1
HR15N	-	-	-	-	259	245	259	1	259	794	286	1
HR3	-	-	-	-	-	1250	2069	107	2114	468	2045	107
HR4	-	-	-	-	-	-	1198	106	1249	289	1185	106
HR5A	-	-	-	-	-	-	-	57	2066	469	2046	57
HR5B	-	-	-	-	-	-	-	-	107	55	57	107
HR6	-	-	-	-	-	-	-	-	-	471	2047	107
HR9B	-	-	-	-	-	-	-	-	-	-	481	55
HR14A	-	-	-	-	-	-	-	-	-	-	-	57

allocated to 20,019, 17,408 and 1865 sources respectively. Elemental abundance determinations are provided as listed in Table 19. Note that in the final abundance release, we do not provide Fe1 and Fe2 abundances and we leave only [Fe/H] to indicate the iron abundance. The [Fe/H] parameter is homogenised together with the other stellar parameters ($T_{\rm eff}$, $\log g$, [Fe/H], ξ, $v \sin i$), while Fe1 and Fe2 are re-computed by Nodes keeping the input stellar parameters fixed. Since the stellar parameters, including [Fe/H], are homogenised using external calibrators, in some cases, the recomputed abundances do not completely fulfill the ionization balance, and there might be differences in Fe1 and Fe2 (in some specific areas of the parameter space, in particular at high metallicity). To avoid misleading results, we provide only [Fe/H].

Discussion of the astrophysical quality and value of the parameters is described in Randich et al. (2022), while an analysis of the precision of the parameters, and external comparisons is in Hourihane & et al, (2022). An example of the power of combining Gaia-ESO and Gaia information in astrophysical analyses is provided by Jackson et al. (2022), who provide membership analysis for 63 open clusters and 7 globular clusters.

13. Conclusions

The Gaia-ESO Public Spectroscopic Survey has been a large ambitious VLT spectroscopic survey of representative samples of the main Galactic stellar populations. One primary aim was to provide high-quality astrophysical parameters, radial velocities to complement Gaia kinematics, and elemental abundances for stars of all accessible ages and abundances, with parameters firmly anchored to open and globular clusters. This links field star properties to tested isochrones, establishing a basis to map temporal as well as spatial evolution in the Galaxy. A second aim was to provide consistent-quality spectroscopic studies of a large sample of open clusters, mapping accessible age-metallicity-location space. For each cluster a wide mass-range is accessed, linking the complementary analysis approaches required for hot and cool stars, (pre-)main sequence and evolved, ensuring consistency. A third aim was to provide a large sample, of order 10^5, field stars, sufficient to map populations across chemical abundance and kinematic properties. A fourth aim was to establish a robust set of calibration stars, suitable for use both in Gaia calibration, and for cross-calibrations between the several recent, current or planned stellar spectroscopic surveys and asteroseismic projects. Another ambition was to bring together the many European stellar spectroscopy groups into successful partnership, providing a robust community foundation for those forthcoming survey projects. Finally, a requirement is that all the data, calibrated spectra and derived parameters, be available in a free public archive for future uses.

Gaia-ESO succeeded in all these ambitions. The ambitious target of 10^5 field stars and $\sim$ 60 open clusters were surveyed, with 114325 stars and 62 open clusters newly surveyed. A very wide range of parameter space was mapped. Substantial scientific advances have been made, with over 100 team science verification refereed papers already published. The spectra are already widely accessed from the ESO SAF, with the astrophysical parameters now also available. The community did come together, learning how to homogenise data from very many different analysis pipelines in a way consistent with the primary

Table 19: Gaia-ESO Survey Final Data Set: elemental abundances determined

He1	C1	C2	C3	C-C2	N2	N3
N-CN	O1	O2	Ne1	Na1	Mg1	Mg2
Al1	Al2	Si1	Si2	Si3	Si4	S1
Ca1	Ca2	Sc1	Sc2	Ti1	Ti2	V1
Cr1	Cr2	Mn1	Co1	Ni1	Cu1	Zn1
Sr1	Y2	Zr1	Zr2	Mo1	Ba2	La2
Ce2	Pr2	Nd2	Sm2	Eu2		

Gaia Benchmark Star calibrations. A community of some 400 scientists from more than 110 institutions came together to deliver the survey. Significant scientific results have already been delivered, some of which are presented in the companion paper Randich et al. (2022).

Acknowledgements. Based on data products from observations made with ESO Telescopes at the La Silla Paranal Observatory under programme ID 188.B-3002. These data products have been processed by the Cambridge Astronomy Survey Unit (CASU) at the Institute of Astronomy, University of Cambridge, and by the FLAMES/UVES reduction team at INAF/Osservatorio Astrofisico di Arcetri. Public access to the data products is via the ESO SAF, and the Gaia-ESO Survey Data Archive, prepared and hosted by the Wide Field Astronomy Unit, Institute for Astronomy, University of Edinburgh, which is funded by the UK Science and Technology Facilities Council. This work was partly supported by the European Union FP7 programme through ERC grant number 320360 and by the Leverhulme Trust through grant RPG-2012-541. We acknowledge the support from INAF and Ministero dell' Istruzione, dell' Università' e della Ricerca (MIUR) in the form of the grant "Premiale VLT 2012". The project presented here benefited in development from discussions held during the Gaia-ESO workshops and conferences supported by the ESF (European Science Foundation) through the GREAT Research Network Programme. This research has made use of the SIMBAD database, operated at CDS, Strasbourg, France. R.Smiljanic acknowledges support from the National Science Centre, Poland (2014/15/B/ST9/03981). This work was partly supported by the INAF grant for mainstream projects: "Enhancing the legacy of the Gaia-ESO Survey for open cluster science". F.J.E. acknowledges financial support from the Spanish MINECO/FEDER through the grant AYA2017-84089 and MDM-2017-0737 at Centro de Astrobiología (CSIC-INTA), Unidad de Excelencia María de Maeztu, and from the European Union's Horizon 2020 research and innovation programme under Grant Agreement no. 824064 through the ESCAPE - The European Science Cluster of Astronomy and Particle Physics ESFRI Research Infrastructures project. T.B. was funded by the "The New Milky Way" project grant from the Knut and Alice Wallenberg Foundation. S.R.B. acknowledges support by the Spanish Government under grants AYA2015-68012-C2-2-P and PGC2018-093741-B-C21/C22 (MICIU/AEI/FEDER, UE). W. J. S. acknowledges CAPES for a PhD studentship. J.M.A. acknowledges support from the Spanish Government Ministerio de Ciencia e Innovación through grants AYA2013-40611-P, AYA2016-75931-C2-2-P, and PGC2018-095049-B-C22. T.M. and others from STAR institute, Liege, Belgium are grateful to Belgian F.R.S.-FNRS for support, and are also indebted for an ESA/PRODEX Belspo contract related to the Gaia Data Processing and Analysis Consortium and for support through an ARC grant for Concerted Research Actions financed by the Federation Wallonie-Brussels.. This research has been partially supported by the following grants: MIUR Premiale "Gaia-ESO survey" (PI S. Randich), MIUR Premiale "MiTiC: Mining the Cosmos" (PI B. Garilli), the ASI-INAF contract 2014-049-R.O: "Realizzazione attività tecniche/scientifiche presso ASDC" (PI Angelo Antonelli), Fondazione Cassa di Risparmio di Firenze, progetto: "Know the star, know the planet" (PI E. Pancino), and Progetto Main Stream INAF: "Chemo-dynamics of globular clusters: the Gaia revolution" (PI E. Pancino). V.A.acknowledges the support from Fundação para a Ciência e Tecnologia (FCT) through Investigador FCT contract nr. IF/00650/2015/CP1273/CT0001. AJK acknowledges support by the Swedish National Space Agency (SNSA). AB acknowledges support by ANID, – Millennium Science Initiative Program – NCN19_171, and FONDECYT regular 1190748. E. M. acknowledges financial support from the Spanish State Research Agency (AEI) through project MDM-2017-0737 Unidad de Excelencia "María de Maeztu" - Centro de Astrobiología (CSIC-INTA). T.Z. acknowledges financial support of the Slovenian Research Agency (research core funding No. P1-0188) and the European Space Agency (Prodex Experiment Arrangement No. C4000127986). P.J. acknowledges support FONDECYT Regular 1200703. The work of I.N. is partially supported by the Spanish Government Ministerio de Ciencia, Innovación y Universidades under grant PGC2018-093741-B-C21 (MICIU/AEI/FEDER, UE). Funding for this work has been provided by the ARC Future Fellowship FT160100402. CAP acknowledges financial support from the Spanish Government through research grants MINECO AYA 2014-56359-P, MINECO AYA2017-86389-P, and MICINN PID2020-117493GB-I00. S.F. was supported by the grants 2011-5042 and 2016- 03412 from the Swedish Research Council and the project grant "The New Milky Way" from the Knut and Alice Wallenberg Foundation. CASU is supported through STFC grants: ST/H004157/1, ST/J00541X/1, ST/M007626/1, ST/N005805/1, ST/T003081/1. Work reported here benefited from support through the GREAT-ITN FP7 project Grant agreement ID: 264895. DKF acknowledges funds from the Alexander von Humboldt Foundation in the framework of the Sofja Kovalevskaja Award endowed by the Federal Ministry of Education and Research and the grant 2016-03412 from the Swedish Research Council. A.H. acknowledges support from the Spanish Government Ministerio de Ciencia e Innovación and ERD Funds through grants PGC-2018-091 3741-B-C22 and CEX2019-000920-S. X.F. acknowledge the support of China Postdoctoral Science Foundation 2020M670023. M. L. L. Dantas acknowledges the Polish NCN grant number 2019/34/E/ST9/00133. Part of this work was funded by the Deutsche Forschungsgemeinschaft (DFG, German Research Foundation) – Project-ID 138713538 – SFB 881 ("The Milky Way System", subproject A09). MZ acknowledge support from the National Agency for Research and Development (ANID) grants: FONDECYT Regular 1191505, Millennium Institute of Astrophysics ICN12-009, BASAL Center for Astrophysics and Associated Technologies AFB-170002. R.B. acknowledges support from the project PRIN-INAF 2019 "Spectroscopically Tracing the Disk Dispersal Evolution". HMT acknowledges financial support from the Agencia Estatal de Investigación of the Ministerio de Ciencia, Innovación y Universidades through projects PID2019-109522GB-C51,54/AEI/10.13039/501100011033, and the Centre of Excellence "María de Maeztu" award to Centro de Astrobiología (MDM-2017-0737). JIGH acknowledges financial support from the Spanish Ministry of Science and Innovation (MICINN) project AYA2017-86389-P, and also from the Spanish MICINN under 2013 Ram©n y Cajal program RYC-2013-14875. V.P.D. is supported by STFC Consolidated grant ST/R000786/1. N.L. acknowledges financial support from "Programme National de Physique Stellaire" (PNPS) and the "Programme National Cosmology et Galaxies (PNCG)" of CNRS/INSU, France. A. R. C. is supported in part by the Australian Research Council through a Discovery Early Career Researcher Award (DE190100656). Parts of this research were supported by the Australian Research Council Centre of Excellence for All Sky Astrophysics in 3 Dimensions (ASTRO 3D), through project number CE170100013. PSB is Supported by the Swedish Research Council through individual project grants with contract Nos. 2016-03765 and 2020-03404. AM acknowledges funding from the European Research Council (ERC) under the European Union's Horizon 2020 research and innovation programme (grant agreement No. 772293 - project ASTEROCHRONOMETRY). JP was supported by the project RVO: 67985815. E.D.M. acknowledges the support from FCT through the research grants UIDB/04434/2020 & UIDP/04434/2020 and through Investigador FCT contract IF/00849/2015/CP1273/CT0003. This work was (partially) supported by the Spanish Ministry of Science, Innovation and University (MICIU/FEDER, UE) through grant RTI2018-095076-B-C21, and the Institute of Cosmos Sciences University of Barcelona (ICCUB, Unidad de Excelencia 'María de Maeztu') through grant CEX2019-000918-M. SLM acknowledges the support of the UNSW Scientia Fellowship program and the Australian Research Council through Discovery Project grant DP180101791. GT acknowledges financial support of the Slovenian Research Agency (research core funding No. P1-0188) and the European Space Agency (Prodex Experiment Arrangement No. C4000127986). S.G.S acknowledges the support from FCT through Investigador FCT contract nr. CEECIND/00826/2018 and POPH/FSE (EC). H.G.L. acknowledges financial support by the Deutsche Forschungsgemeinschaft (DFG, German Research Foundation) – Project-ID 138713538 – SFB 881 ("The Milky Way System", subproject A04). This work was (partially) supported by the Spanish Ministry of Science, Innovation and University (MICIU/FEDER, UE) through grant RTI2018-095076-B-C21, and the Institute

of Cosmos Sciences University of Barcelona (ICCUB, Unidad de Excelencia 'María de Maeztu') through grant CEX2019-000918-M. T.K. is supported by STFC Consolidated grant ST/R000786/1. MV acknowledges the support of the Deutsche Forschungsgemeinschaft (DFG, project number: 428473034). T.M. is supported by a grant from the Fondation ULB. We acknowledge financial support from the Universidad Complutense de Madrid (UCM) and by the Spanish Ministerio de Ciencia, Innovación y Universidades, Ministerio de Economía y Competitividad, from project AYA2016-79425-C3-1-P and PID2019-109522GB-C5[4]/AEI/10.13039/501100011033. U.H. acknowledges support from the Swedish National Space Agency (SNSA/Rymdstyrelsen). D.G. gratefully acknowledges support from the Chilean Centro de Excelencia en Astrofísica y Tecnologías Afines (CATA) BASAL grant AFB-170002. D.G. also acknowledges financial support from the Dirección de Investigación y Desarrollo de la Universidad de La Serena through the Programa de Incentivo a la Investigación de Académicos (PIA-DIDULS). A. Lobel acknowledges support in part by the Belgian Federal Science Policy Office under contract No. BR/143/A2/BRASS. We acknowledge financial support from the Universidad Complutense de Madrid (UCM) and by the Spanish Ministerio de Ciencia, Innovación y Universidades, Ministerio de Economía y Competitividad, from project AYA2016-79425-C3-1-P and PID2019-109522GB-C5[4]/AEI/10.13039/501100011033. AM acknowledges the support from the Portuguese Fundação para a Ciência e a Tecnologia (FCT) through the Portuguese Strategic Programme UID/FIS/00099/2019 for CENTRA. TM acknowledges financial support from the Spanish Ministry of Science and Innovation (MICINN) through the Spanish State Research Agency, under the Severo Ochoa Program 2020-2023 (CEX2019-000920-S). EJA acknowledges funding from the State Agency for Research of the Spanish MCIU through the "Center of Excellence Severo Ochoa" award to the Instituto de Astrofisica de An- dalucia (SEV-2017-0709).

References

Ahn, C. P., Alexandroff, R., Allende Prieto, C., et al. 2014, ApJS, 211, 17
Allende Prieto, C., Fernández-Alvar, E., Schlesinger, K. J., et al. 2014, A&A, 568, A7
Allende Prieto, C., Sivarani, T., Beers, T. C., et al. 2008, AJ, 136, 2070
Alvarez, R. & Plez, B. 1998, A&A, 330, 1109
Asplund, M., Grevesse, N., & Jacques Sauval, A. 2006, Nucl. Phys. A, 777, 1
Asplund, M., Grevesse, N., Sauval, A. J., & Scott, P. 2009, ARA&A, 47, 481
Battistini, C. & Bensby, T. 2015, A&A, 577, A9
Battistini, C. & Bensby, T. 2016, A&A, 586, A49
Bensby, T., Adén, D., Meléndez, J., et al. 2011, A&A, 533, A134
Bensby, T., Feltzing, S., & Oey, M. S. 2014, A&A, 562, A71
Blanco-Cuaresma, S., Soubiran, C., Jofré, P., & Heiter, U. 2014, A&A, 566, A98
Bland-Hawthorn, J., Krumholz, M. R., & Freeman, K. 2010, ApJ, 713, 166
Blomme, R., Daflon, S., Gebran, M., et al. 2022, arXiv e-prints, arXiv:2202.08662
Bonito, R., Prisinzano, L., Venuti, L., et al. 2020, A&A, 642, A56
Bragaglia, A., Alfaro, E. J., Flaccomio, E., et al. 2022, A&A, 659, A200
Butler, K. 1984, PhD thesis, UNIVERSITY OF LONDON, UK
Cantat-Gaudin, T., Donati, P., Pancino, E., et al. 2014, A&A, 562, A10
Casali, G., Magrini, L., Tognelli, E., et al. 2019, A&A, 629, A62
Castelli, F. & Kurucz, R. L. 2003, in IAU Symposium, Vol. 210, Modelling of Stellar Atmospheres, ed. N. Piskunov, W. W. Weiss, & D. F. Gray, A20
Cirasuolo, M., Fairley, A., Rees, P., et al. 2020, The Messenger, 180, 10
Cui, X.-Q., Zhao, Y.-H., Chu, Y.-Q., et al. 2012, Research in Astronomy and Astrophysics, 12, 1197
Dalton, G. 2016, in Astronomical Society of the Pacific Conference Series, Vol. 507, Multi-Object Spectroscopy in the Next Decade: Big Questions, Large Surveys, and Wide Fields, ed. I. Skillen, M. Balcells, & S. Trager, 97
Damiani, F., Prisinzano, L., Micela, G., et al. 2014a, A&A, 566, A50
Damiani, F., Prisinzano, L., Micela, G., et al. 2014b, A&A, 566, A50
David, M., Blomme, R., Frémat, Y., et al. 2014, A&A, 562, A97
de Jong, R. S., Agertz, O., Berbel, A. A., et al. 2019, The Messenger, 175, 3
de Laverny, P., Recio-Blanco, A., Worley, C. C., et al. 2013, The Messenger, 153, 18
de Laverny, P., Recio-Blanco, A., Worley, C. C., & Plez, B. 2012, A&A, 544, A126
De Silva, G. M., Freeman, K. C., Bland-Hawthorn, J., et al. 2015, MNRAS, 449, 2604
Franchini, M., Morossi, C., Di Marcantonio, P., et al. 2018, ApJ, 862, 146
Franciosini, E., Tognelli, E., Degl'Innocenti, S., et al. 2022, A&A, 659, A85
Frasca, A., Alcalá, J. M., Covino, E., et al. 2003, A&A, 405, 149
Frasca, A., Guillout, P., Marilli, E., et al. 2006, A&A, 454, 301
Freeman, K. & Bland-Hawthorn, J. 2002, ARA&A, 40, 487
Gaia Collaboration, Prusti, T., de Bruijne, J. H. J., et al. 2016, A&A, 595, A1
Gavel, A., Gruyters, P., Heiter, U., et al. 2019, A&A, 629, A74
Gebran, M., Farah, W., Paletou, F., Monier, R., & Watson, V. 2016, A&A, 589, A83
Gilmore, G., Norris, J. E., Monaco, L., et al. 2013, ApJ, 763, 61
Gilmore, G., Randich, S., Asplund, M., et al. 2012, The Messenger, 147, 25
Grevesse, N., Asplund, M., & Sauval, A. J. 2007, Space Sci. Rev., 130, 105
Guiglion, G., de Laverny, P., Recio-Blanco, A., et al. 2016, A&A, 595, A18
Gustafsson, B., Edvardsson, B., Eriksson, K., et al. 2008, A&A, 486, 951
Hartigan, P., Hartmann, L., Kenyon, S., Hewett, R., & Stauffer, J. 1988, in Bulletin of the American Astronomical Society, Vol. 20, 1092
Hawkins, K., Jofré, P., Heiter, U., et al. 2016a, A&A, 592, A70
Hawkins, K., Masseron, T., Jofré, P., et al. 2016b, A&A, 594, A43
Heiter, U., Jofré, P., Gustafsson, B., et al. 2015, A&A, 582, A49
Heiter, U., Lind, K., Bergemann, M., et al. 2021, A&A, 645, A106
Hillier, D. J. & Miller, D. L. 1998, ApJ, 496, 407
Hourihane, A. P. & et al,. 2022, in preparation
Hubeny, I. & Lanz, T. 1992, A&A, 262, 501
Hubeny, I. & Lanz, T. 1995, ApJ, 439, 875
Hubeny, I. & Lanz, T. 2017, arXiv e-prints, arXiv:1706.01859
Jackson, R. J., Jeffries, R. D., Lewis, J., et al. 2015, A&A, 580, A75
Jackson, R. J., Jeffries, R. D., Wright, N. J., et al. 2022, MNRAS, 509, 1664
Jofré, P., Heiter, U., & Buder, S. 2017a, in Astronomical Society of India Conference Series, Vol. 14, Astronomical Society of India Conference Series, 37–44
Jofré, P., Heiter, U., & Soubiran, C. 2019, ARA&A, 57, 571
Jofré, P., Heiter, U., Soubiran, C., et al. 2015, A&A, 582, A81
Jofré, P., Heiter, U., Soubiran, C., et al. 2014, A&A, 564, A133
Jofré, P., Heiter, U., Tucci Maia, M., et al. 2018, Research Notes of the American Astronomical Society, 2, 152
Jofré, P., Heiter, U., Worley, C. C., et al. 2017b, A&A, 601, A38
Kang, W. & Lee, S.-G. 2012, MNRAS, 425, 3162
Kassounian, S., Gebran, M., Paletou, F., & Watson, V. 2019, Open Astronomy, 28, 68
Kirby, E. N., Guhathakurta, P., Bolte, M., Sneden, C., & Geha, M. C. 2009, ApJ, 705, 328
Koposov, S. E., Casey, A. R., Belokurov, V., et al. 2015, ApJ, 811, 62
Koposov, S. E., Gilmore, G., Walker, M. G., et al. 2011, ApJ, 736, 146
Kormendy, J., Drory, N., Bender, R., & Cornell, M. E. 2010, ApJ, 723, 54
Korotin, S., Andrievsky, S., Caffau, E., & Bonifacio, P. 2017, in Astronomical Society of the Pacific Conference Series, Vol. 510, Stars: From Collapse to Collapse, ed. Y. Y. Balega, D. O. Kudryavtsev, I. I. Romanyuk, & I. A. Yakunin, 141
Kovalev, M., Bergemann, M., Ting, Y.-S., & Rix, H.-W. 2019, A&A, 628, A54
Kurucz, R. L. 1992, Rev. Mexicana Astron. Astrofis., 23
Kurucz, R. L. 1993, in Astronomical Society of the Pacific Conference Series, Vol. 44, IAU Colloq. 138: Peculiar versus Normal Phenomena in A-type and Related Stars, ed. M. M. Dworetsky, F. Castelli, & R. Faraggiana, 87
Lanz, T. & Hubeny, I. 2007, ApJS, 169, 83
Lanzafame, A. C., Frasca, A., Damiani, F., et al. 2015, A&A, 576, A80
Lee, Y. S., Beers, T. C., Sivarani, T., et al. 2008a, AJ, 136, 2022
Lee, Y. S., Beers, T. C., Sivarani, T., et al. 2008b, AJ, 136, 2050
Lobel, A. 2011, Canadian Journal of Physics, 89, 395
Magrini, L., Randich, S., Friel, E., et al. 2013, A&A, 558, A38
Marsh, T. R. 1989, PASP, 101, 1032
Masseron, T. & et al. 2022, in preparation
McMahon, R. G., Banerji, M., Gonzalez, E., et al. 2013, The Messenger, 154, 35
Merle, T., Van der Swaelmen, M., Van Eck, S., et al. 2020, A&A, 635, A155
Merle, T., Van Eck, S., Jorissen, A., et al. 2017, A&A, 608, A95
Morel, T. & Butler, K. 2008, A&A, 487, 307
Morel, T., Butler, K., Aerts, C., Neiner, C., & Briquet, M. 2006, A&A, 457, 651
Natta, A., Testi, L., Muzerolle, J., et al. 2004, A&A, 424, 603
Nissen, P. E. 2013, Chemical Abundances as Population Tracers, ed. T. D. Oswalt & G. Gilmore, Vol. 5, 21
Nissen, P. E. & Gustafsson, B. 2018, A&A Rev., 26, 6
Nissen, P. E. & Schuster, W. J. 2010, A&A, 511, L10
Norris, J. E., Wyse, R. F. G., Gilmore, G., et al. 2010a, ApJ, 723, 1632
Norris, J. E., Yong, D., Gilmore, G., & Wyse, R. F. G. 2010b, ApJ, 711, 350
Paletou, F., Gebran, M., Houdebine, E. R., & Watson, V. 2015, A&A, 580, A78
Pancino, E., Lardo, C., Altavilla, G., et al. 2017a, A&A, 598, A5
Pancino, E., Romano, D., Tang, B., et al. 2017b, A&A, 601, A112
Pasquini, L., Avila, G., Blecha, A., et al. 2002, The Messenger, 110, 1
Peebles, P. J. E., Tully, R. B., & Shaya, E. J. 2011, arXiv e-prints, arXiv:1105.5596
Pereira, S. H., Holanda, R. F. L., & Souza, A. P. S. 2017, EPL (Europhysics Letters), 120, 31001
Piatti, A. E. 2019, Research Notes of the American Astronomical Society, 3, 104
Piskunov, N. & Valenti, J. A. 2017, A&A, 597, A16
Prugniel, P. & Soubiran, C. 2001, A&A, 369, 1048
Puls, J., Kudritzki, R. P., Herrero, A., et al. 1996, A&A, 305, 171

Puls, J., Urbaneja, M. A., Venero, R., et al. 2005, A&A, 435, 669
Puspitarini, L., Lallement, R., Babusiaux, C., et al. 2015, A&A, 573, A35
Randich, S., Gilmore, G., & et al. 2022, companion paper
Randich, S., Gilmore, G., & Gaia-ESO Consortium. 2013, The Messenger, 154, 47
Randich, S., Tognelli, E., Jackson, R., et al. 2018, A&A, 612, A99
Recio-Blanco, A., Bijaoui, A., & de Laverny, P. 2006, MNRAS, 370, 141
Recio-Blanco, A., de Laverny, P., Kordopatis, G., et al. 2014, A&A, 567, A5
Reddy, B. E., Lambert, D. L., & Allende Prieto, C. 2006, MNRAS, 367, 1329
Reddy, B. E., Tomkin, J., Lambert, D. L., & Allende Prieto, C. 2003, MNRAS, 340, 304
Ruffoni, M. P., Den Hartog, E. A., Lawler, J. E., et al. 2014, MNRAS, 441, 3127
Sacco, G. G., Morbidelli, L., Franciosini, E., et al. 2014, A&A, 565, A113
Sahlholdt, C. L., Feltzing, S., Lindegren, L., & Church, R. P. 2019, MNRAS, 482, 895
Santolaya-Rey, A. E., Puls, J., & Herrero, A. 1997, A&A, 323, 488
Sbordone, L., Bonifacio, P., Buonanno, R., et al. 2007, A&A, 465, 815
Sbordone, L., Bonifacio, P., Castelli, F., & Kurucz, R. L. 2004, Memorie della Societa Astronomica Italiana Supplementi, 5, 93
Skrutskie, M. F., Cutri, R. M., Stiening, R., et al. 2006, AJ, 131, 1163
Smiljanic, R., Korn, A. J., Bergemann, M., et al. 2014, A&A, 570, A122
Sneden, C., Bean, J., Ivans, I., Lucatello, S., & Sobeck, J. 2012, MOOG: LTE line analysis and spectrum synthesis
Soubiran, C., Jasniewicz, G., Chemin, L., et al. 2018, A&A, 616, A7
Sousa, S. G., Santos, N. C., Adibekyan, V., Delgado-Mena, E., & Israelian, G. 2015, A&A, 577, A67
Sousa, S. G., Santos, N. C., Israelian, G., Mayor, M., & Monteiro, M. J. P. F. G. 2007, A&A, 469, 783
Steinmetz, M., Zwitter, T., Siebert, A., et al. 2006, AJ, 132, 1645
Stetson, P. B. & Pancino, E. 2008, PASP, 120, 1332
Stonkutė, E., Koposov, S. E., Howes, L. M., et al. 2016, MNRAS, 460, 1131
Tabernero, H. M., Marfil, E., Montes, D., & González Hernández, J. I. 2019, A&A, 628, A131
Takeda, Y., Omiya, M., Harakawa, H., & Sato, B. 2016, PASJ, 68, 81
Traven, G., Matijevič, G., Zwitter, T., et al. 2017, ApJS, 228, 24
Traven, G., Zwitter, T., Van Eck, S., et al. 2015, A&A, 581, A52
Turon, C., Primas, F., Binney, J., et al. 2008, ESA-ESO Working Group on Galactic Populations, Chemistry and Dynamics, ESA-ESO Working Group reports
Valenti, J. A. & Piskunov, N. 1996, A&AS, 118, 595
Van der Swaelmen, M. & et al. 2022, in preparation
Van der Swaelmen, M., Merle, T., van Eck, S., Jorissen, A., & Zwitter, T. 2018, in Astrometry and Astrophysics in the Gaia Sky, ed. A. Recio-Blanco, P. de Laverny, A. G. A. Brown, & T. Prusti, Vol. 330, 350–351
Van Eck, S. & et al. 2022, in preparation
Venn, K. A., Shetrone, M. D., Irwin, M. J., et al. 2012, ApJ, 751, 102
Worley, C. C., de Laverny, P., Recio-Blanco, A., Hill, V., & Bijaoui, A. 2016a, A&A, 591, A81
Worley, C. C., de Laverny, P., Recio-Blanco, A., Hill, V., & Bijaoui, A. 2016b, A&A, 591, A81
Worley, C. C. & et al. 2022, in preparation
Worley, C. C., Jofré, P., Rendle, B., et al. 2020, A&A, 643, A83

[1] Institute of Astronomy, University of Cambridge, Madingley Road, Cambridge CB3 0HA, United Kingdom
e-mail: gil@ast.cam.ac.uk
[2] INAF - Osservatorio Astrofisico di Arcetri, Largo E. Fermi, 5, 50125, Firenze, Italy
[3] GEPI, Observatoire de Paris, PSL Research University, CNRS, Univ. Paris Diderot, Sorbonne Paris Cité, 61 avenue de l'Observatoire, 75014, Paris, France
[4] Astrophysics Group, Keele University, Keele, Staffordshire ST5 5BG, United Kingdom
[5] Institute for Astronomy, Royal Observatory, University of Edinburgh, Blackford Hill, Edinburgh EH9 3HJ, UK
[6] INAF - Osservatorio di Astrofisica e Scienza dello Spazio, via P. Gobetti 93/3, 40129 Bologna, Italy
[7] Instituto de Astrofísica de Andalucía, CSIC, Glorieta de la Astronomía s/n, Granada 18008, Spain
[8] Instituto de Astrofísica de Canarias, Vía Láctea s/n, E-38205 La Laguna, Tenerife, Spain
[9] Departamento de Astrofísica, Universidad de La Laguna, E-38205 La Laguna, Tenerife, Spain
[10] ROB - Royal Observatory of Belgium, Ringlaan 3, B-1180 Brussels, Belgium
[11] Observational Astrophysics, Division of Astronomy and Space Physics, Department of Physics and Astronomy, Uppsala University, Box 516, 75120 Uppsala, Sweden
[12] Dipartimento di Fisica e Astronomia, Sezione Astrofisica, Universitá di Catania, via S. Sofia 78, 95123, Catania, Italy
[13] Space Science Data Center - Agenzia Spaziale Italiana, via del Politecnico, s.n.c., I-00133, Roma, Italy
[14] Université Côte d'Azur, Observatoire de la Côte d'Azur, CNRS, Laboratoire Lagrange, Bd de l'Observatoire, CS 34229, 06304 Nice cedex 4, France
[15] Nicolaus Copernicus Astronomical Center, Polish Academy of Sciences, ul. Bartycka 18, 00-716, Warsaw, Poland
[16] Institut d'Astronomie et d'Astrophysique, Université Libre de Bruxelles, CP 226, Boulevard du Triomphe, B-1050 Bruxelles, Belgium
[17] Faculty of Mathematics and Physics, University of Ljubljana, Jadranska 19, 1000 Ljubljana, Slovenia
[18] Lund Observatory, Department of Astronomy and Theoretical Physics, Box 43, SE-22100 Lund, Sweden
[19] INAF - Osservatorio Asronomico di Palermo, Piazza del Parlamento, 1 90134 Palermo, Italy
[20] Astronomy Department, Indiana University, 727 East 3rd St, Bloomington, IN 47405, USA
[21] Armagh Observatory and Planetarium, College Hill, Armagh BT61 9DG, United Kingdom
[22] INAF - Osservatorio Astrofisico di Torino, via Osservatorio 20, I-10025 Pino Torinese, Italy
[23] Section of Astrophysics, Astronomy and Mechanics, Department of Physics, National and Kapodistrian University of Athens, GR15784, Athens, Greece
[24] IAASARS, National Observatory of Athens, GR15236, Penteli, Greece
[25] INAF - Osservatorio Astronomico di Padova, Vicolo dell'Osservatorio 5, I-35122, Padova, Italy
[26] Institut de Ciències del Cosmos (ICCUB), Universitat de Barcelona (IEEC-UB), Martí i Franquès 1, E-08028 Barcelona, Spain
[27] Department of Theoretical Physics and Astrophysics, Faculty of Science, Masaryk University, Kotlarska 2, 611 37 Brno, Czech Republic
[28] Centro de Astrobiología (CSIC-INTA), Departamento de Astrofísica, campus ESAC. Camino bajo del castillo s/n. 28 692 Villanueva de la Cañada, Madrid, Spain.
[29] Australian Academy of Science, Box 783, Canberra ACT 2601, Australia
[30] GEPI, Observatoire de Paris, Université PSL, CNRS, 5 Place Jules Janssen, 92190 Meudon, France
[31] Rudolf Peierls Centre for Theoretical Physics, Clarendon Laboratory, Parks Road, Oxford OX1 3PU, United Kingdom
[32] Department of Physics and Astronomy, University College London, Gower Street, London WC1E 6BT, United Kingdom
[33] Institute for Astronomy, University of Edinburgh, Blackford Hill, Edinburgh EH9 3HJ UK
[34] Departamento de Física Aplicada, Facultad de Ciencias, Universidad de Alicante, 03690 San Vicente del Raspeig, Alicante, Spain
[35] European Space Agency (ESA), European Space Research and Technology Centre (ESTEC), Keplerlaan 1, 2201 AZ Noordwijk, The Netherlands
[36] Max-Planck-Institut f
ur Astronomie, Königstuhl 17, D-69117 Heidelberg, Germany
[37] Niels Bohr International Academy, Niels Bohr Institute, Blegdamsvej 17, DK-2100 Copenhagen Ø, Denmark
[38] School of Physics and Astronomy, Monash University, Wellington Road, Clayton 3800, Victoria, Australia
[39] INAF - Osservatorio Astrofisico di Catania, Via S. Sofia 78, 95123 Catania, Italy
[40] Department of Astronomy, Stockholm University, AlbaNova University Center, SE-106 91 Stockholm, Sweden

[41] ESO - European Organisation for Astronomical Research in the Southern Hemisphere, Alonso de Córdova 3107, Vitacura, 19001 Casilla, Santiago de Chile, Chile
[42] Instituto de Astrofísica e Ciências do Espaço, Universidade do Porto, CAUP, Rua das Estrelas, 4150-762 Porto, Portugal
[43] Observatório Nacional - MCTI (ON), Rua Gal. José Cristino 77, São Cristóvão, 20921-400, Rio de Janeiro, Brazil
[44] Department of Chemistry and Physics, Saint Mary's College, Notre Dame, IN 46556, USA
[45] Leibniz-Institut für Astrophysik Potsdam (AIP), An der Sternwarte 16, 14482 Potsdam, Germany
[46] Institute of Theoretical Physics and Astronomy, Vilnius University, Sauletekio av. 3, LT-10257 Vilnius, Lithuania
[47] Departamento de Física de la Tierra y Astrofísica and IPARCOS-UCM (Instituto de Física de Partículas y del Cosmos de la UCM), Facultad de Ciencias Físicas, Universidad Complutense de Madrid, E-28040 Madrid, Spain
[48] Space Sciences, Technologies, and Astrophysics Research (STAR) Institute, Université de Liège, Quartier Agora, Bât B5c, Allée du 6 août, 19c, 4000 Liège, Belgium
[49] Laboratoire d'astrophysique de Bordeaux, Univ. Bordeaux, CNRS, B18N, allée Geoffroy Saint-Hilaire, 33615 Pessac, France
[50] Centro de Astrobiología (CSIC-INTA), Carretera de Ajalvir km 4, E-28850 Torrejón de Ardoz, Madrid, Spain
[51] Departamento de Astronomía, Casilla 160-C, Universidad de Concepción, Concepción, Chile
[52] Instituto de Física y Astronomía, Facultad de Ciencias, Universidad de Valparaíso, Chile
[53] Núcleo Milenio Formación Planetaria - NPF, Universidad de Valparaíso, Chile
[54] INAF - Osservatorio Astronomico di Roma, Via Frascati 33, I-00040 Monte Porzio Catone (Roma), Italy
[55] Department of Physics and Astronomy, University of Padova, v. dell'Osservatorio 2, 35122, Padova, Italy
[56] Theoretical Astrophysics, Department of Physics and Astronomy, Uppsala University, Box 516, SE-751 20 Uppsala, Sweden
[57] Núcleo de Astronomía, Facultad de Ingeniería y Ciencias, Universidad Diego Portales, Av. Ejército 441, Santiago, Chile
[58] Departamento de Ciencias Fisicas, Universidad Andres Bello, Fernandez Concha 700, Las Condes, Santiago, Chile
[59] Stellar Astrophysics Centre, Department of Physics and Astronomy, Aarhus University, Ny Munkegade 120, DK-8000 Aarhus C, Denmark
[60] University of Vienna, Dept. Astrophysics, Türkenschanzstrasse 17, 1180 Vienna, Austria
[61] Centro de Astrobiología (INTA-CSIC), Camino Bajo del Castillo s/n, 28692, Villanueva de la Cañada, Madrid, Spain
[62] Massachusetts Institute of Technology, Kavli Institute for Astrophysics and Space Research, 77 Massachusetts Ave., Cambridge, MA 02139, USA
[63] SISSA, via Bonomea, 265 - 34136 Trieste, Italy
[64] Dep. of Physics, Sapienza, University of Roma, Roma, Italy
[65] Research School of Astronomy and Astrophysics, Australian National University, ACT 2611, Australia
[66] Jeremiah Horrocks Institute, University of Central Lancashire, Preston PR1 2HE, United Kingdom
[67] INAF - Osservatorio Astronomico di Trieste, Via G.B Tiepolo, 11 I-34143 Trieste, Italy
[68] Université de Strasbourg, CNRS, Observatoire Astronomique de Strasbourg, UMR 7550, F-67000 Strasbourg, France
[69] The Kavli Institute for Astronomy and Astrophysics at Peking University, 100871, Beijing, PR China
[70] Instituto de Investigación Multidisciplinario en Ciencia y Tecnología, Universidad de La Serena, Avenida Raúl Bitrán s/n, La Serena, Chile
[71] Departamento de Astronomía, Facultad de Ciencias, Universidad de La Serena, Av. Juan Cisternas 1200, La Serena, Chile
[72] Max-Planck-Institute for Ex. Physics, Giessenbachstr.1, 85748 Garching, Germany
[73] Astronomisches Rechen-Institut, Zentrum für Astronomie der Universität Heidelberg, Mönchhofstr. 12–14, 69120 Heidelberg, Germany
[74] Materials Science and Applied Mathematics, Malmö University, SE-205 06 Malmö, Sweden
[75] Institut UTINAM, CNRS UMR6213, Univ. Bourgogne Franche-Comté, OSU THETA Franche-Comté-Bourgogne, Observatoire de Besançon, BP 1615, 25010 Besançon Cedex, France
[76] Zentrum für Astronomie der Universität Heidelberg, Landessternwarte, Königstuhl 12, 69117 Heidelberg, Germany
[77] School of Physics, University of New South Wales, Sydney 2052, Australia
[78] Dipartimento di Fisica e Astronomia, Università degli Studi di Bologna, Via Gobetti 93/2, I-40129 Bologna, Italy
[79] CENTRA, Faculdade de Ciências, Universidade de Lisboa, Ed. C8, Campo Grande, 1749-016 Lisboa, Portugal
[80] Departamento de Física e Astronomia, Faculdade de Ciéncias da Universidade do Porto, Portugal
[81] Department of Astronomy, University of Geneva, 51 chemin Pegasi, 1290 Versoix, Switzerland
[82] Université de Toulouse, Observatoire Midi-Pyrénées, CNRS, IRAP, 14 av. E. Belin, F-31400 Toulouse
[83] Astronomical Institute, CAS, Boční II 1401, 141 00 Prague 4, Czech Republic
[84] Physics Department, Imperial College London, Prince Consort Road, London SW7 2BZ, United Kingdom
[85] University of Surrey, Physics Department, Guildford, GU2 7XH, UK
[86] Mullard Space Science Laboratory, University College London, Holmbury St Mary, Dorking, Surrey, RH5 6NT, United Kingdom
[87] INAF - Astronomical Observatory of Padua, Vicolo dell'Osservatorio, 5, 35122 Padua PD, Italy
[88] Astronomical Observatory, Institute of Theoretical Physics and Astronomy, Vilnius University, Sauletekio av. 3, 10257 Vilnius, Lithuania
[89] Department of Physics and Astronomy, Johns Hopkins University, Baltimore, MD 21218, USA
[90] Institute of Astrophysics, Pontificia Universidad Católica de Chile, Av. Vicuña Mackenna 4860, Macul, Santiago, Chile
[91] Sorbonne Université, CNRS, UPMC, UMR7095 Institut d'Astrophysique de Paris, 98bis Bd. Arago, F-75014 Paris, France
[92] Department of Physics and Astronomy, Macquarie University, Sydney, NSW 2109, Australia